ARMY RESEARCH LABORATORY

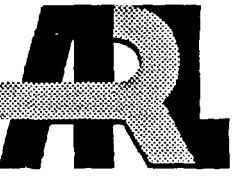

Multipath-Induced, Low-Angle Tracking Error at 140 GHz

Suzanne R. Stratton
Donald G. Bauerle
H. Bruce Wallace

JUN 3 0 1994

ARL-MR-140 June 1994

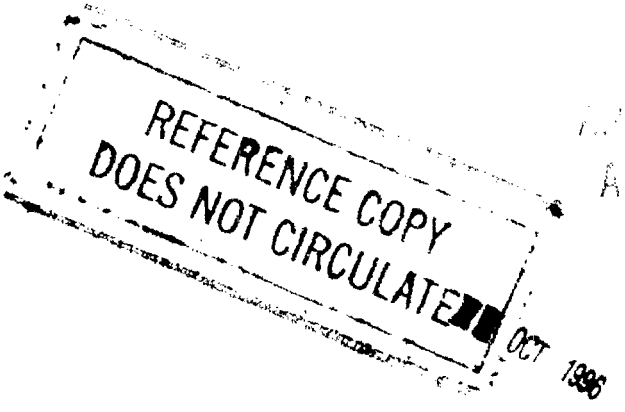

APG, MD. 21005-5066

APPROVED FOR PUBLIC RELEASE; DISTRIBUTION IS UNLIMITED.

NOTICES

Destroy this report when it is no longer needed. DO NOT return it to the originator.

Additional copies of this report may be obtained from the National Technical Information Service, U.S. Department of Commerce, 5285 Port Royal Road, Springfield, VA 22161.

The findings of this report are not to be construed as an official Department of the Army position, unless so designated by other authorized documents.

The use of trade names or manufacturers' names in this report does not constitute indorsement of any commercial product.

REPORT DOCUMENTATION PAGE

Form Approved
OMB No. 0704-0188

Public reporting burden for this collection of information is estimated to average 1 hour per response, including the time for reviewing instructions, searching existing data sources, gathering and maintaining the data needed, and completing and reviewing the collection of information. Send comments regarding this burden estimate or any other aspect of this collection of information, including suggestions for reducing this burden, to Washington Headquarters Services, Directorate for Information Operations and Reports, 1215 Jefferson Davis Highway, Suite 1204, Arlington, VA 22202-4302, and to the Office of Management and Budget, Paperwork Reduction Project (0704-0188), Washington, DC 20503.

1. AGENCY USE ONLY (Leave blank)	2. REPORT DATE	3. REPORT TYPE AND DATES COVERED
	June 1994	Final, 3–19 September 1991

4. TITLE AND SUBTITLE
Mulitpath-Induced, Low-Angle Tracking Error at 140 GHz

5. FUNDING NUMBERS
PR: 1L161102AH43

6. AUTHOR(S)
Suzanne R. Stratton, Donald G. Bauerle, and H. Bruce Wallace

7. PERFORMING ORGANIZATION NAME(S) AND ADDRESS(ES)
U.S. Army Research Laboratory
ATTN: AMSRL-SS-SD
Aberdeen Proving Ground, MD 21005-5066

8. PERFORMING ORGANIZATION REPORT NUMBER

9. SPONSORING / MONITORING AGENCY NAME(S) AND ADDRESS(ES)
U.S. Army Research Laboratory
ATTN: AMSRL-OP-AP-L
Aberdeen Proving Ground, MD 21005-5066

10. SPONSORING / MONITORING AGENCY REPORT NUMBER
ARL-MR-140

11. SUPPLEMENTARY NOTES

12a. DISTRIBUTION / AVAILABILITY STATEMENT
Approved for public release; distribution is unlimited.

12b. DISTRIBUTION CODE

13. ABSTRACT *(Maximum 200 words)*

This report describes a measurement program to characterize multipath-induced errors which can affect missile guidance. Measurements of angular position errors were made using a 140-GHz amplitude monopulse radar and a vertical probe. Data was collected at ranges out to 4.8 km. The longest ranges give propagation geometries that are typical for a missile trajectory in close proximity to the earth. Angular positioning errors due to diffuse multipath, specular multipath, and atmospheric-induced noise were measured.

14. SUBJECT TERMS
missiles, monopulse radar, multipath, tracking

15. NUMBER OF PAGES
75

16. PRICE CODE

17. SECURITY CLASSIFICATION OF REPORT	18. SECURITY CLASSIFICATION OF THIS PAGE	19. SECURITY CLASSIFICATION OF ABSTRACT	20. LIMITATION OF ABSTRACT
UNCLASSIFIED	UNCLASSIFIED	UNCLASSIFIED	SAR

ACKNOWLEDGMENTS

The authors would like to thank Mr. Donald E. Testerman of the Sensors, Signatures, Signal, and Information Processing (S^3I) Directorate of the U.S. Army Research Laboratory (ARL) for fabricating and assembling parts of the experimental apparatus and assisting in the conduct of the experiment.

Victor Leitzke of Weapons Technology Directorate and Robert L. Bender of S^3I Directorate reviewed this report and provided many thoughtful comments to the authors.

The authors would also like to thank Mike Christian of the U.S. Army Missile Command (MICOM) who was very helpful in providing the Redstone Arsenal meteorological data used in this report.

TABLE OF CONTENTS

		Page
	ACKNOWLEDGMENTS	iii
	LIST OF FIGURES	vii
	LIST OF TABLES	xi
1.	INTRODUCTION	1
2.	INSTRUMENTATION	2
3.	TEST SETUP AND TEST PROCEDURES	5
4.	DATA COLLECTED	11
5.	ANALYSIS OF MULTIPATH PROPAGATION DATA	11
6.	MULTIPATH DIFFUSE AND SPECULAR ANGULAR VARIATIONS	13
7.	ATMOSPHERIC NOISE	15
8.	CONCLUSIONS	16
9.	REFERENCES	19
	APPENDIX A: MULTIPATH MEASUREMENTS	21
	APPENDIX B: NOISE MEASUREMENTS	41
	APPENDIX C: METEOROLOGICAL DATA	63
	DISTRIBUTION LIST	71

INTENTIONALLY LEFT BLANK.

LIST OF FIGURES

Figure		Page
1.	Block diagram of RF and IF sections	3
2.	140-GHz two-way antenna pattern, elevation plane	4
3.	Typical measured vertical difference and sum outputs	5
4.	Vertical probe	6
5.	Television still frame of corner reflector at 4 km	8
6.	Typical calibration S-curve	8
7.	Terrain profile for the Redstone Arsenal Test Area 3	9
8.	Monopulse antenna and instrumentation trailer	10
9.	Typical difference and sum signals vs. probe position	12
A-1.	Trial 24, 0.8 km	23
A-2.	Trial 25, 0.8 km	24
A-3.	Trial 29, 0.8 km	25
A-4.	Trial 17, 1.8 km	26
A-5.	Trial 21, 1.8 km	27
A-6.	Trial 20, 1.8 km	28
A-7.	Trial 53, 1.8 km	29
A-8.	Trial 54, 1.8 km	30
A-9.	Trial 3, 2.8 km	31
A-10.	Trial 6, 2.8 km	32
A-11.	Trial 32, 2.8 km	33
A-12.	Trial 36, 2.8 km	34
A-13.	Trial 44, 2.8 km	35

Figure Page

A-14. Trial 47, 2.8 km 36

A-15. Trial 11, 2.8 km 37

A-16. Trial 14, 2.8 km 38

A-17. Trial 39, 3.8 km 39

A-18. Trial 42, 4.8 km 40

B-1. Noise measurement at 0.4 km and 3 km, Trials 5 and 4 43

B-2. Noise measurement at 0.4 km and 3 km, Trials 8 and 7 44

B-3. Noise measurement at 0.4 km and 3 km, Trials 9 and 10 45

B-4. Noise measurement at 0.4 km and 3 km, Trials 12 and 13 46

B-5. Noise measurement at 0.4 km and 2 km, Trials 15 and 16 47

B-6. Noise measurement at 0.4 km and 2 km, Trials 18 and 19 48

B-7. Noise measurement at 0.4 km and 1 km, Trials 22 and 23 49

B-8. Noise measurement at 0.4 km and 5 km, Trials 22 and 26 50

B-9. Noise measurement at 0.4 km and 1 km, Trials 27 and 28 51

B-10. Noise measurement at 0.4 km and 3 km, Trials 30 and 31 52

B-11. Noise measurement at 0.4 km and 3 km, Trials 34 and 33 53

B-12. Noise measurement at 0.4 km and 3 km, Trials 34 and 35 54

B-13. Noise measurement at 0.4 km and 4 km, Trials 37 and 38 55

B-14. Noise measurement at 0.4 km and 5 km, Trials 37 and 40 56

B-15. Noise measurement at 0.4 km and 5 km, Trials 37 and 41 57

B-16. Noise measurement at 0.4 km and 3 km, Trials 37 and 43 58

B-17. Noise measurement at 0.4 km and 3 km, Trials 45 and 46 59

B-18. Noise measurement at 0.4 km and 3 km, Trials 48 and 49 60

Figure Page

B-19. Noise measurement at 0.4 km and 2 km, Trials 51 and 52 61

B-20. Noise measurement at 0.4 km and 2 km, Trials 51 and 55 62

INTENTIONALLY LEFT BLANK.

LIST OF TABLES

Table		Page
1.	Mean and Standard Deviation of Angular Error for Path Lengths of 1, 2, 3, 4, and 5 km	14
2.	Mean and Standard Deviation of Angular Error for Noise Runs Over Path Lengths of 422 m, and 1, 2, 3, 4, and 5 km	17
C-1.	Meteorological Data Recorded at 2-km Mark of Test Area 3	65
C-2.	Meteorological Data Recorded at 5-km Mark of Test Area 3	68

INTENTIONALLY LEFT BLANK.

1. INTRODUCTION

The U.S. Army's new generation of advanced radar-guided antiarmor munitions will be required to track low-angle targets on the battlefield. Such systems must deal with the potential problem of multipath propagation. The development of munitions flying at longer ranges in many different environments has created a need for more substantive data collected under a variety of conditions and over greater distances.

Various aspects of multipath propagation have been investigated over the years by the U.S. Army Ballistic Research Laboratory (BRL),* Aberdeen Proving Ground (APG), MD. Two earlier studies will be cited here for comparison with more recent results. One study (Kammerer and Richer 1964) at 68 GHz found that angular pointing errors of less than 1/10th of the beamwidth could be achieved with null-type conical scan pointing techniques. Another BRL investigation (Wallace 1979) at 140 GHz concluded that multipath effects are less serious when propagating over vegetated surfaces than over surfaces such as asphalt because the power of the undesired reflected signals will be reduced by absorption and the reflected signals diffused by a relatively rougher surface.

A more recent measurement program was conducted to collect data on millimeter wave (MMW) propagation over natural terrain with a variety of ground cover conditions (Stratton, Wallace, and Bauerle 1991). Measurements of tracking errors at 95 and 140 GHz were recorded with a conical scan antenna tracking a trihedral corner reflector that was moved through a continuous range of heights between 0.4 m and 3.6 m above the ground. Antenna diameters of 0.92 m (3 ft) and 0.61 m (2 ft) were used for propagation paths of 2,850.0 m and 838.4 m, respectively. The results indicated that tracking error is substantially higher when tracking over snow and ice than when tracking over grass.

This report describes the results of the most recent joint Army Research Laboratory (ARL) and Army Missile Command (MICOM) program to measure the effects of multipath interference on the guidance of a missile or projectile to a distant target. The radar instrumentation consisted of 95- and 140-GHz monopulse radars set up for simultaneous measurements. This report includes the results of the ARL 140-GHz measurements. Results of the 95-GHz measurements are available in Christian, Wintler, and Woods (1992).

---

* The U.S. Army Ballistic Research Laboratory was deactivated on 30 September 1992 and subsequently became a part of the U.S. Army Research Laboratory on 1 October 1992.

2. INSTRUMENTATION

The radar system used in this test is a 139.5-GHz amplitude monopulse system designed and fabricated at the former BRL. Figure 1 is a block diagram of the complete radio frequency (RF) and intermediate frequency (IF) sections of this radar. The monopulse antenna, comparator, and the local oscillator (LO) distribution network were built under contract by the TRG Division of Alpha Industries. (The antenna/comparator is a 0.61-m monopulse reflector-type antenna with amplitude sensing of the multiplicative and additive sensing functions of the comparator.) The operational frequency of this unit is 140 GHz ±600 MHz. Figure 2 is an antenna pattern in the vertical plane of this system measured at the operational frequency of 139.5 GHz.

The LO distribution network distributes the 138.5-GHz LO signal to each of three mixers with equal phase shift. A fourth mixer connected directly to the transmitting tube through a 30-dB directional coupler is used for automatic frequency control (AFC). The LO is a Hughes continuous wave (CW) IMPATT oscillator with an output power of +18 dBm. Each of the three receiver mixers operates with +5.5-dBm LO drive. The noise figure of each mixer with this level of drive is 6 dB.

The transmitter tube is a Varian Pulsed Extended Interaction Oscillator. The peak output power of this tube is 260 W. An external modulator built into the radar is set up for 100-ns pulses at a 20 KHz-repetition rate. Ferrite switches in synchronism with the transmitted pulses are used for receiver protection. Failure of any one or all of these switches will shut down the transmitter. AFC is implemented in the second conversion process. A 160-MHz discriminator samples the transmitter signal and, through the gated integrator, controls the frequency of the second 1,160-MHz LO. This tracks the received signals into the 20-MHz bandwidths of the 160-MHz (IF) amplifiers and monopulse processor.

The Monopulse Detector Subsystem is a complete unit that was purchased from RHG Electronics Laboratory. This device is a complete three-channel monopulse IF processing subsystem. The unit consists of an IF matrix, a detector matrix, and three matched limiter channels. This detector subsystem determines difference nulls by measuring the difference (Δ) to sum (Σ) ratio. Each output error signal is proportional to this ratio and to the cosine of the phase angle between the Δ and Σ signals. The output is of the form,

$$E_o = \frac{1.4\ (\Delta/\Sigma)\ \cos\ \phi}{\left(1 + 2\ (\Delta/\Sigma)\ \sin\ \phi + (\Delta/\Sigma)^2\right)^{1/2}} \ ,$$

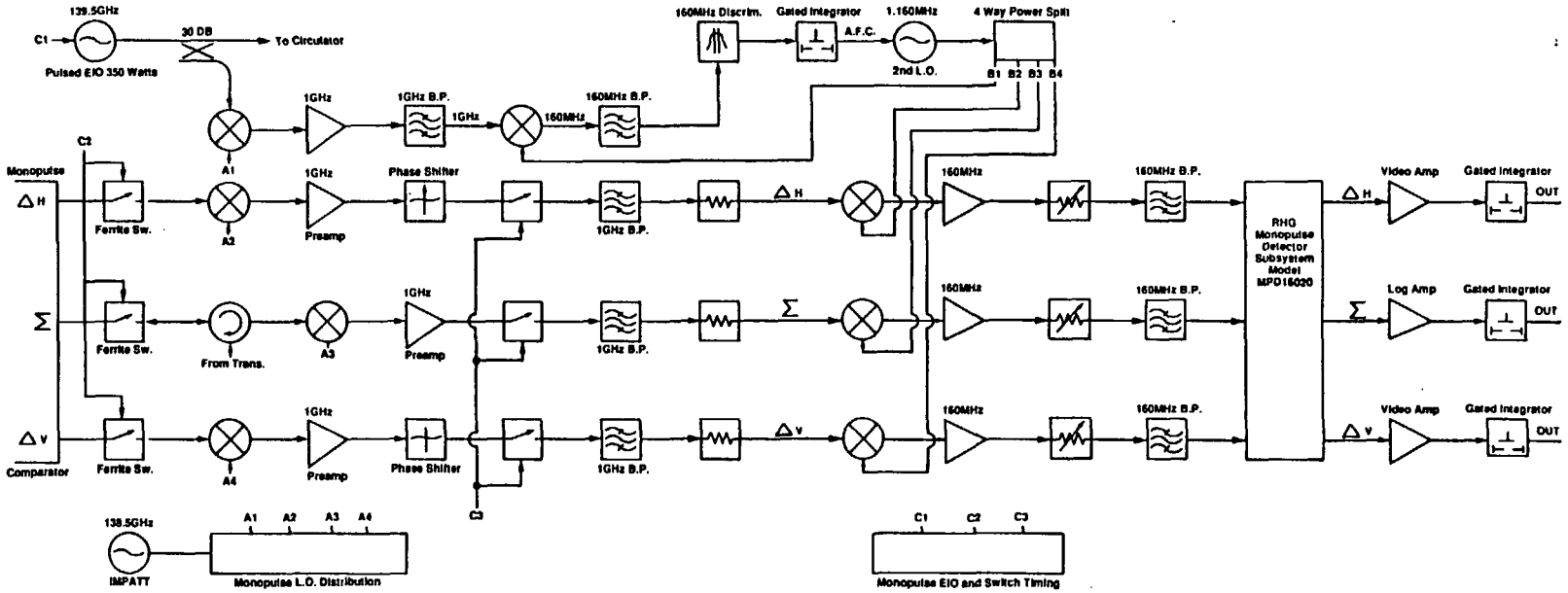

Figure 1. Block diagram of RF and IF sections.

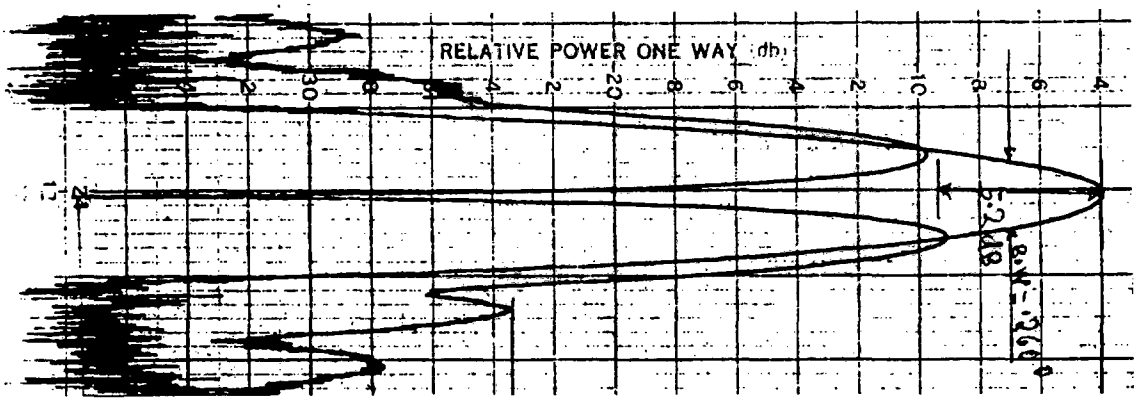

Figure 2. 140-GHz two-way antenna pattern, elevation plane.

where

E_o = difference output voltage,

Δ/Σ = voltage ratio between Δ and Σ, and

ϕ = phase angle between Δ and Σ .

The difference and sum channel outputs, still in the form of a 100-ns pulse, are passed on to the gated integrator modules (Evans Electronics Modules Model 4130A). Each unit is a fast, low-leakage integrator with an input-isolative gate that is opened under external control, which is a function of the range to the target. The output voltages of these devices closely approximates 1/RCx, the time integral of the input voltage, with integration proceeding only during the open gate intervals. The integral is held constant while the gate is closed. Figure 3 is an example of sum and vertical difference voltage outputs of the radar.

Initial alignment of the radar was accomplished with precise adjustments of the antenna, comparators, and phase shift adjustments in the first 1-GHz IF sections at the mixer outputs. Phase stability was maintained by temperature stabilizing all of the electronic components and the comparator.

The computer system used with this radar is a Hewlett-Packard (HP) Series 6900 Multiprogrammer with an HP 9000 CPU board and sufficient I/O cards for radar control functions and data input and output.

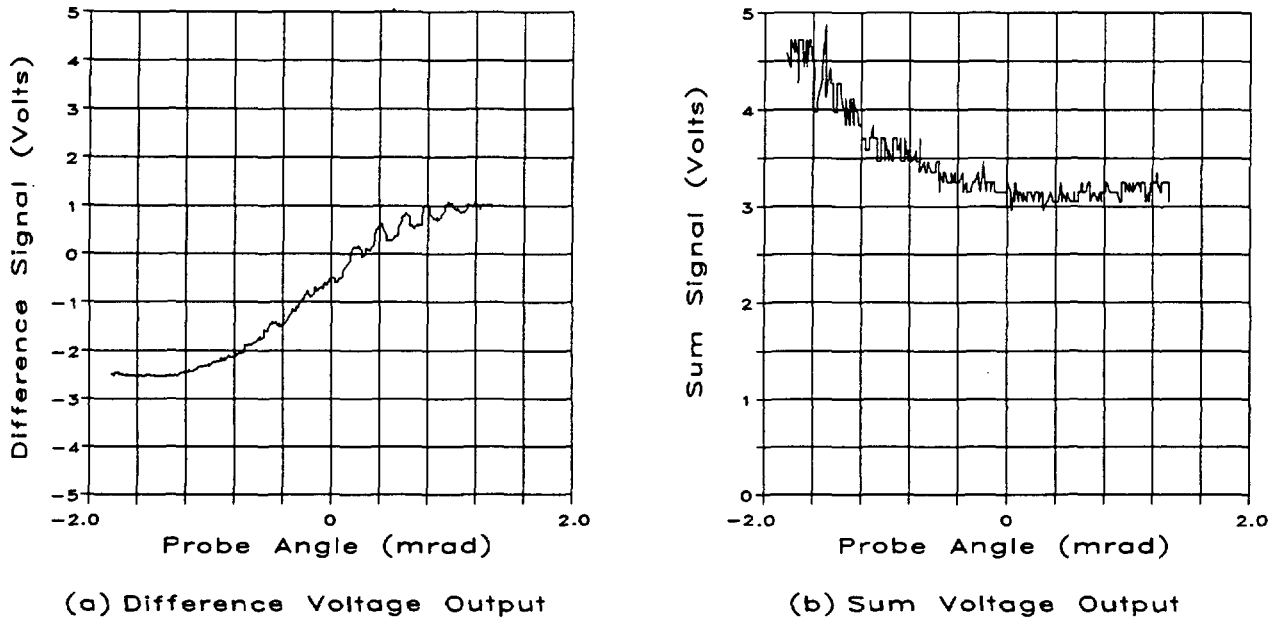

Figure 3. Typical measured vertical difference and sum outputs.

The vertical probe used for this test was designed and fabricated at the former BRL. The object of this device was to move a trihedral reflector through the fixed monopulse antenna beam at extended ranges from the radar. The probe shown in Figure 4 was mounted on a four-wheel trailer for ease of transportation and positioning. A radar reflector could be moved from near ground to a height of 5.36 m. The tower was constructed such that it had very low radar cross section. The vertical position of the reflector was continuously monitored and telemetered back to the transmitter trailer.

3. TEST SETUP AND TEST PROCEDURES

The radar was set up on an elevation over azimuth positioning mount located in the rear of an instrumentation trailer. The mount was attached to a special floor rack assembly that was detachable from the trailer and secured directly to the ground under the trailer. This was necessary to maintain the stability required for precise angular error measurements. The elevation axis of the positioning mount was instrumented for angle readout into the computer. The antenna was located 3 m above the ground for all the tests.

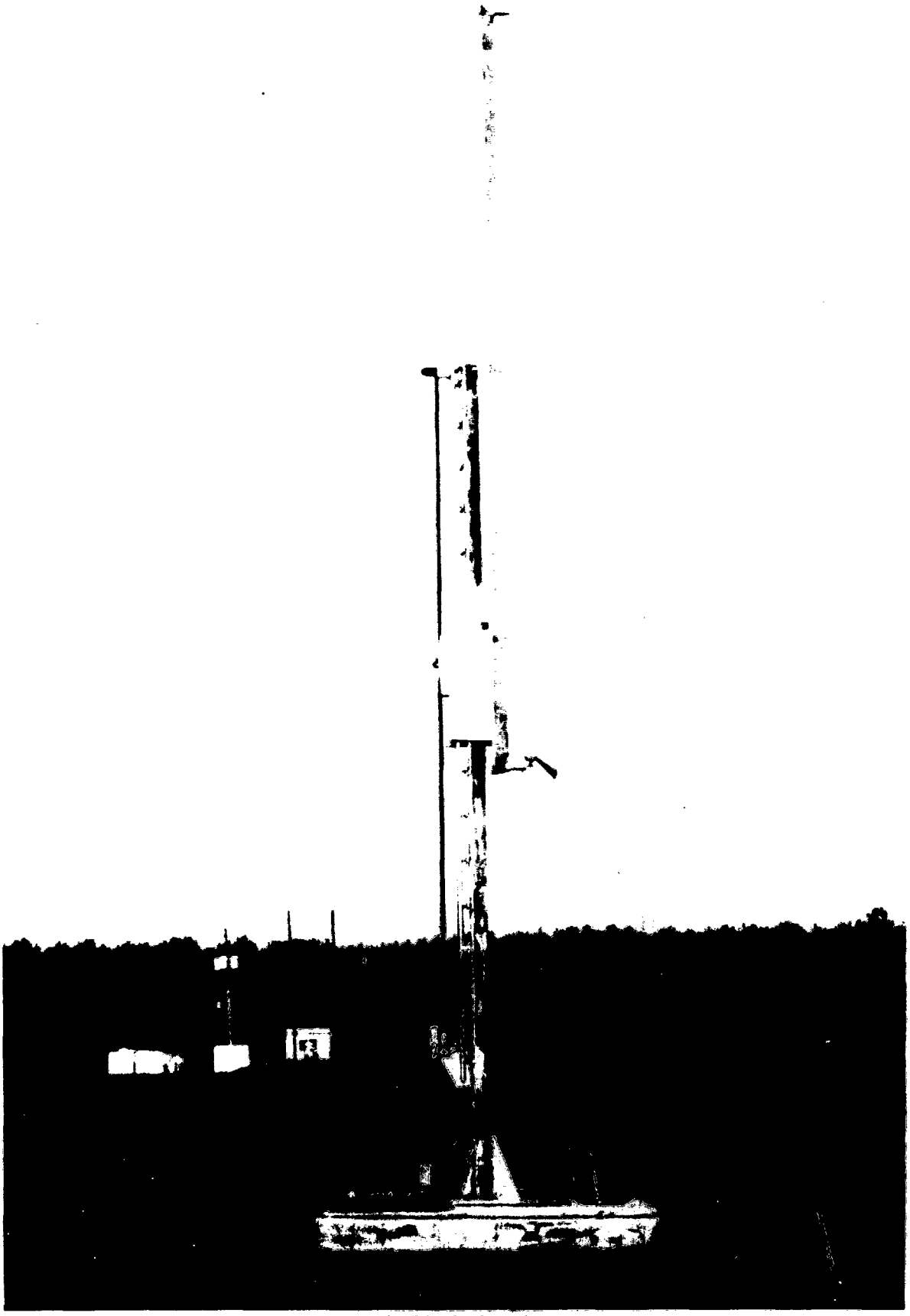

Figure 4. Vertical probe.

The site for this series of measurements was Test Area 3 at Redstone Arsenal, AL. These tests were designed to represent a radar locked on to a target at a range of 5 km and height above the ground of 1.5 m. The vertical probe was used to measure the effects multipath reflections would have on the guidance of a missile or projectile directed at the target.

A line of sight was set up between the radar and a target board at a range of 5 km. This line of sight was held constant, in both azimuth and elevation, for all but one of the measurements along the 5-km path. This optical boresight varied between 1 m and 3.6 m above the ground, depending on the terrain.

A calibrated corner reflector was set up at a range of 422 m at a height of 9 m. This point source was out of the antenna nearfield and high enough to ensure there were no multipath effects. The radar was boresighted with a television and Questar telephoto lens system. This high-resolution optical system was parallax aligned in the monopulse azimuth null plane and on the true elevation null. All subsequent multipath measurements were made relative to this optical boresight. The optics were boresighted to within 0.05 mrad of the true vertical null of the monopulse antenna. Figure 5 is a television still frame of a corner reflector at a range of 4 km.

Prior to each test, a series of calibration measurements was recorded using the calibration reflector. A complete vertical difference pattern was recorded. This was accomplished by sweeping the antenna beam, in the vertical plane, across the calibration reflector. One of these calibration patterns is shown in Figure 6. Long-term noise measurements of the vertical difference null signal were also recorded. This difference noise signal is calibrated in terms of angle offset from the zero null in the vertical difference channel. This angular variation is caused by receiver noise and atmospheric perturbations in the propagation path. Atmospheric noise was very low in the calibration measurements but was evident during subsequent long-range measurements.

The vertical probe was used for all the multipath measurements recorded during this series of tests. The probe was set up at various ranges out to 4.8 km in the direct line of sight to the target board. The boresighted optics were used to align the probe within the line of sight. Vertical error signals were recorded as the corner moved up through the antenna beam. Variations in these error signals are a measure of specular multipath. The measure of diffuse multipath error was the difference between the true optical calibration null and the apparent electrical null measured with the vertical probe. Long-term angular error noise was also recorded with the probe reflector adjusted to the electrical null of the antenna.

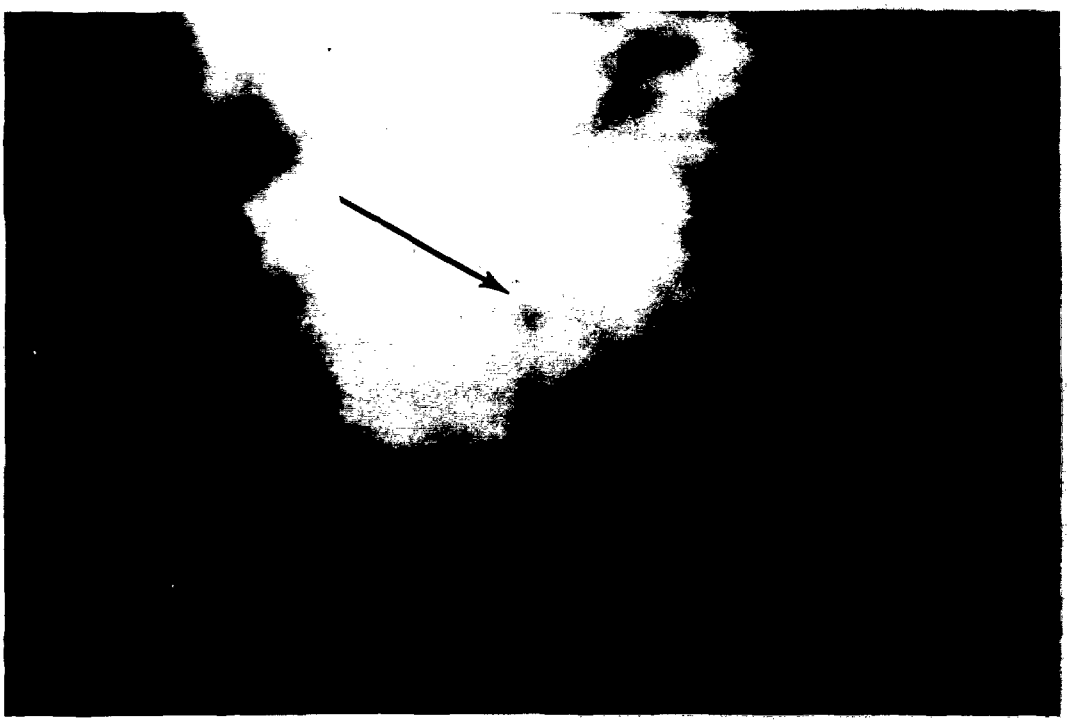

Figure 5. Television still frame of corner reflector at 4 km.

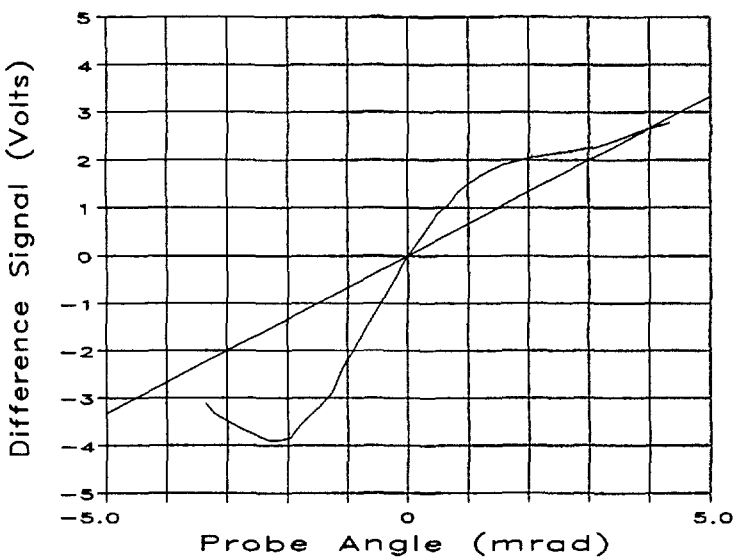

Figure 6. Typical calibration S-curve.

This noise was only recorded in the vertical error channel. The sum channel output was also recorded during each test. A corner reflector was set up approximately 20 m in front of the probe for each test. The sum range gate was alternately switched between this reflector and the probe to measure signal stability during each test. This precluded any errors associated with instabilities within the radar system or some momentary obstruction within the propagation path.

The test area, Redstone Arsenal Test Area 3, is a relatively flat field with a medium level of grass covering most of the propagation path. The terrain profile for part of the path is shown in Figure 7. Note that the vertical scale is significantly larger than the horizontal scale, to show that the profile is not perfectly flat. The profile was surveyed using a laser over the first 2,770 m of the propagation path. This short range was the limit of the laser system. The remaining 2,230 m of the path did not differ significantly in character from the measured path.

Figure 7. Terrain profile for the Redstone Arsenal Test Area 3.

Figure 8 is a photograph of the radar mounted in the trailer. The second antenna mounted on the tripod was the telemeter receiver used to transfer probe position data to the computer.

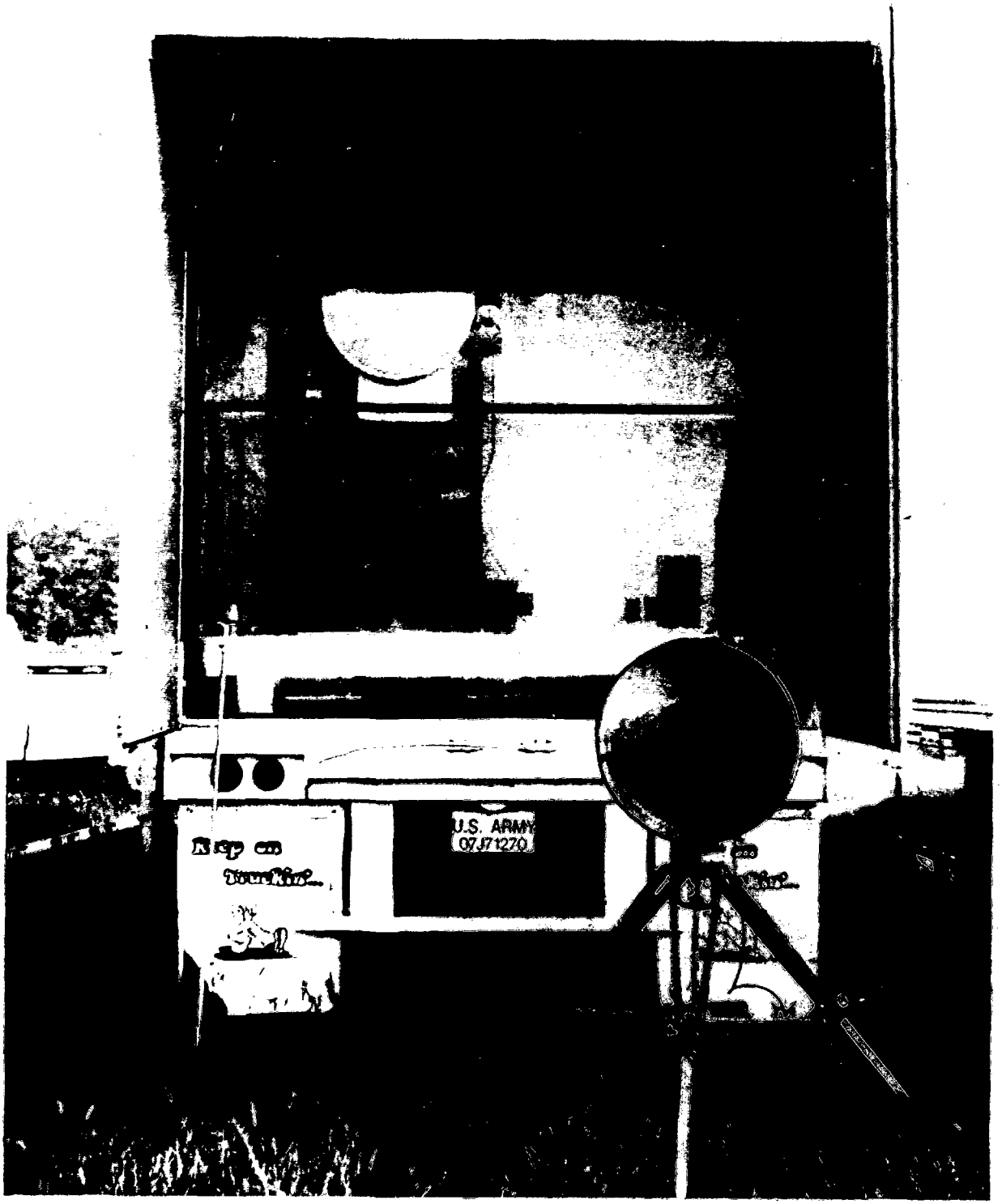

Figure 8. Monopulse antenna and instrumentation trailer.

4. DATA COLLECTED

Data was recorded on 11, 12, 13, 16, 17, and 18 September 1991. Measurements were made at six different ranges between 0.4 and 4.8 km. Additional measurements were made of static angular errors as a function of atmospheric weather conditions. A total of 18 usable measurements were made with the vertical probe. The total number of multipath tests was limited due to problems encountered with the 95-GHz monopulse radar system. The overall test plan called for simultaneous 95- and 140-GHz measurements. In one test, TR53, the optical boresight was raised 1.3 mrad above the normal optical boresight to determine if the multipath error would be reduced if there was a fixed vertical offset in the target track.

5. ANALYSIS OF MULTIPATH PROPAGATION DATA

Figure 9 shows typical difference and sum channel signals vs. probe position before calibration and filtering. Processing the raw error signal data was a three-step process that consisted of 1) converting angular vertical difference voltages to apparent angular difference in milliradians; 2) converting the probe position units to probe angle in milliradians; and 3) filtering the data with a smoothing algorithm.

The angular difference voltage was calibrated to give apparent angular difference by using information derived from the calibration S-curves recorded before each trial. The straight-line section in the middle of each S-curve was used to compute a slope. The slope is in units of volts/mrad, as can be seen in Figure 6. Digitized values of the angular difference voltage were scaled by this slope value, resulting in angular difference in milliradians.

Next, the position axis of the raw data was calibrated. The pulse-generated output from the vertical probe contained position information in terms of uncalibrated oscillator period "units," that changed linearly as the position along the probe pole changed. The maximum and minimum raw values were assumed to correspond to the highest and lowest positions of the probe in meters. The conversion to position in angle (with respect to the optical boresight) was accomplished by first converting the period value to probe distance from the boresight in meters using this linear relationship and then computing the angle by using the simple geometric relationship between the range and the probe height:

$$\text{angle (from boresight)} = \arctan\left[\frac{(\text{probe height}) \times (\text{datafreq} - \text{nullfreq})}{(\text{range to probe}) \times (\text{maxfreq} - \text{minfreq})}\right].$$

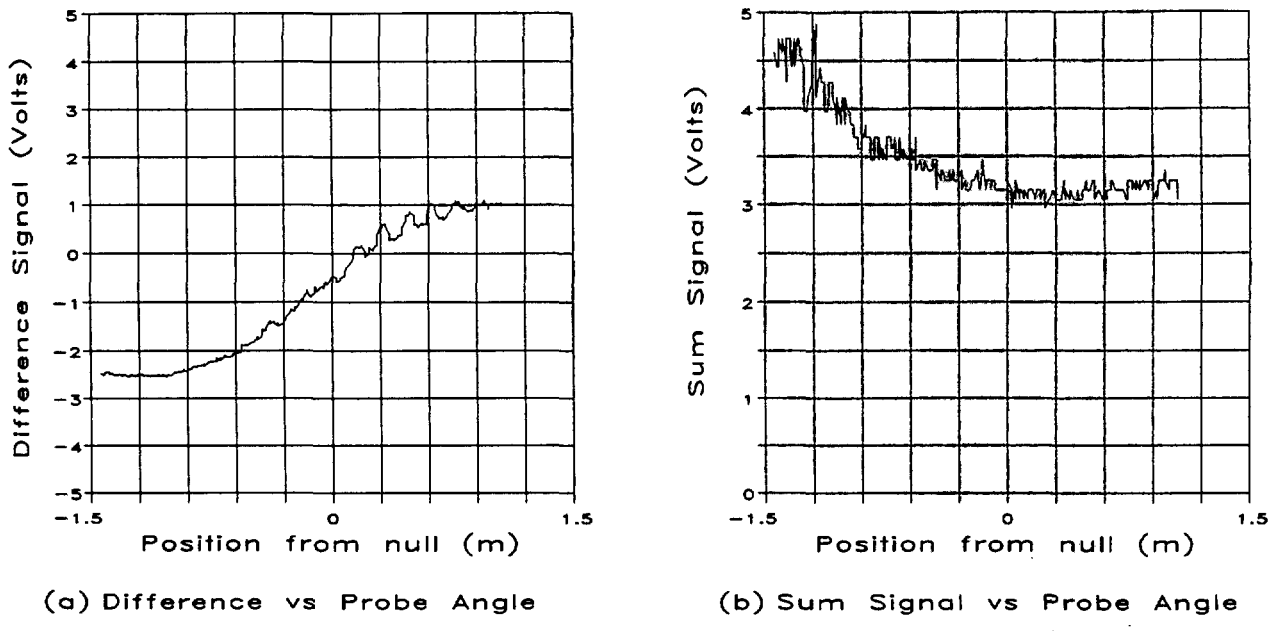

Figure 9. Typical difference and sum signals vs. probe position.

The last step in reducing the multipath probe data was smoothing to get rid of the noise that may have otherwise obscured the specular multipath variations. The bandwidth of the integrated signal was calculated to be 0.025 Hz by using the formula associated with the gated integrators (Evans Electronics),

$$\text{Noise factor} = \frac{(RC)}{n\,(t2-t1)} = 0.025 \text{ Hz},$$

where

R = integrator resistance = 10×10^3 Ohms

C = integrator capacitance = 10×10^{-9} F

n = repitition rate = 20×10^3 Hz, and

t2 – t1 = integration time = 200 ns .

With a noise factor of 0.025 Hz, a smoothing constant can be determined using Shannon's Law of Sampling, (i.e., freq (sampling) $\geq 2 \times$ signal BW). The sampling rate used in this experiment was approximately 160 Hz; therefore, it was well within acceptable bounds to use a three-point moving average to smooth the data without introducing any aliasing effects. The resulting calibrated apparent angular error vs. true (or probe) angular error curves are shown in Appendix A (A-1 through A-18). Note that the x-axis scale is not constant over the entire set of data. The axis was expanded with increasing path length to allow the features of the difference curves to be seen more easily. At the longer distances, the length of the probe pole subtends a smaller angle than at the shorter distances, making for a smaller measured angular error curve.

The vertical difference-axis of the atmospheric noise plots shown in Appendix B (B-1 through B-20) was calibrated in the same way as the difference-axis of the plots in Appendix A. The difference data was calibrated with the S-curve taken closest in time to the noise run. The sum voltage was calibrated with the voltage calibration curve recorded on the day of the noise run. The points of the calibration curve were used as a lookup table to convert the sum voltages to decibels. Linear interpolation was used for voltage values that fell between points on the calibration curve.

6. MULTIPATH DIFFUSE AND SPECULAR ANGULAR VARIATIONS

Computations of all the probe measurements of diffuse and specular multipath vertical channel difference variations are shown in Table 1. All multipath tests were set up so the optical boresight, which was the center null of the antenna beam, was aligned with the boresight mark on the target board. The vertical probe was then set up along the propagation path within the optical boresight. The radar reflector was moved up the probe until it was aligned with the optical boresight. This point on the probe was noted as the zero null or crossover point of the antenna. The reflector was then lowered to the bottom of the vertical beam probe and slowly raised to the top, while sum and vertical difference channels were recorded. If there were no multipath effects, the zero crossover in the vertical difference channel would occur at the optical boresight level. Diffuse multipath causes the measured null or crossover to be biased below the optical boresight. The computed measure of diffuse multipath is noted in Table 1 as the mean difference calibrated in terms of angle.

Specular multipath would cause cyclical variations in the vertical difference channel output as the vertical probe reflector is moved through the antenna monopulse beam. The period of this variation is

Table 1. Mean and Standard Deviation of Angular Error for Path Lengths of 1, 2, 3, 4, and 5 km

Target Reflector				Calibration Reflector		
Trial No.	Distance (km)	Mean (mrad)	Std. Dev. (mrad)	Trial No.	Mean (mrad)	Std. Dev. (mrad)
TR 24	0.8	−0.14	0.36	TR 22	0.00	0.05
TR 25	0.8	−0.07	0.43	TR 22	0.00	0.05
TR 29	0.8	−0.06	0.25	TR 27	0.02	0.03
[1]TR 17	1.8	−1.03	0.56	TR 18	−0.07	0.06
TR 20	1.8	0.01	0.23	TR 18	−0.07	0.06
[1]TR 21	1.8	−0.52	0.54	TR 18	−0.07	0.06
TR 53	1.8	−0.13	0.15	TR 51	−0.02	0.06
TR 54	1.8	−0.12	0.23	TR 51	−0.02	0.06
TR 3	2.8	−0.18	0.38	TR 5	0.01	0.03
TR 6	2.8	−0.07	0.32	TR 5	0.01	0.03
TR 11	2.8	−0.45	0.48	TR 9	0.01	0.03
TR 14	2.8	0.08	0.16	TR 9	0.01	0.03
TR 32	2.8	−0.05	0.15	TR 30	0.00	0.03
TR 36	2.8	−0.38	0.39	TR 34	0.06	0.03
TR 44	2.8	−0.04	0.15	TR 37	−0.06	0.02
TR 47	2.8	−0.41	0.26	TR 48	0.10	0.09
[2]TR 39	3.8	—	0.25	TR 37	−0.06	0.02
[2]TR 42	4.8	—	0.13	TR 37	−0.06	0.02

[1] Data probably bad, probe sitting below optical boresight.
[2] Optical boresighting impossible at these lengths due to haze, so no mean error has been calculated.

a function of range to the probe (Barton and Ward 1984). The computed measure of specular multipath variations is noted in Table 1 as the standard deviation, calibrated in terms of angle. The data was filtered so that atmospheric angular variations were removed. This set of multipath data is shown in Appendix A.

Four separate plots are shown for each trial. Plot "a" (difference vs. probe angle) is the raw data (voltages) out of the vertical difference channel vs. the position of the vertical probe reflector in terms of angle—negative angle below the optical boresight and positive angle above the optical boresight. In Figure A-1, the specular and diffuse multipath-induced difference signals are apparent. Plot "b" (sum vs. angular probe position) shows the sum signal amplitude as a function of the vertical probe reflector position. This sum data is not filtered and shows the atmospheric signal amplitude variations. Plot "c" (difference voltage vs. vertical angle antenna mount position) is the raw data output (voltages) of the vertical difference channel when the monopulse antenna beam is swept vertically past the calibration

reflector. The calibration curve is used to calibrate the vertical difference channel in terms of angular difference. Plot "d" (apparent angle vs. probe angle) shows the calibrated multipath-induced vertical differences in terms of angle, plot "a," calibrated with plot "c," along with the theoretical straight-line difference curve that would have been achievable if there were no multipath errors. The mean difference from the theoretical straight line is the diffuse angular difference. The cyclical amplitude variations are the specular multipath differences.

At the longest ranges, 3.8 km and 4.8 km, haze conditions due to the hot, humid air limited the range of the optical boresight. Diffuse multipath at these ranges could not be measured with any degree of accuracy. Appendix C contains tabular data on water vapor values that were computed from meterological data measure during the testing.

For Trial 53, the optical boresight was raised 1.3 mrad in the vertical plane above the target board. This is approximately one-quarter of the sum of the antenna beam pattern beamwidth. This test was performed to measure the difference in multipath-induced errors if a slight bias in the vertical plane was applied to the tracking loop. Trials 53 and 54 were run for direct comparison at 1.8 km (Figures A-7 and A-8). There is a definite difference in the data sets. Trial 54, with boresight on the target board, shows both specular and diffuse multipath-induced errors. When the antenna beam was raised for Trial 53, there was no trace of specular multipath and the diffuse error at 0° probe angle is very small. In Trial 54, the lower optical boresight allows more of the antenna beam to intercept the ground, causing a stronger surface-reflected signal that can interfere with the direct radar-target-radar signal. The error is less in Trial 53 because the higher boresight implies less illumination of the ground, hence a weaker surface-reflected signal.

7. ATMOSPHERIC NOISE

The weather pattern during this series of tests consisted of extremely high temperatures with high levels of relative humidity. Large variations in difference channel and sum channel noise were noted throughout the course of this measurement program. It has been noted in other measurement programs (McMillan, Wiltse, and Snider 1979) that atmospheric noise and phase front distortions increase as the moisture content of the atmosphere increases. Water vapor is a continuously changing medium with areas of variable concentrations (scale sizes 10–100 m and strata of approximately 1 m). MMWs traveling through changing media are subject to random variations in both amplitude and phase (Deepak, Wilkerson, and Ruhnke 1980).

A series of measurements was made to ascertain the effects of this atmospheric noise on monopulse tracking accuracies. The antenna monopulse boresight was set up on the probe with the corner reflector set at the height of the target board boresight. Static measurements of the sum and vertical difference channels were recorded at all the measurement ranges out to 4.8 km, as a function of time. These static measurements were also recorded on the 0.4-km calibration reflector prior to or after each long-range measurement. Direct comparisons are shown in the data set which is in Appendix B.

Computations of all the static noise measurements are shown in Table 2. The vertical difference channel output was calibrated in terms of angular differences. The sum channel outputs are calibrated in terms of decibels. The measurements at 0.4 km of the calibration reflector are essentially system noise. This data is shown for comparison. The amplitude of the difference channel angular noise increases with range out to 2.8 km. The standard deviations of the data sets, shown in Table 2, characterize the relative magnitudes of the noise in terms of angular error. The number of measurements made at the longer ranges, 3.8 and 4.8 km, were not enough to indicate any further trend.

Phase front distortions and signal amplitude fluctuations could cause the angular difference fluctuations noted in both the vertical and horizontal difference channels. The RHG monopulse processor in this system employs hard limiters in the sum and delta processing channels. The return signal levels out to ranges of 3 km were of such amplitude to be hard limited; thus, signal amplitude fluctuations would not be a dominant factor in the processed difference channel outputs. The static angular variations measured out to 2.8 km in range are believed to be caused by phase front distortions. The sum channel outputs shown in Appendix B were not hard limited.

8. CONCLUSIONS

The measurements made during this test characterize errors that can affect the guidance of a missile or projectile to a distant target. Consider a missile that flies within a radar monopulse antenna beam. The monopulse radar tracking a target would measure the instantaneous position of the missile relative to the target, and guidance commands would be issued to the missile to correct its flight path to the target. There are three major sources of missile position error other than the tracking accuracies associated with the radar system: 1) atmospheric noise, 2) diffuse multipath, and 3) specular multipath.

Table 2. Mean and Standard Deviation of Angular Error for Noise Runs Over Path Lengths of 422 m, and 1, 2, 3, 4, and 5 km

Trial No.	Distance (km)	Mean (mrad)	Std. Dev. (mrad)
TR 5	0.4	0.01	0.03
TR 8	0.4	–0.01	0.04
TR 9	0.4	0.01	0.03
TR 12	0.4	0.00	0.04
TR 15	0.4	0.04	0.08
TR 18	0.4	–0.07	0.06
TR 22	0.4	0.00	0.05
TR 27	0.4	0.02	0.03
TR 30	0.4	0.00	0.03
TR 34	0.4	0.06	0.03
TR 37	0.4	–0.06	0.02
TR 45	0.4	–0.02	0.02
TR 48	0.4	0.10	0.09
TR 51	0.4	–0.02	0.06
TR 23	0.8	–0.01	0.07
TR 28	0.8	–0.01	0.07
TR 16	1.8	0.00	0.22
TR 19	1.8	0.00	0.06
TR 52	1.8	–0.02	0.06
TR 55	1.8	0.00	0.08
TR 4	2.8	0.02	0.12
TR 7	2.8	0.04	0.25
TR 10	2.8	–0.01	0.05
TR 13	2.8	–0.02	0.13
TR 31	2.8	–0.08	0.15
TR 33	2.8	0.00	0.04
TR 35	2.8	–0.01	0.11
TR 43	2.8	0.05	0.10
TR 46	2.8	0.09	0.09
TR 49	2.8	0.00	0.12
TR 38	3.8	–0.04	0.06
TR 26	4.8	–0.04	0.08
TR 40	4.8	0.01	0.04
TR 41	4.8	0.00	0.05

Atmospheric noise, which manifests itself in signal amplitude and phase front distortions, is a variable factor dependent on the water vapor continuum. In the damp atmosphere of summer, this angular variation was measured to be as great as ±0.15 mrad. Atmospheric noise can be reduced through closed loop bandwidth reduction when tracking a slow-moving distant target. Position tracking of a missile or projectile requires a very wide open loop bandwidth, which would include atmospheric noise.

Diffuse multipath error is variable depending on terrain features and surface moisture conditions. This source of error manifests itself in a negative bias error below the radar aimpoint. Diffuse errors measured during this test were as great as -0.45 mrad.

Specular multipath errors are also dependent on terrain and surface moisture conditions. The magnitude of this error increases as diffuse bias errors increase. Specular multipath is coherent in nature and will cycle with range. The error is impressed on the diffuse bias; thus, it will add to or subtract from the bias error. Specular multipath errors measured during this test had an average magnitude of 0.25 mrad.

Both diffuse and specular multipath errors can be reduced by introducing a small positive bias in the antenna boresight so that less of the beam intercepts the ground. This was shown to be the case in Trials 53 and 54. This simple method of reducing multipath error can be exploited to allow for more accurate tracking at low elevation angles.

9. REFERENCES

Barton, D., and H. Ward. Handbook of Radar Measurement. Englewood Cliffs, NJ, Pentice-Hall, 1984.

Christian, M. R., J. B. Winter, and T. D. Woods. "W Band Low Angle Multipath Measurements." Proceedings Precision Munitions Guidance Symposium, 1992.

Deepak, A., T. Wilkerson, and L. Ruhnke. Atmospheric Water Vapor. Academic Press, 1980.

Evans Electronics. "Gated Integrator Module - Model 4130A." Operator's Manual, Berkeley, CA.

Kammerer, J. E., and V. A. Richer. "4-mm Near-Earth Antenna Multipath Pointing Errors." BRL-MR-1559, U.S. Army Ballistic Research Laboratory, Aberdeen Proving Ground, MD, March 1964.

McMillan, R. W., J. C. Wiltse, and D. E. Snider. "Atmospheric Turbulence Effects on Millimeter Wave Propagation." IEEE EASCON 79 Conference Records, vol. 1, 1979.

Stratton, S. R., H. B. Wallace, and D. G. Bauerle. "Multipath Induce Tracking Errors at 95- and 140-GHz." BRL-MR-3947, U.S. Army Ballistic Research Laboratory, Aberdeen Proving Ground, MD, 1991.

Wallace, H. B. "140-GHz Propagation Measurements Over Varied Terrain Covers." IEEE EASCON-79 Conference Record, vol. 2, p. 256, 1979.

INTENTIONALLY LEFT BLANK.

APPENDIX A:

MULTIPATH MEASUREMENTS

INTENTIONALLY LEFT BLANK.

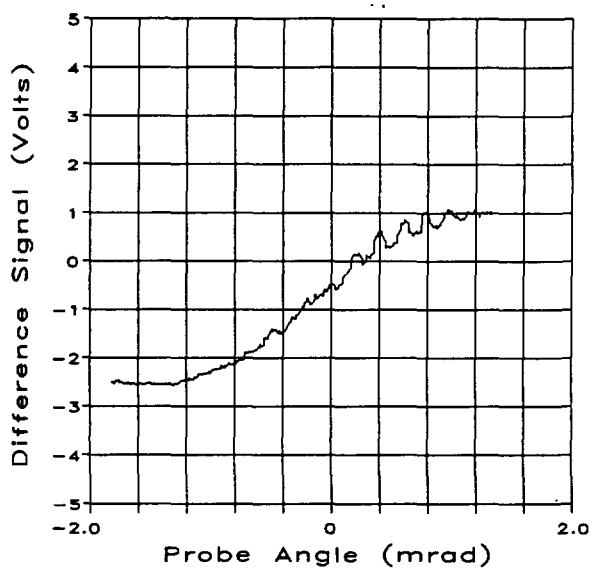

(a) Difference vs Probe Angle

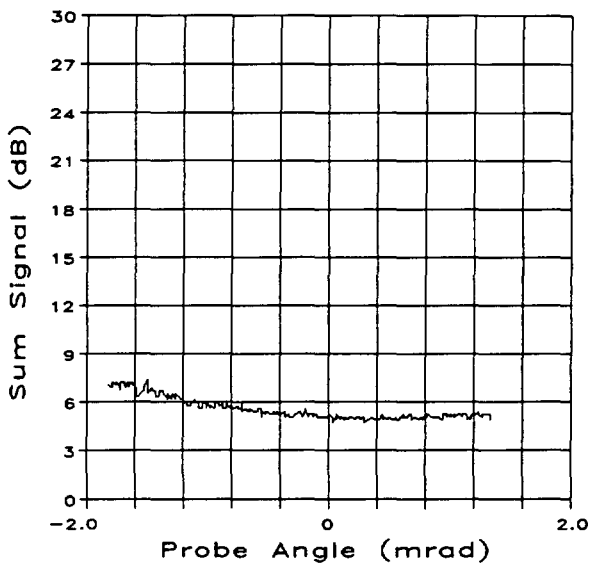

(b) Sum Signal vs Probe Angle

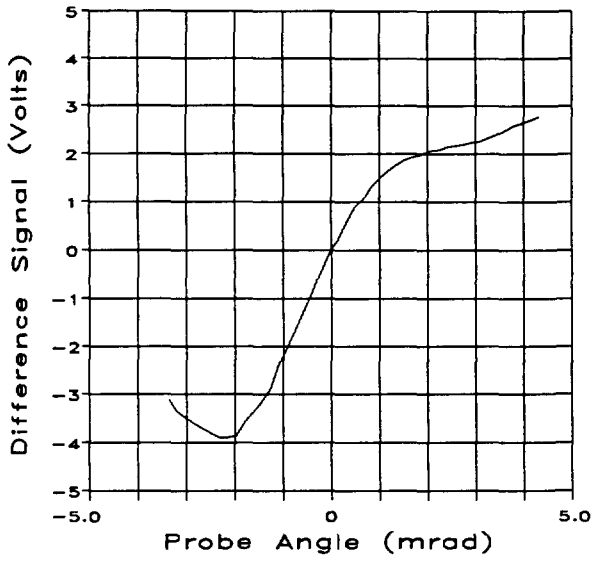

(c) Calibration Diff. vs Probe Angle

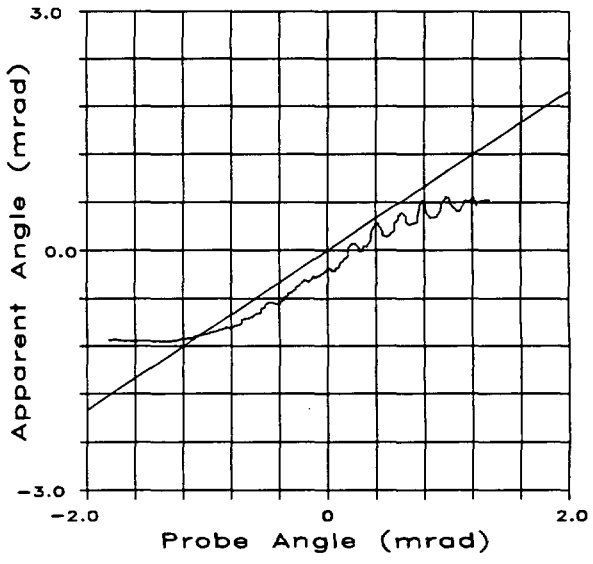

(d) Apparent Angle vs Probe Angle

Figure A-1. Trial 24, 0.8 km.

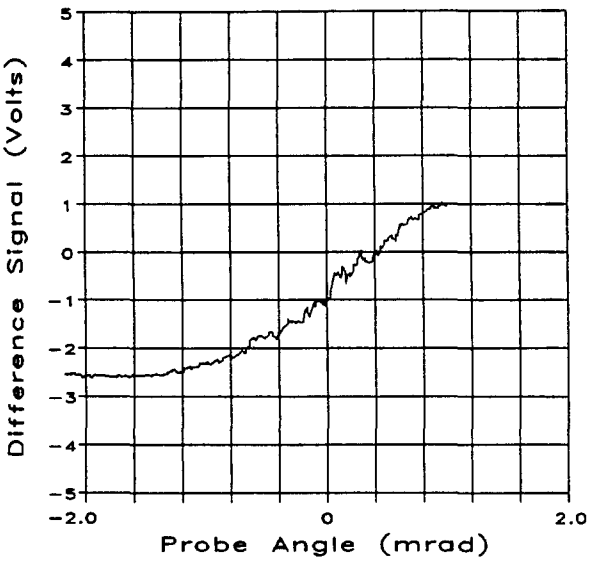

(a) Difference vs Probe Angle

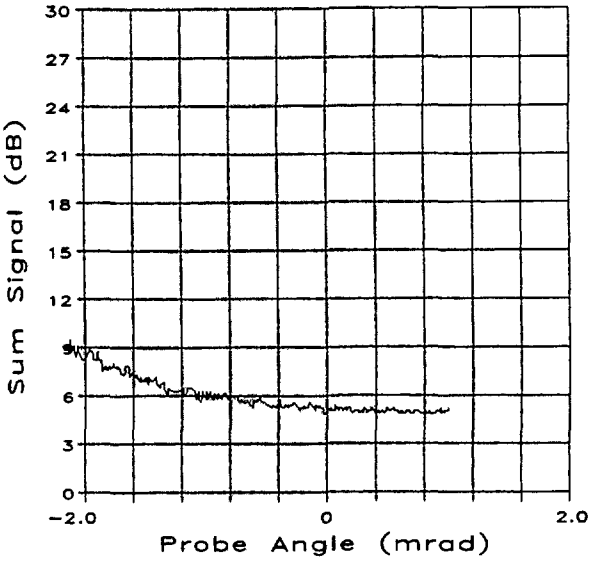

(b) Sum Signal vs Probe Angle

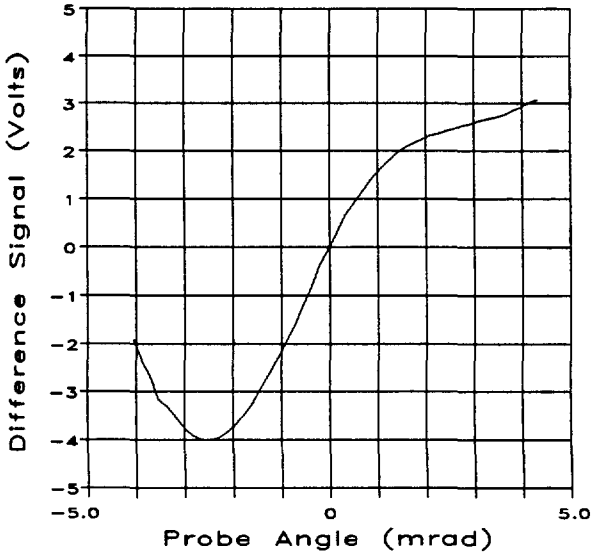

(c) Calibration Diff. vs Probe Angle

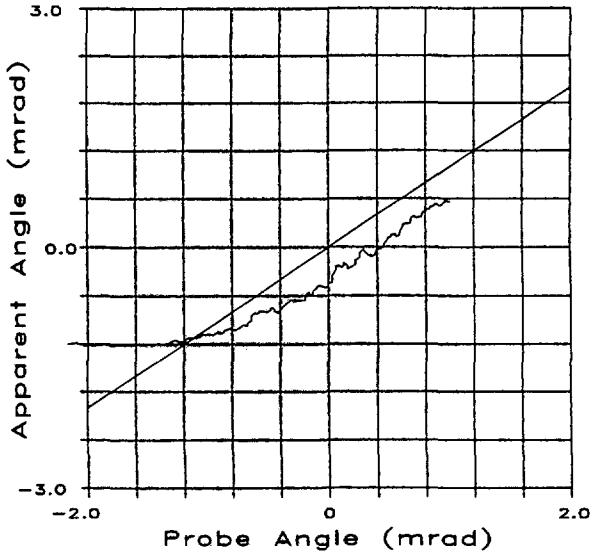

(d) Apparent Angle vs Probe Angle

Figure A-2. Trial 25, 0.8 km.

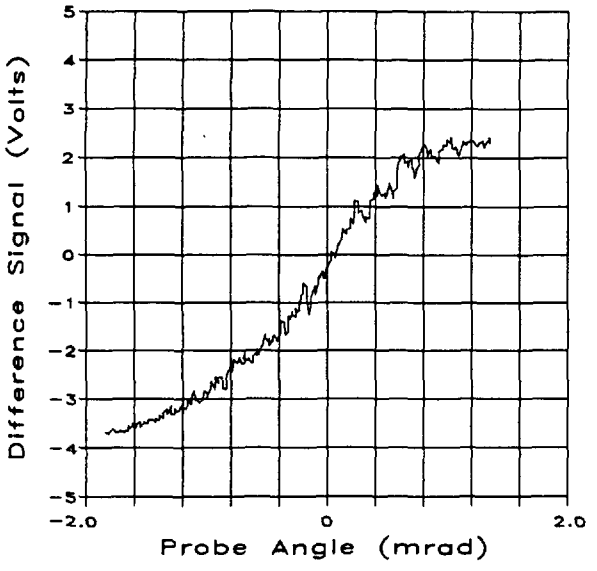

(a) Difference vs Probe Angle

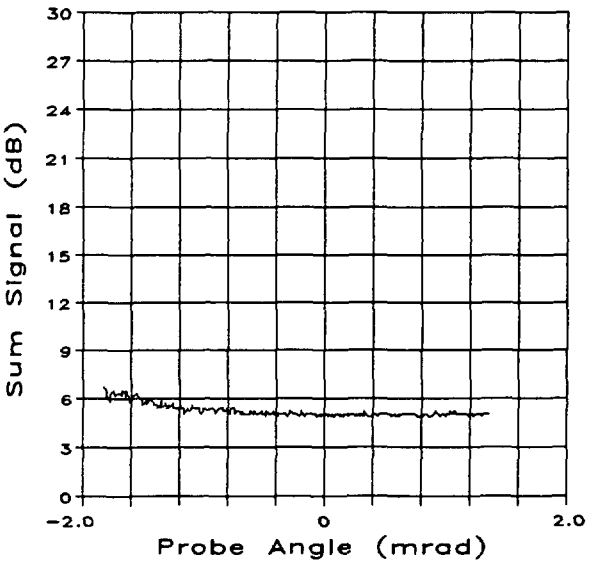

(b) Sum Signal vs Probe Angle

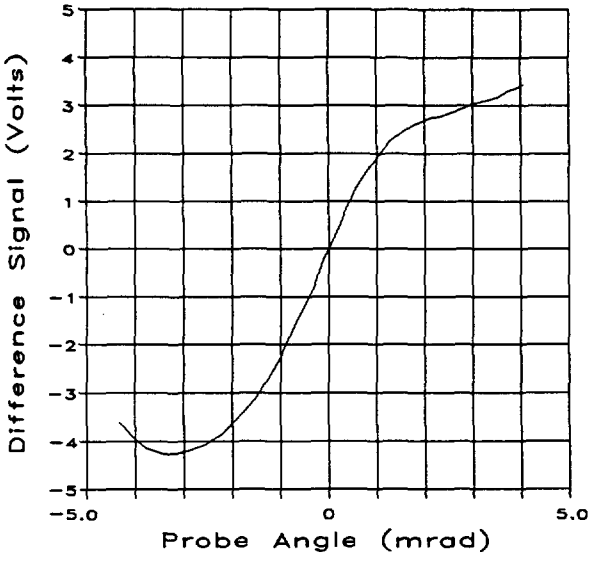

(c) Calibration Diff. vs Probe Angle

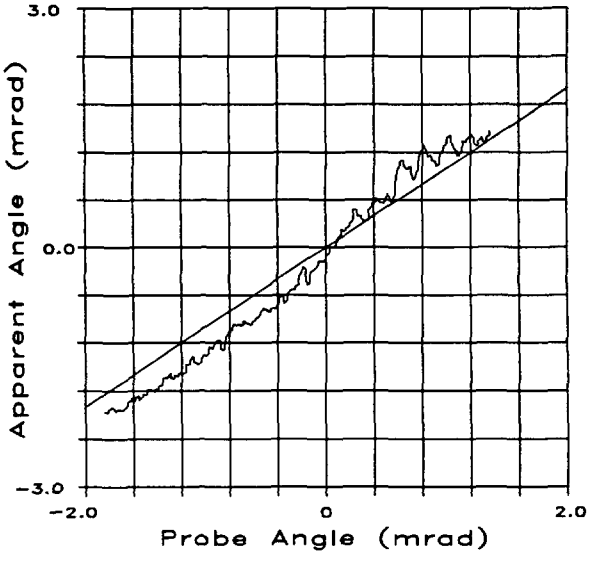

(d) Apparent Angle vs Probe Angle

Figure A-3. Trial 29, 0.8 km.

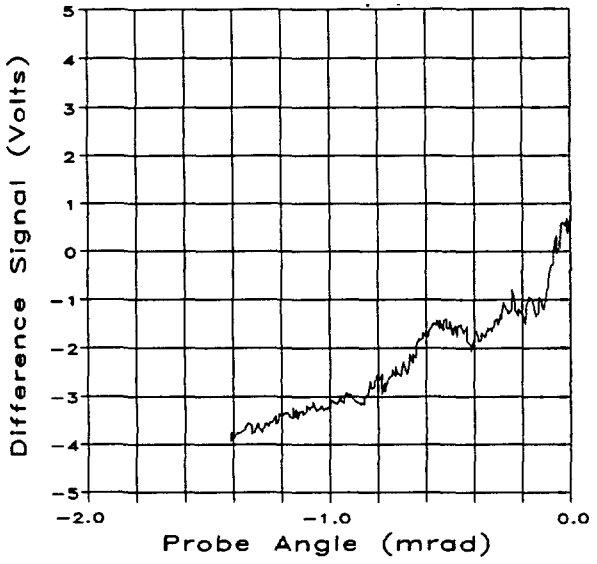

(a) Difference vs Probe Angle

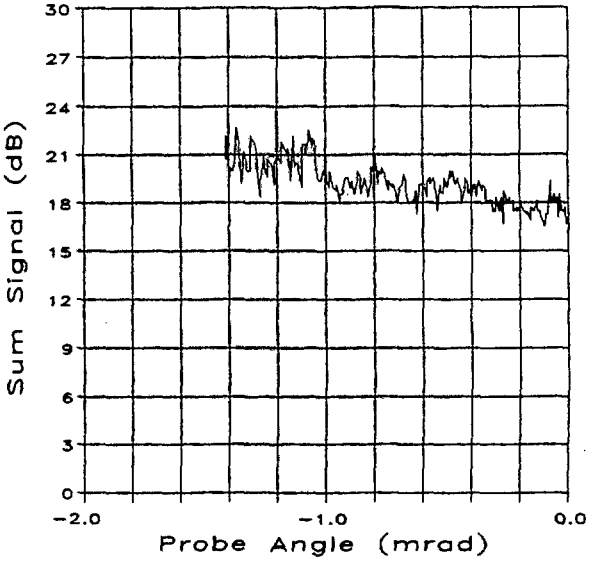

(b) Sum Signal vs Probe Angle

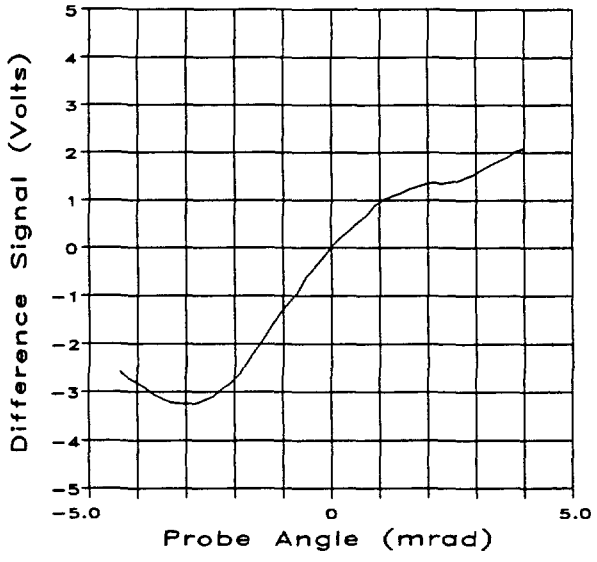

(c) Calibration Diff. vs Probe Angle

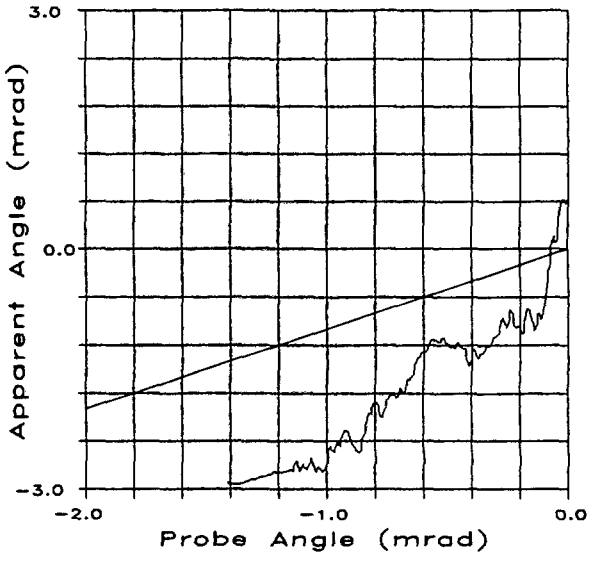

(d) Apparent Angle vs Probe Angle

Figure A-4. Trial 17, 1.8 km.

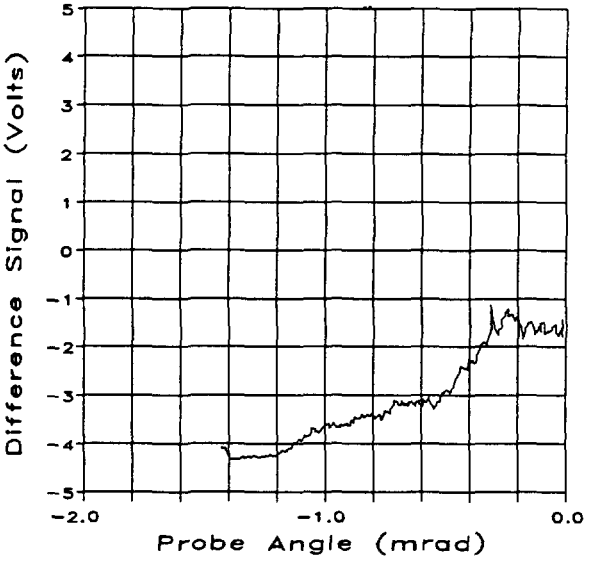

(a) Difference vs Probe Angle

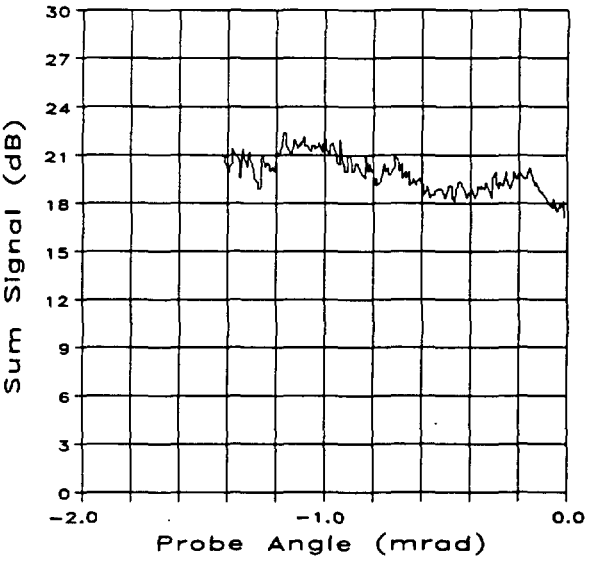

(b) Sum Signal vs Probe Angle

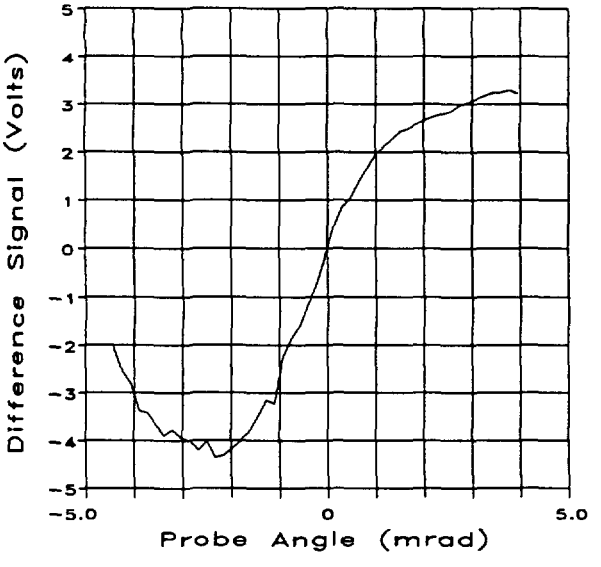

(c) Calibration Diff. vs Probe Angle

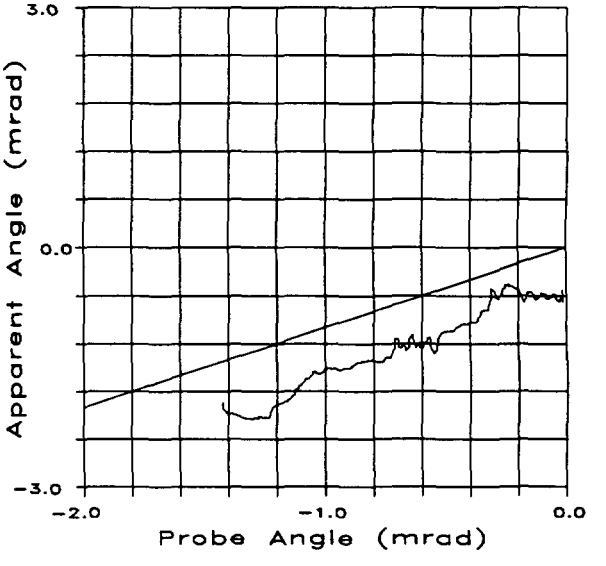

(d) Apparent Angle vs Probe Angle

Figure A-5. Trial 21, 1.8 km.

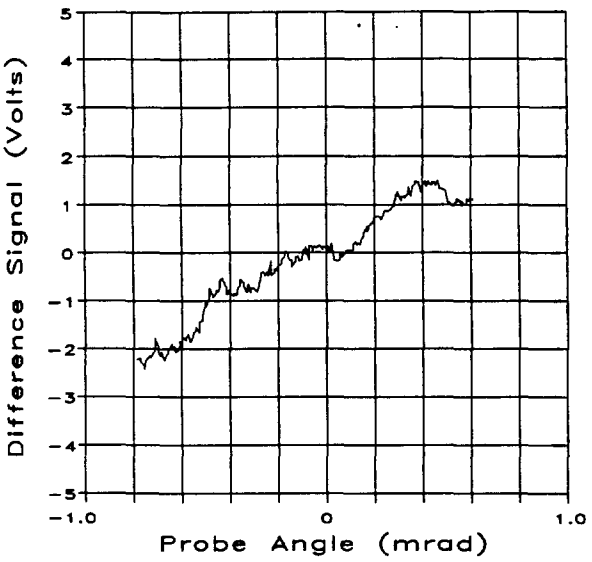

(a) Difference vs Probe Angle

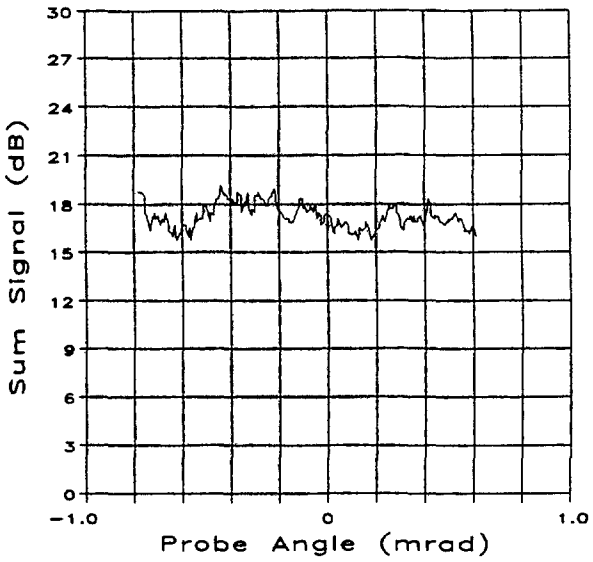

(b) Sum Signal vs Probe Angle

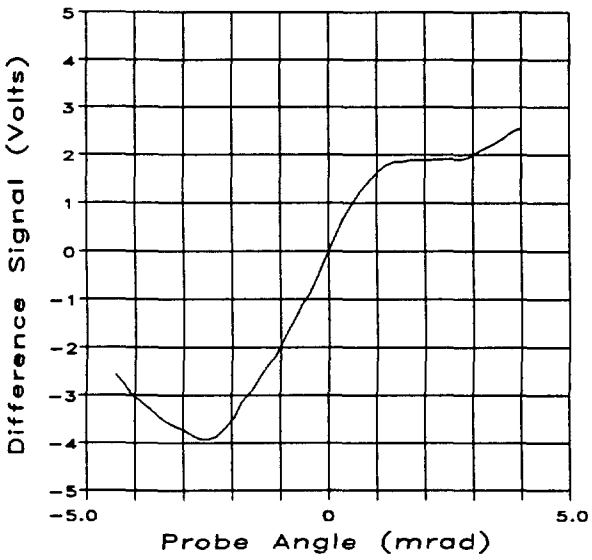

(c) Calibration Diff. vs Probe Angle

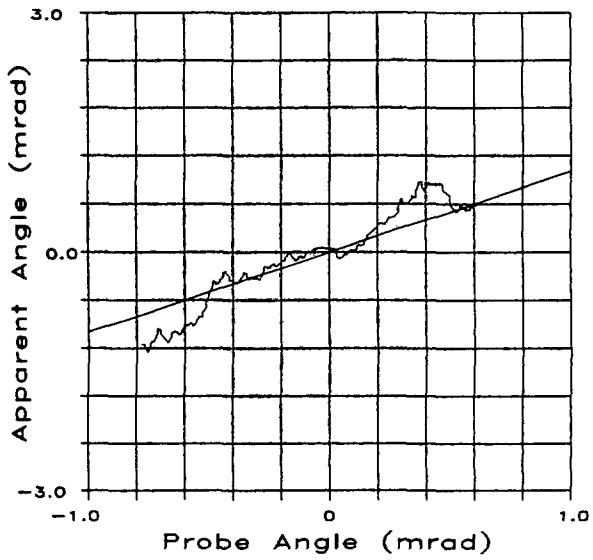

(d) Apparent Angle vs Probe Angle

Figure A-6. Trial 20, 1.8 km.

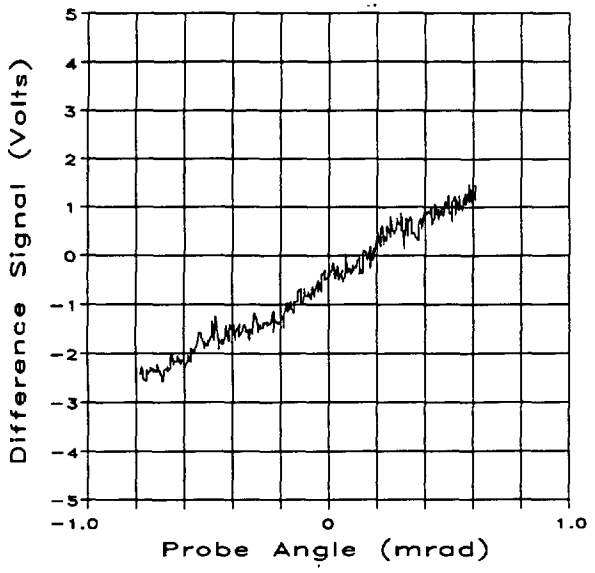

(a) Difference vs Probe Angle

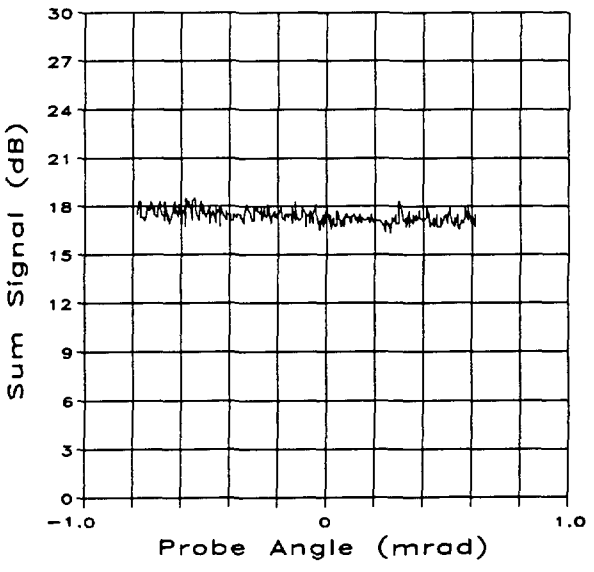

(b) Sum Signal vs Probe Angle

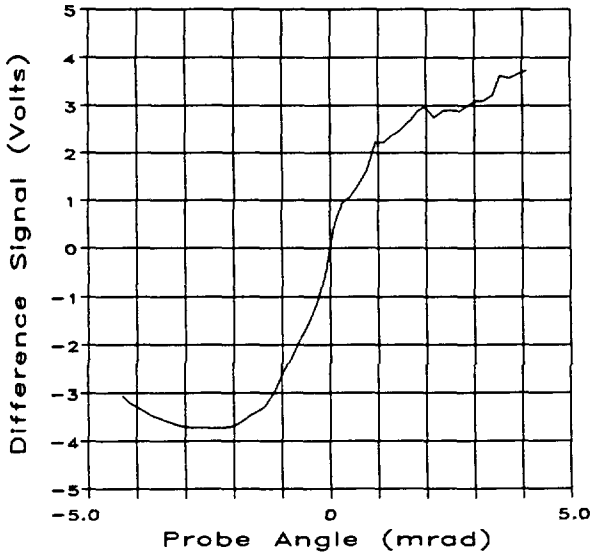

(c) Calibration Diff. vs Probe Angle

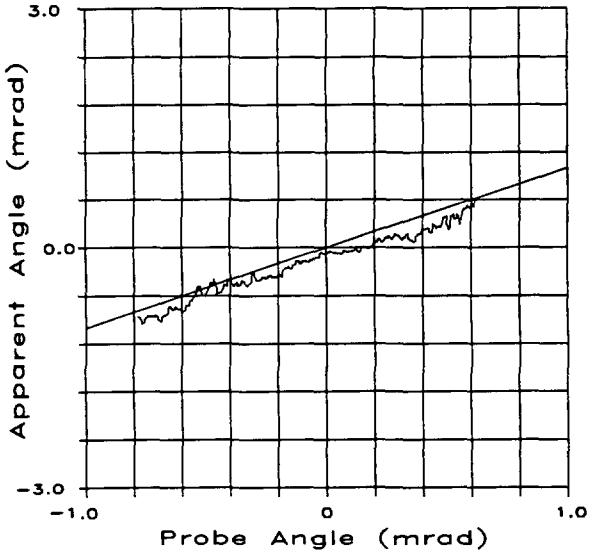

(d) Apparent Angle vs Probe Angle

Figure A-7. Trial 53, 1.8 km.

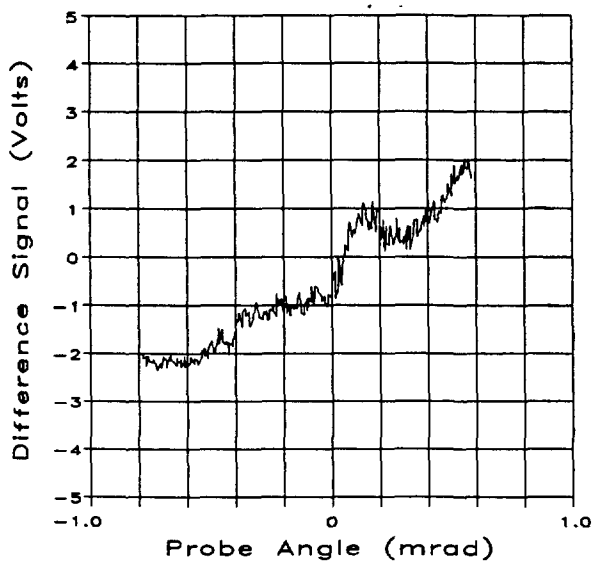

(a) Difference vs Probe Angle

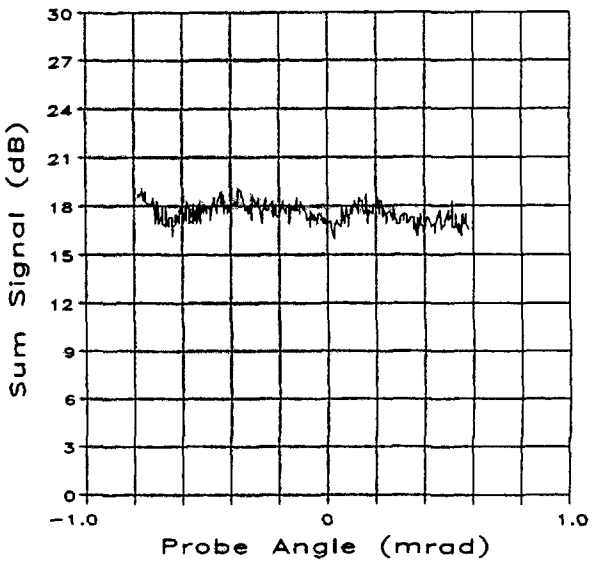

(b) Sum Signal vs Probe Angle

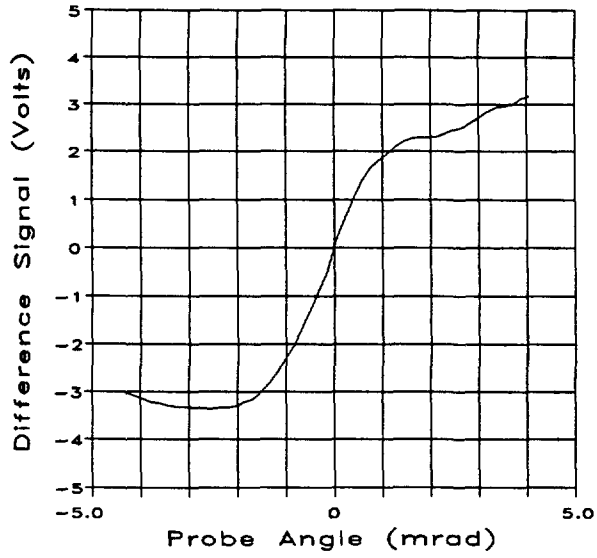

(c) Calibration Diff. vs Probe Angle

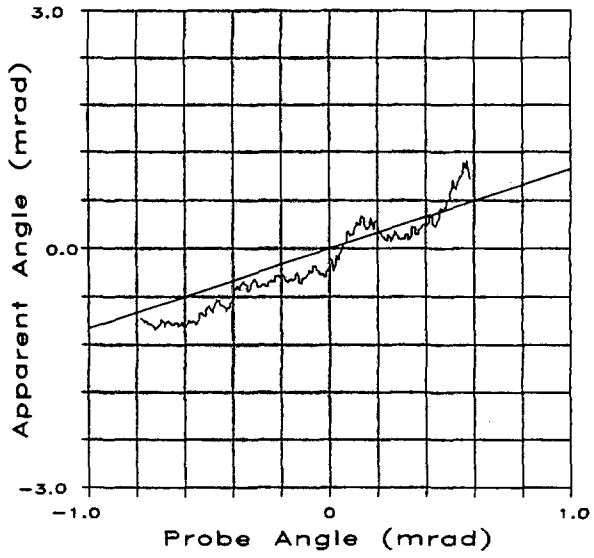

(d) Apparent Angle vs Probe Angle

Figure A-8. Trial 54, 1.8 km.

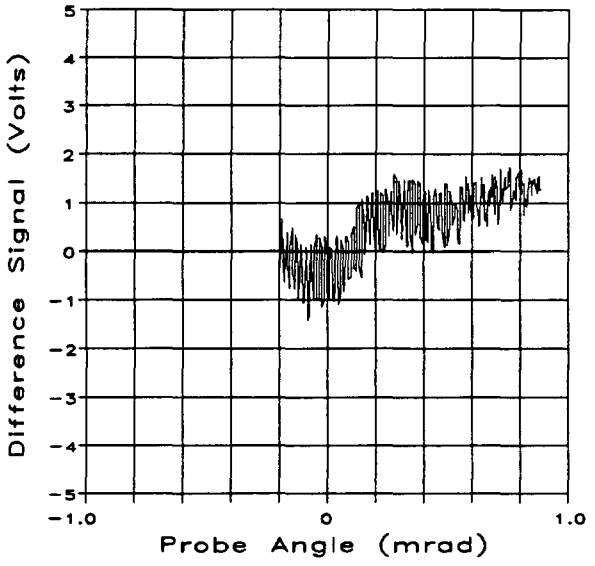

(a) Difference vs Probe Angle

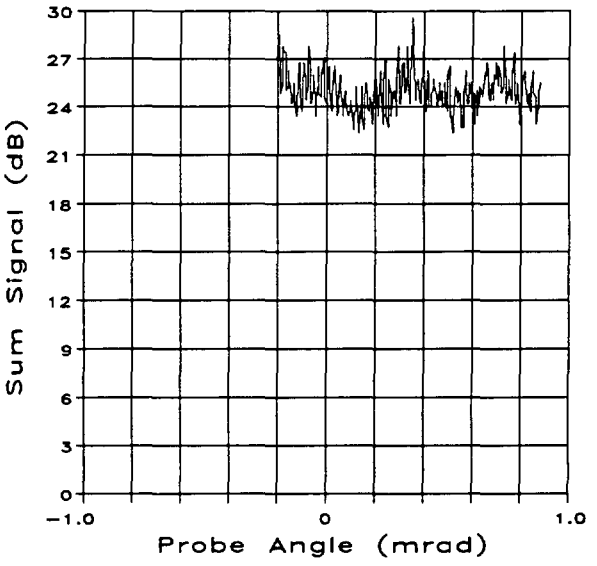

(b) Sum Signal vs Probe Angle

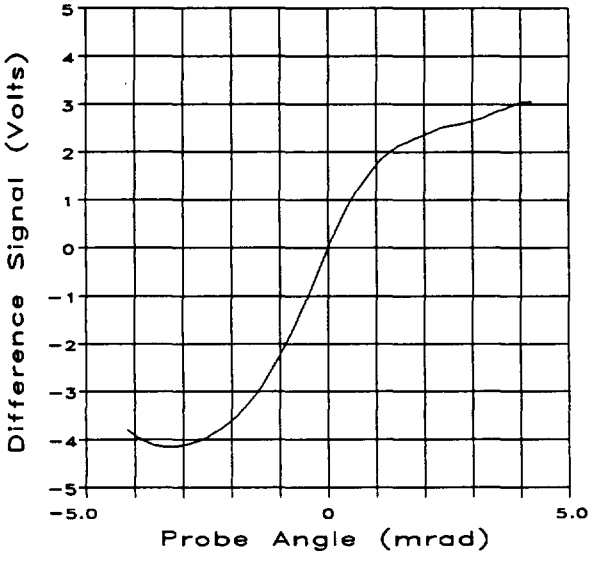

(c) Calibration Diff. vs Probe Angle

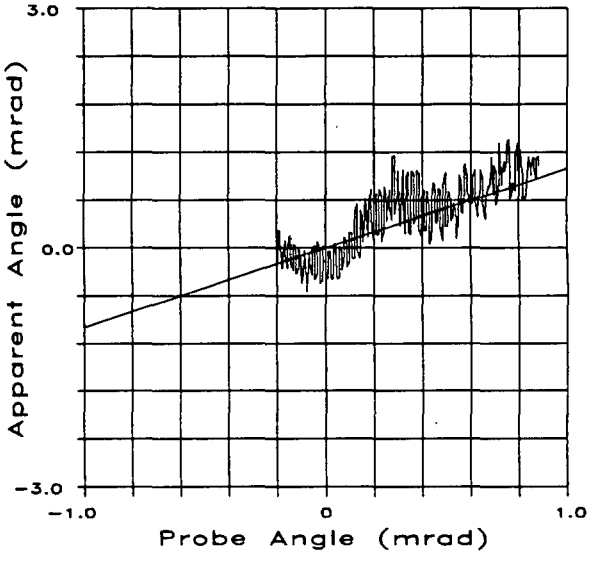

(d) Apparent Angle vs Probe Angle

Figure A-9. Trial 3, 2.8 km.

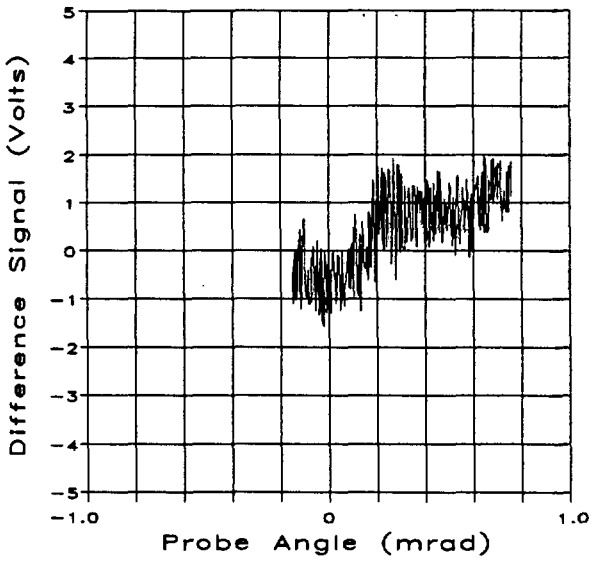

(a) Difference vs Probe Angle

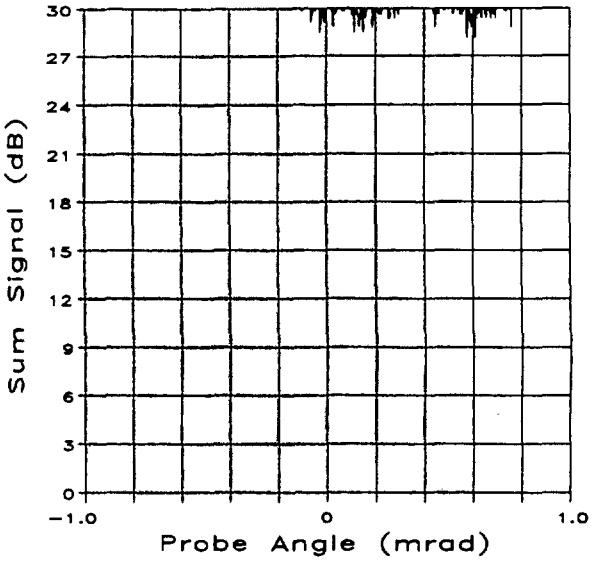

(b) Sum Signal vs Probe Angle

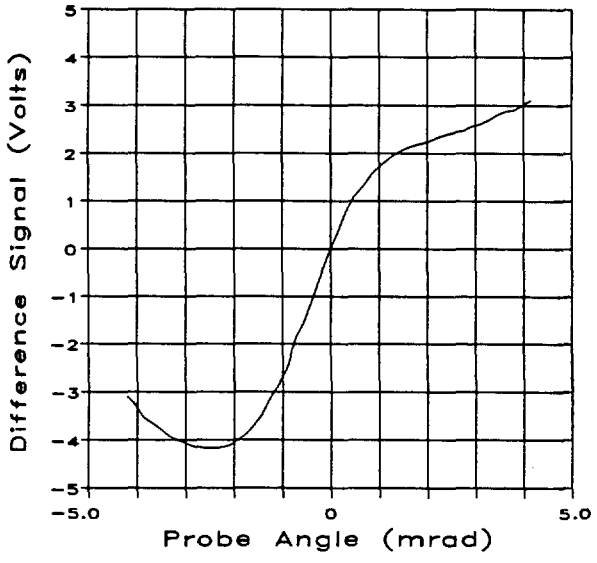

(c) Calibration Diff. vs Probe Angle

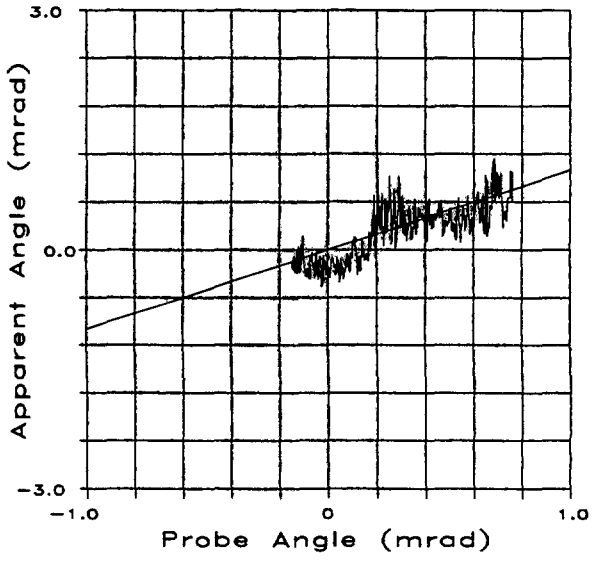

(d) Apparent Angle vs Probe Angle

Figure A-10. Trial 6, 2.8 km.

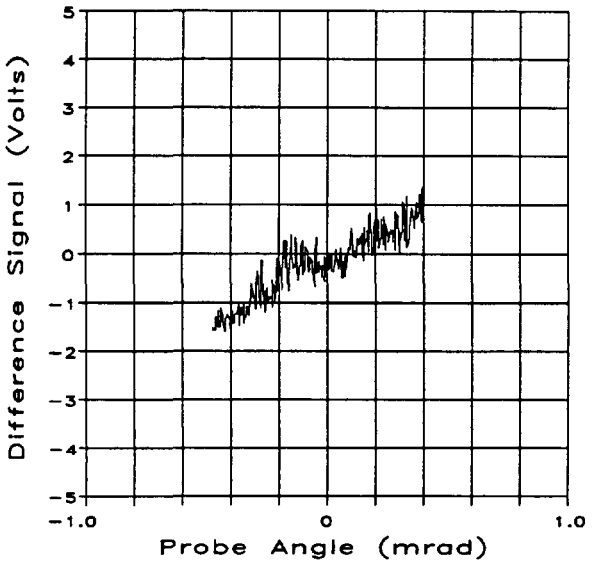

(a) Difference vs Probe Angle

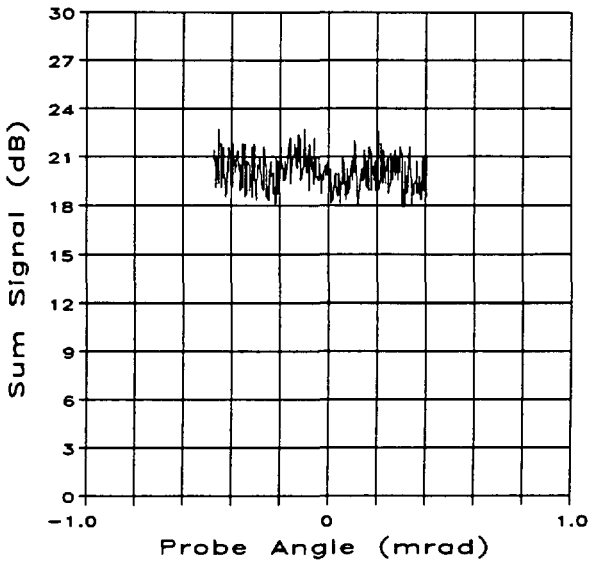

(b) Sum Signal vs Probe Angle

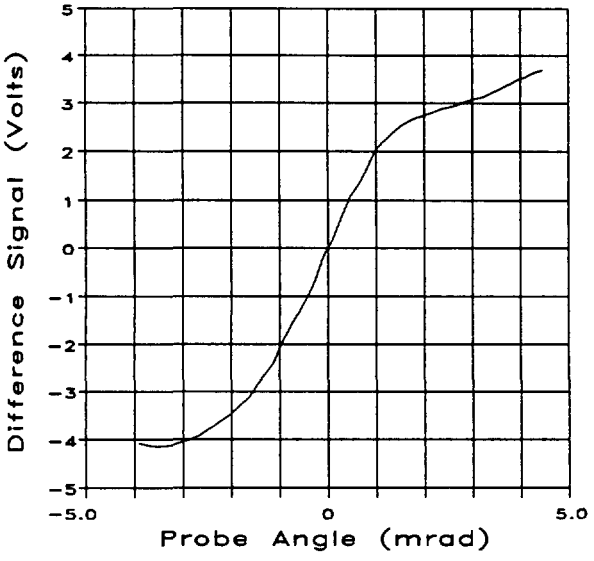

(c) Calibration Diff. vs Probe Angle

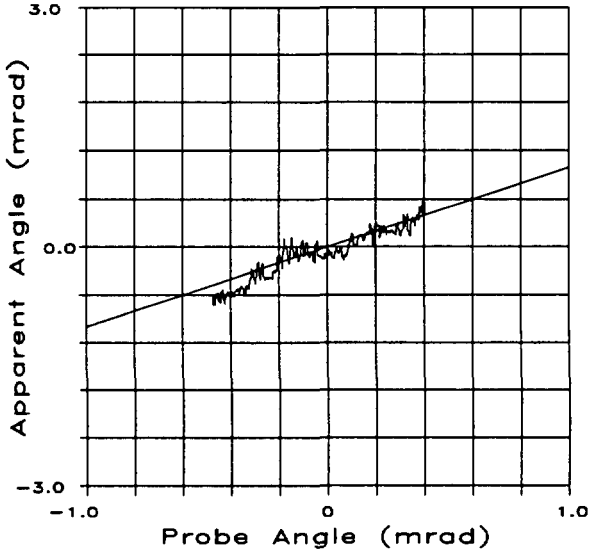

(d) Apparent Angle vs Probe Angle

Figure A-11. Trial 32, 2.8 km.

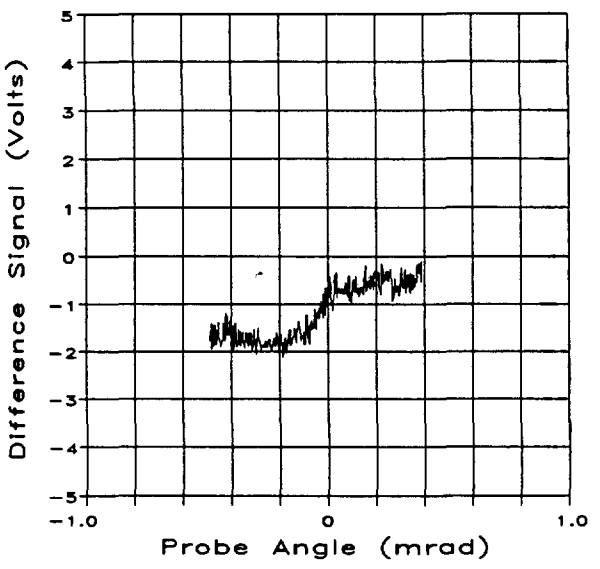

(a) Difference vs Probe Angle

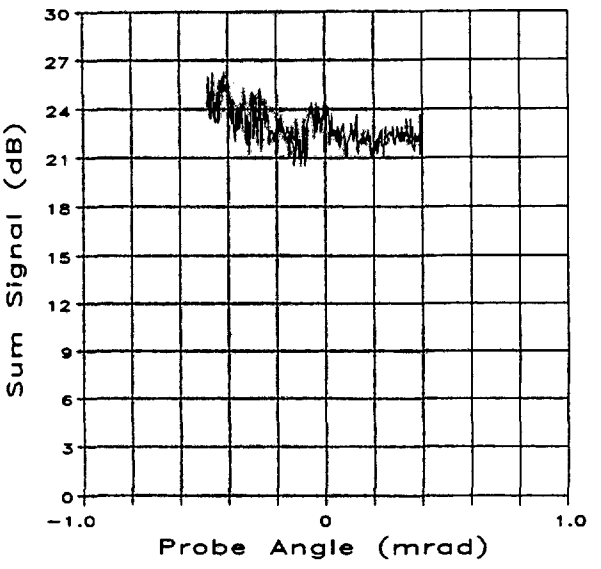

(b) Sum Signal vs Probe Angle

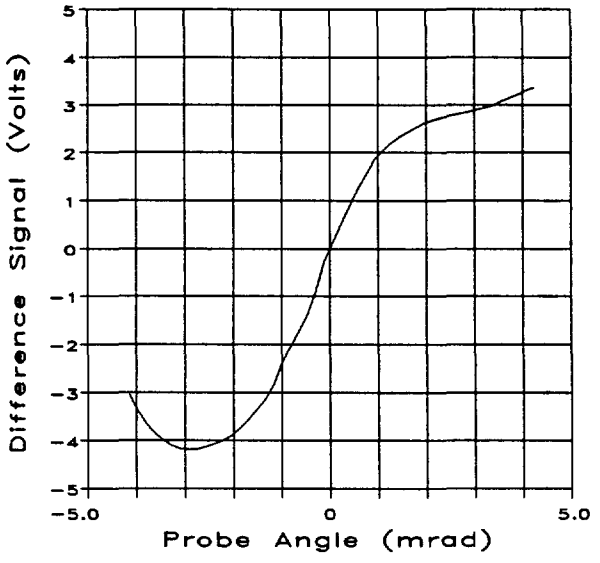

(c) Calibration Diff. vs Probe Angle

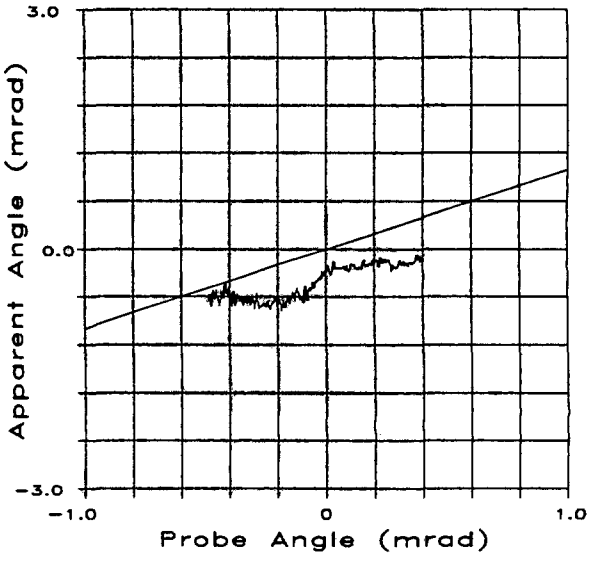

(d) Apparent Angle vs Probe Angle

Figure A-12. Trial 36, 2.8 km.

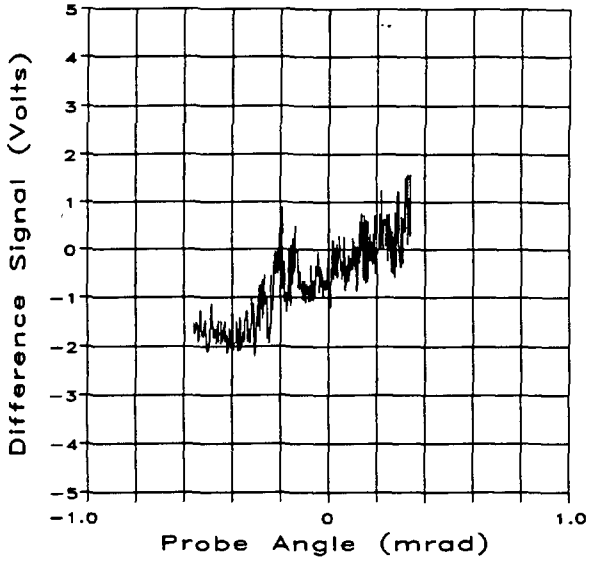

(a) Difference vs Probe Angle

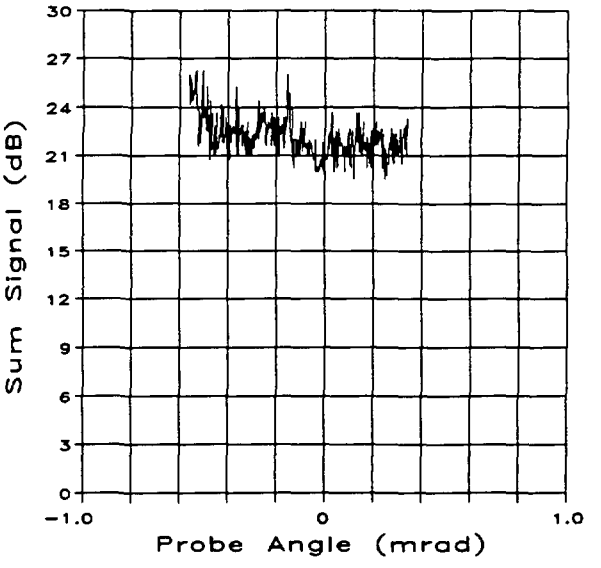

(b) Sum Signal vs Probe Angle

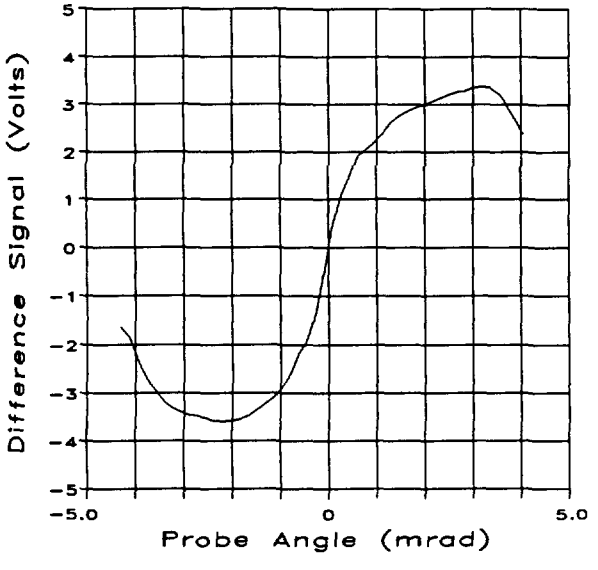

(c) Calibration Diff. vs Probe Angle

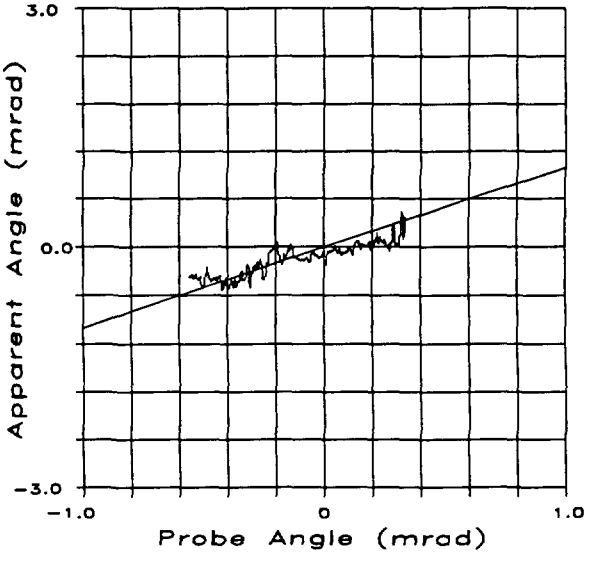

(d) Apparent Angle vs Probe Angle

Figure A-13. Trial 44, 2.8 km.

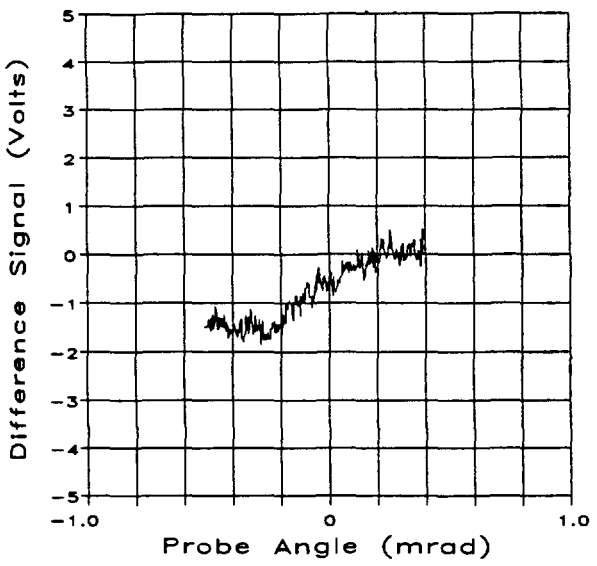

(a) Difference vs Probe Angle

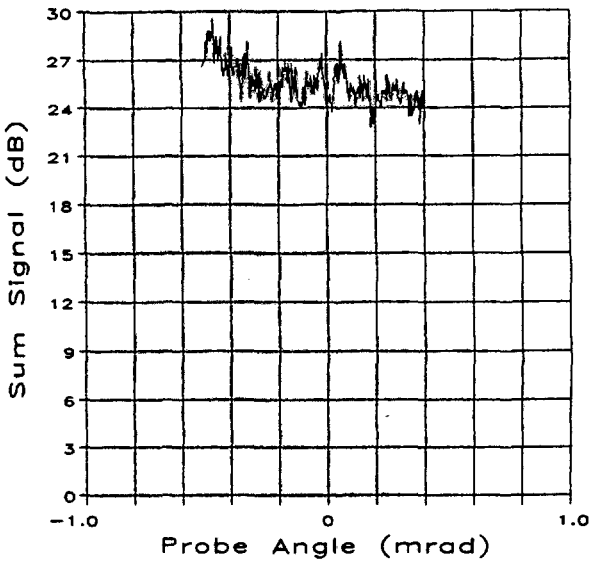

(b) Sum Signal vs Probe Angle

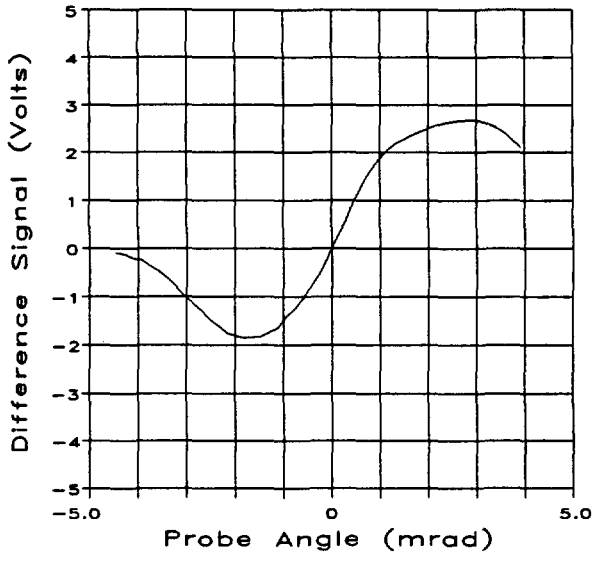

(c) Calibration Diff. vs Probe Angle

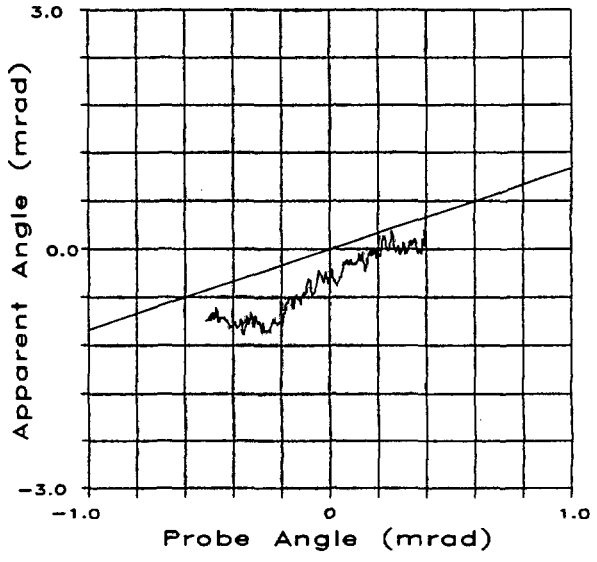

(d) Apparent Angle vs Probe Angle

Figure A-14. Trial 47, 2.8 km.

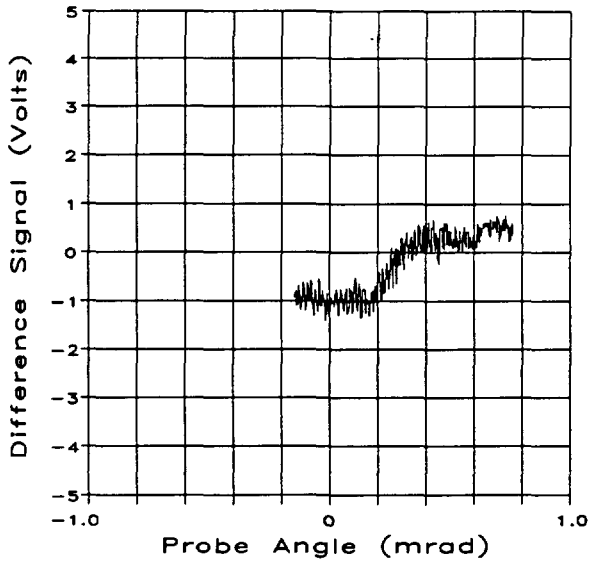

(a) Difference vs Probe Angle

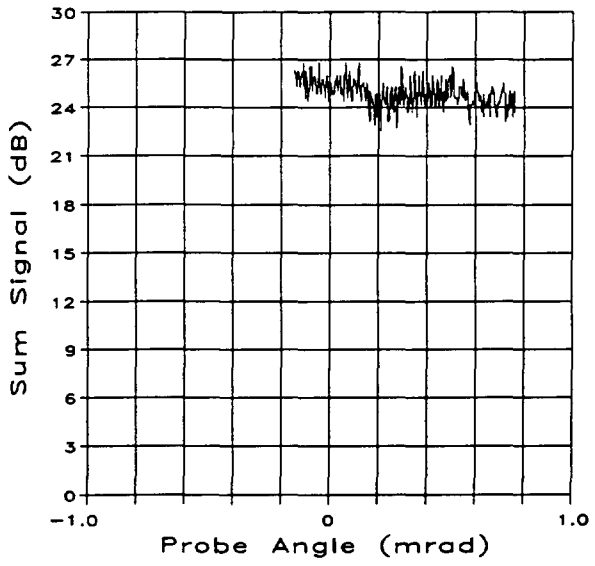

(b) Sum Signal vs Probe Angle

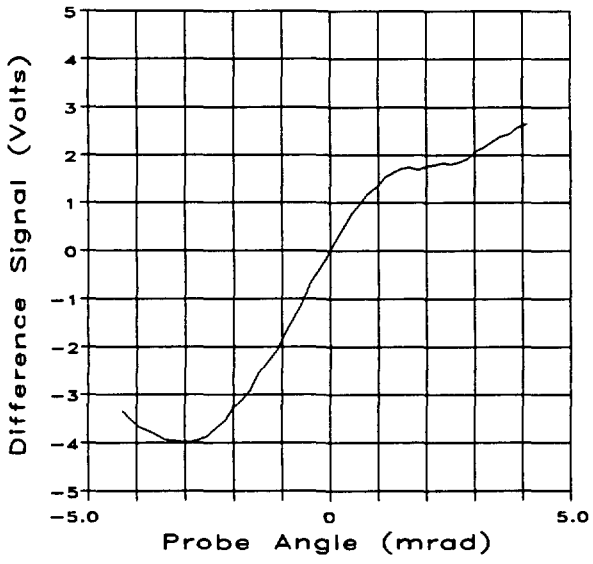

(c) Calibration Diff. vs Probe Angle

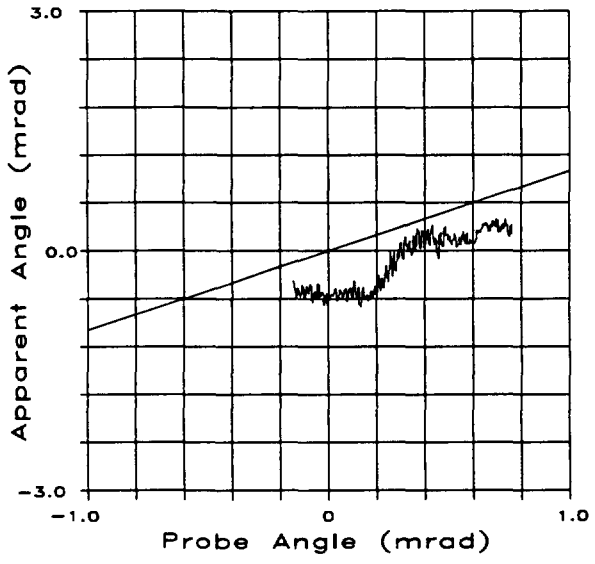

(d) Apparent Angle vs Probe Angle

Figure A-15. Trial 11, 2.8 km.

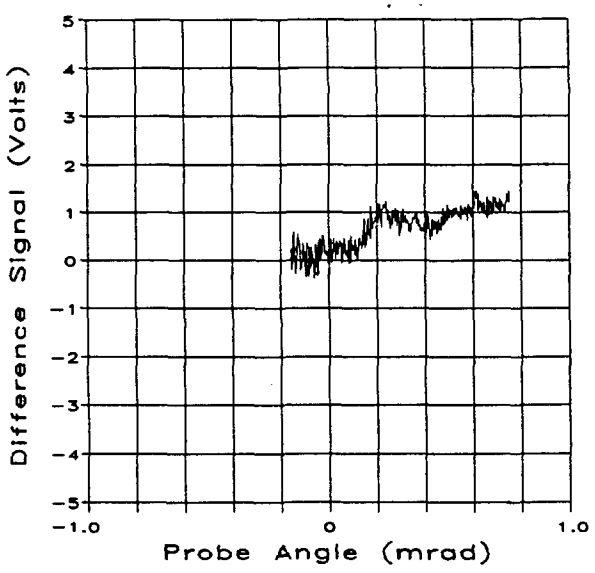

(a) Difference vs Probe Angle

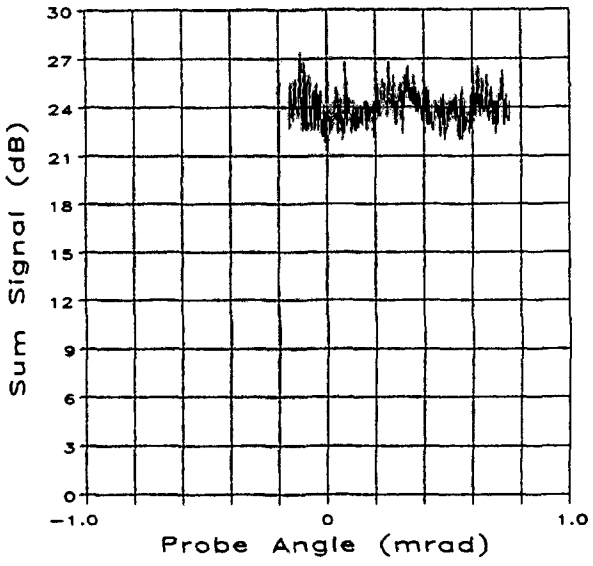

(b) Sum Signal vs Probe Angle

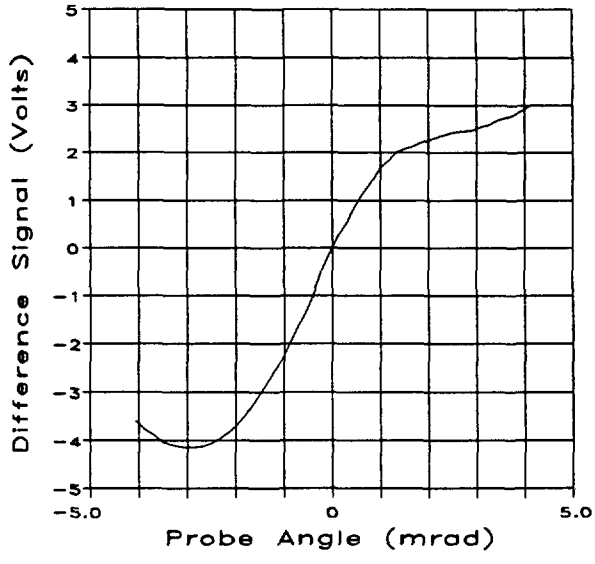

(c) Calibration Diff. vs Probe Angle

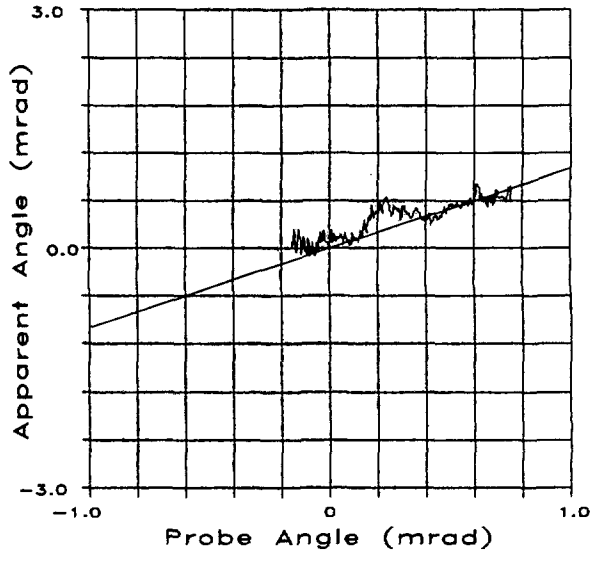

(d) Apparent Angle vs Probe Angle

Figure A-16. Trial 14, 2.8 km.

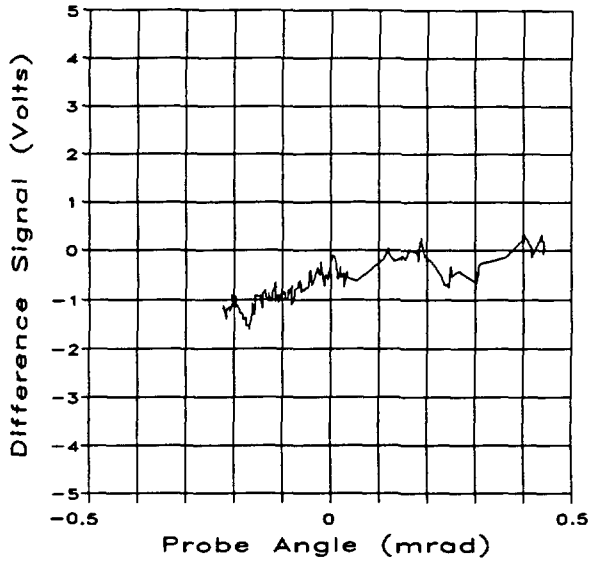

(a) Difference vs Probe Angle

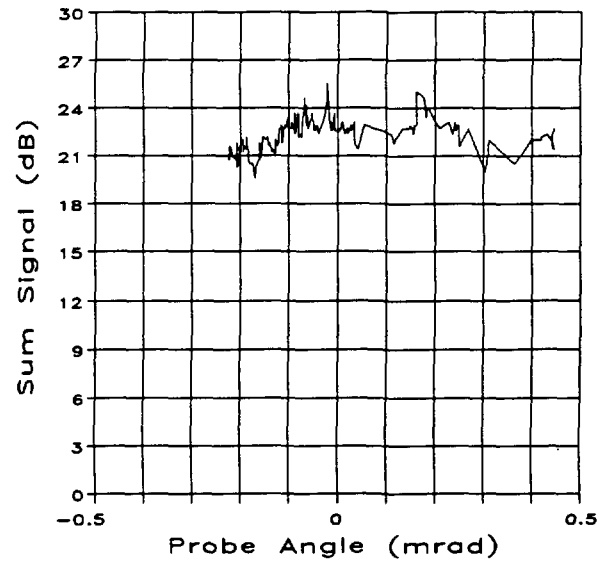

(b) Sum Signal vs Probe Angle

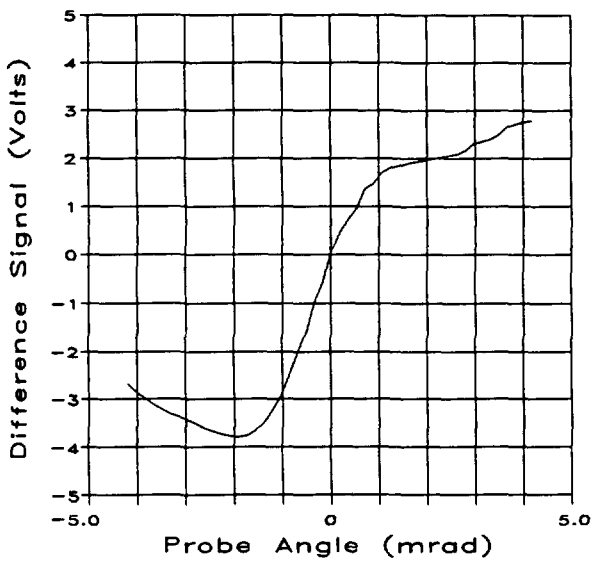

(c) Calibration Diff. vs Probe Angle

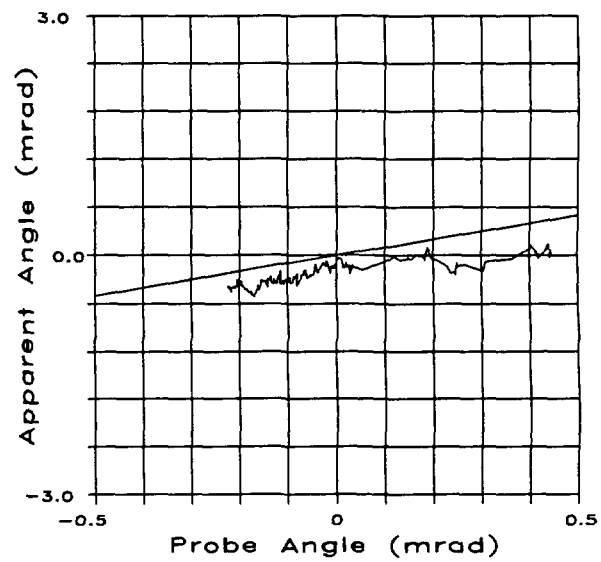

(d) Apparent Angle vs Probe Angle

Figure A-17. Trial 39, 3.8 km.

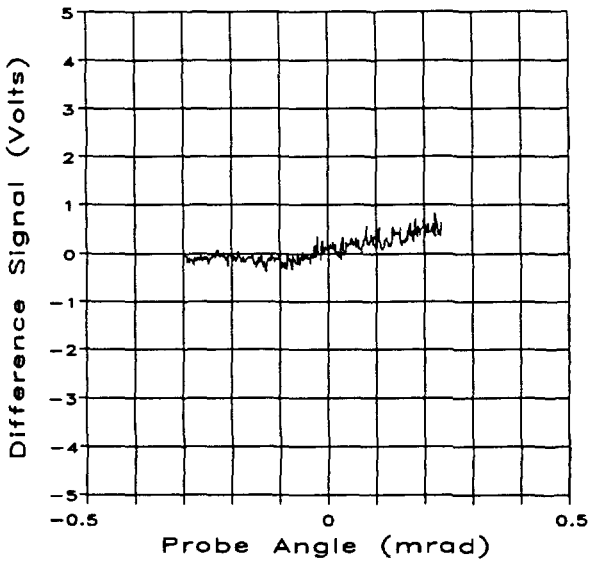

(a) Difference vs Probe Angle

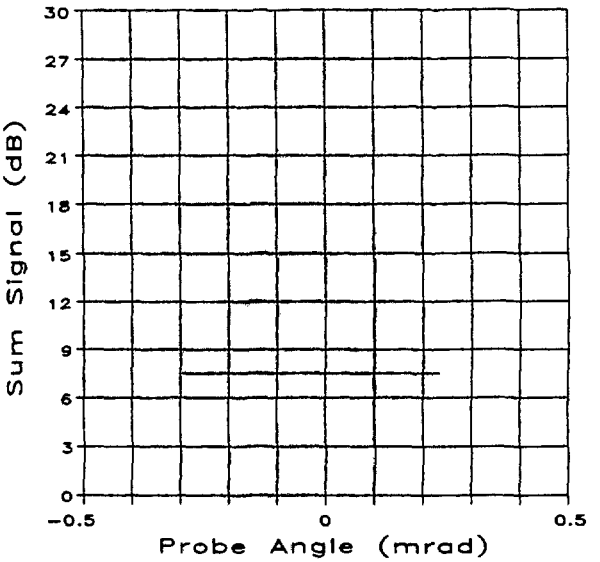

(b) Sum Signal vs Probe Angle

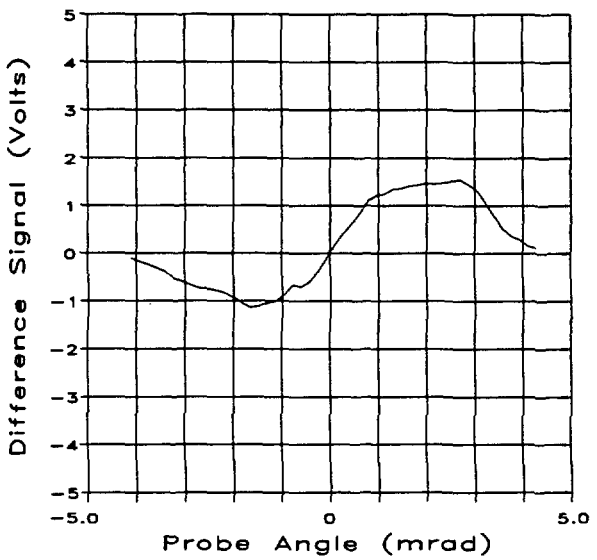

(c) Calibration Diff. vs Probe Angle

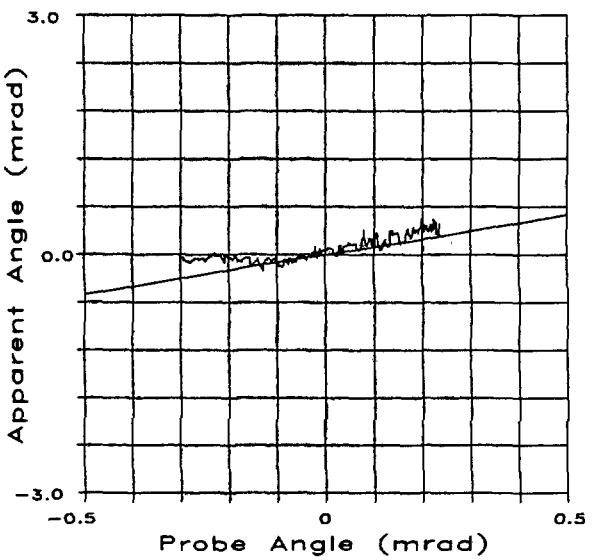

(d) Apparent Angle vs Probe Angle

Figure A-18. Trial 42, 4.8 km.

APPENDIX B:

NOISE MEASUREMENTS

INTENTIONALLY LEFT BLANK.

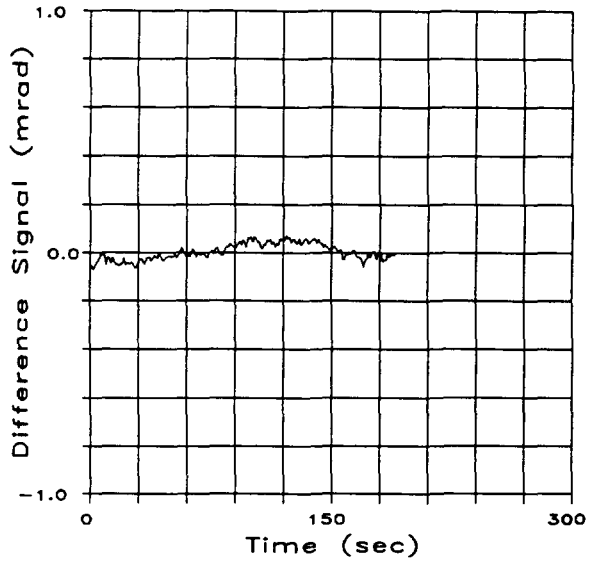

TR5, 11Sep91, 0850 hours

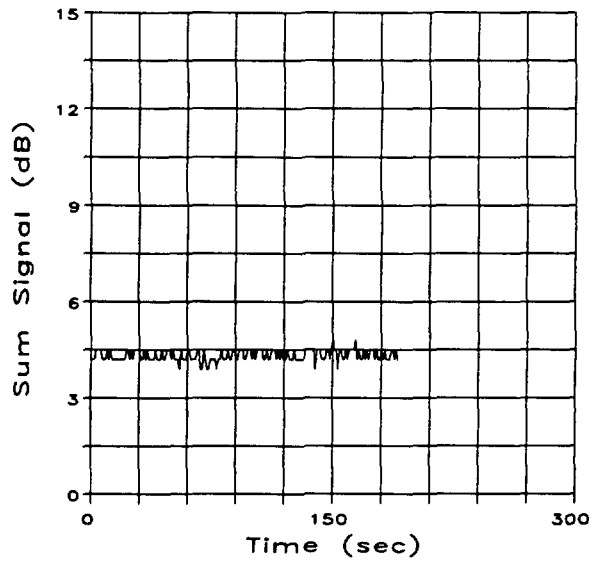

TR5, 11Sep91, 0850 hours

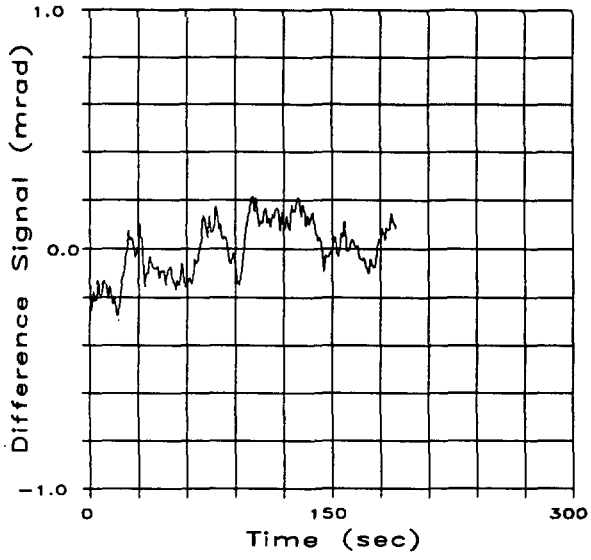

TR4, 11Sep91, 0830 hours

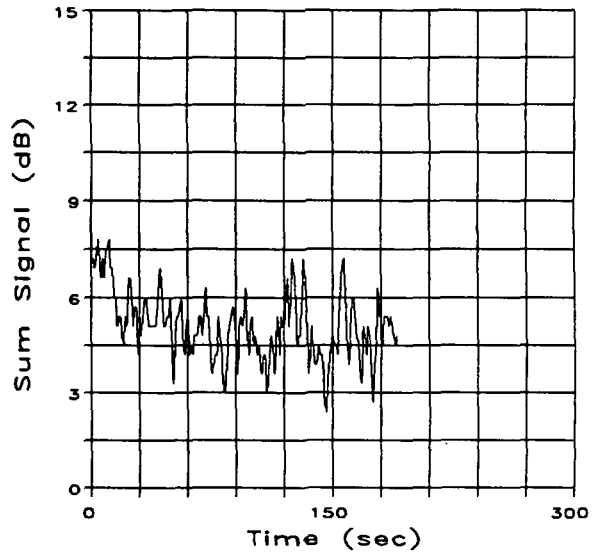

TR4, 11Sep91, 0830 hours

Figure B-1. Noise measurement at 0.4 km and 3 km, Trials 5 and 4.

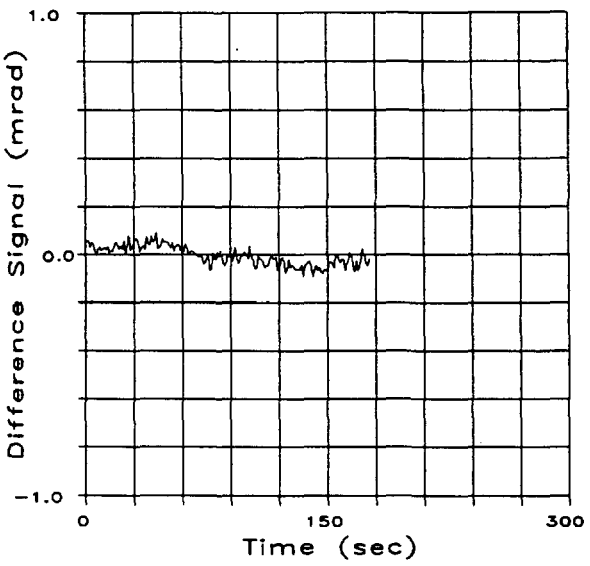

TR8, 11Sep91, 1445 hours

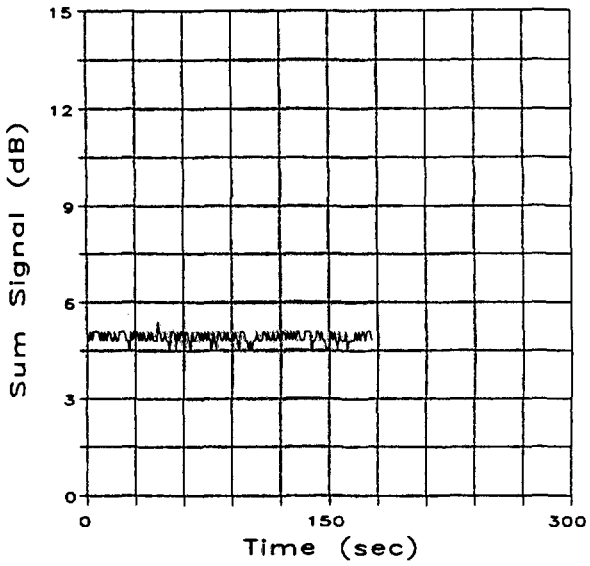

TR8, 11Sep91, 1445 hours

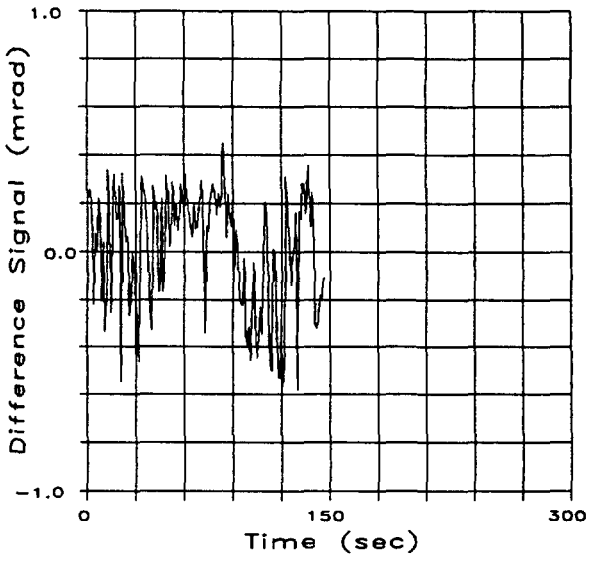

TR7, 11Sep91, 1400 hours

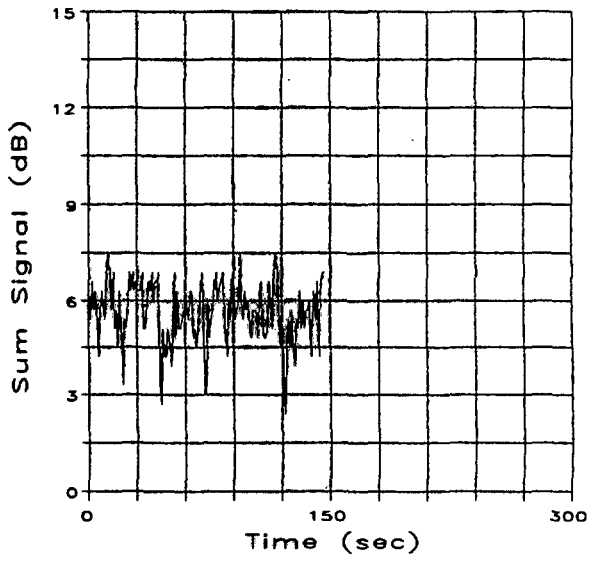

TR7, 11Sep91, 1400 hours

Figure B-2. Noise measurement at 0.4 km and 3 km, Trials 8 and 7.

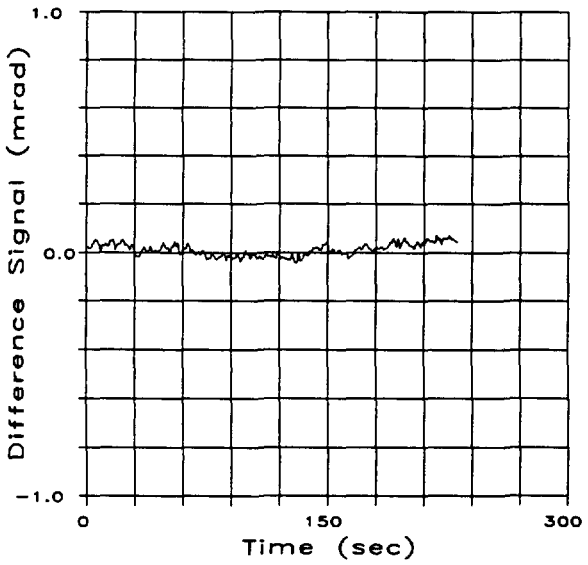

TR9, 12Sep91, 0817 hours

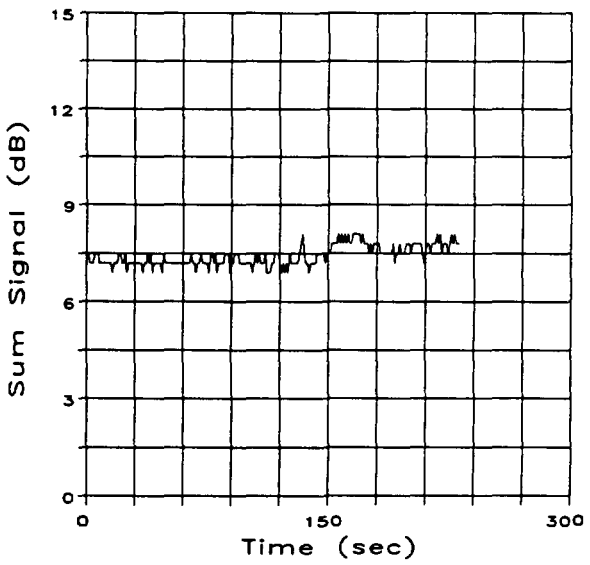

TR9, 12Sep91, 0817 hours

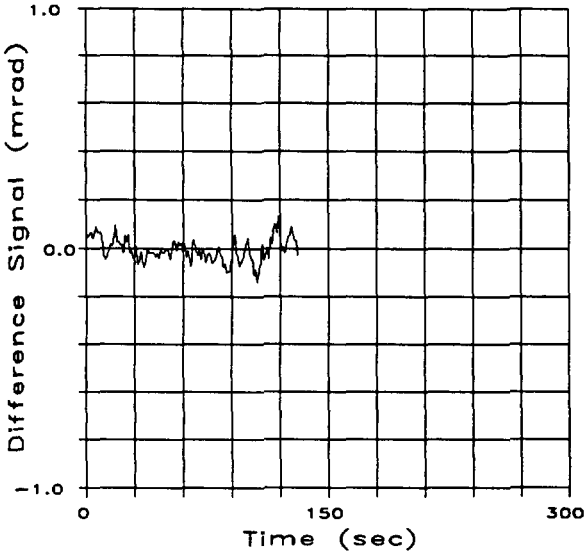

TR10, 12Sep91, 0830 hours

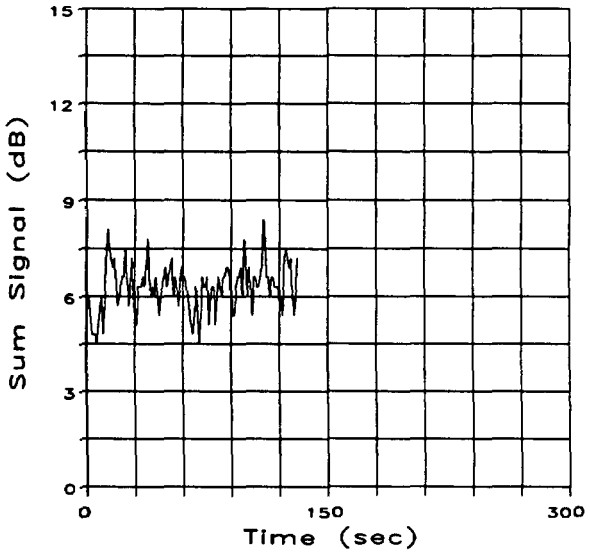

TR10, 12Sep91, 0830 hours

Figure B-3. Noise measurement at 0.4 km and 3 km, Trials 9 and 10.

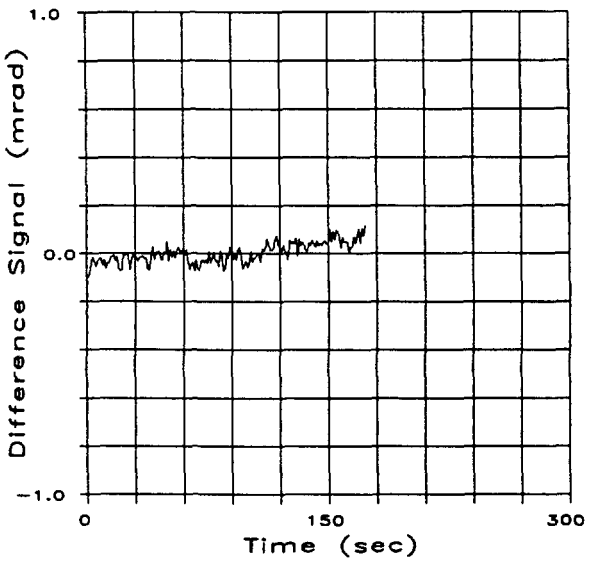

TR12, 12Sep91, 1207 hours

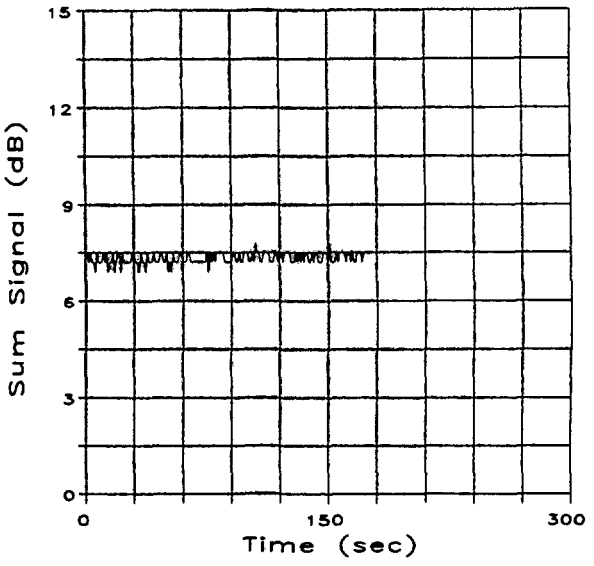

TR12, 12Sep91, 1207 hours

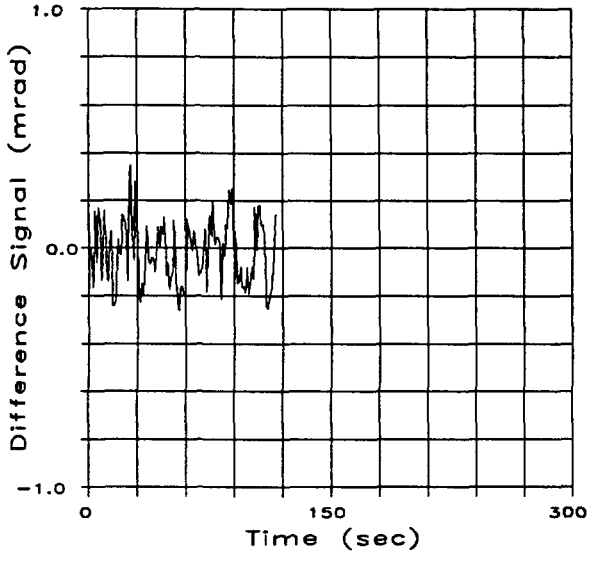

TR13, 12Sep91, 1220 hours

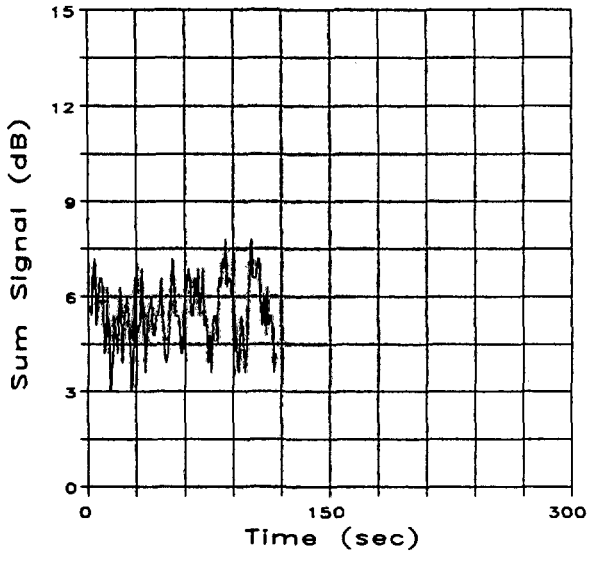

TR13, 12Sep91, 1220 hours

Figure B-4. Noise measurement at 0.4 km and 3 km, Trials 12 and 13.

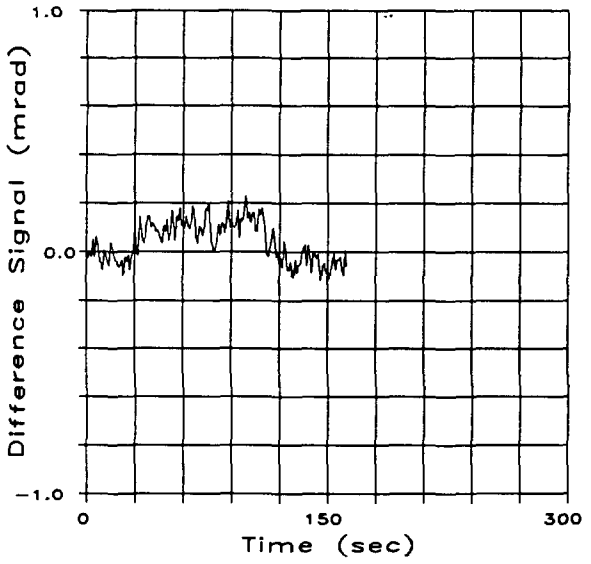

TR15, 12Sep91, 1425 hours

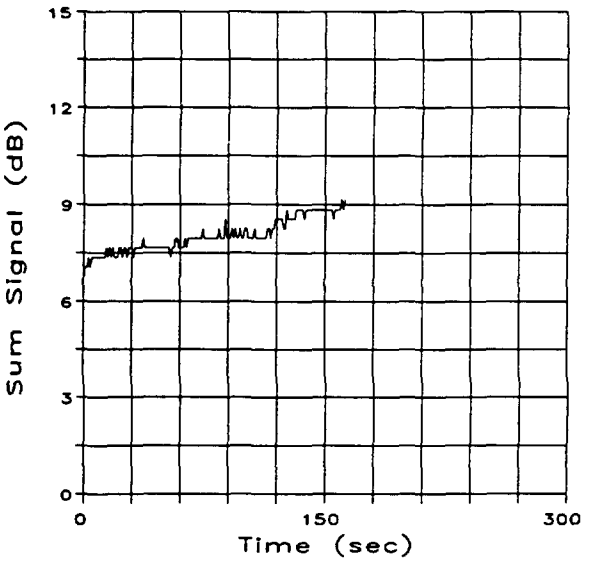

TR15, 12Sep91, 1425 hours

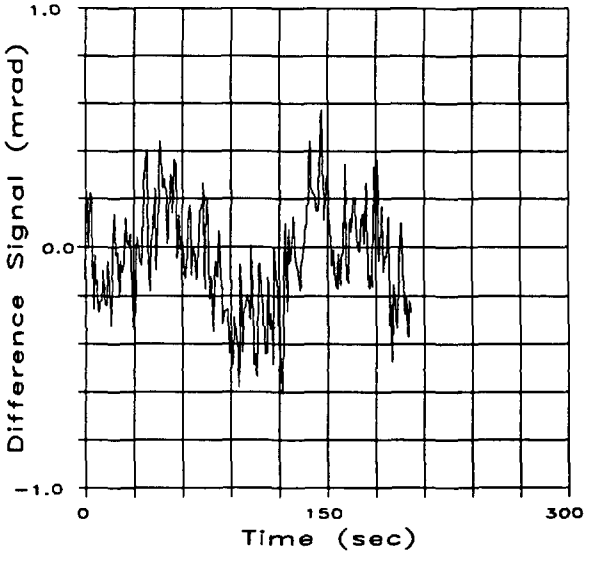

TR16, 12Sep91, 1430 hours

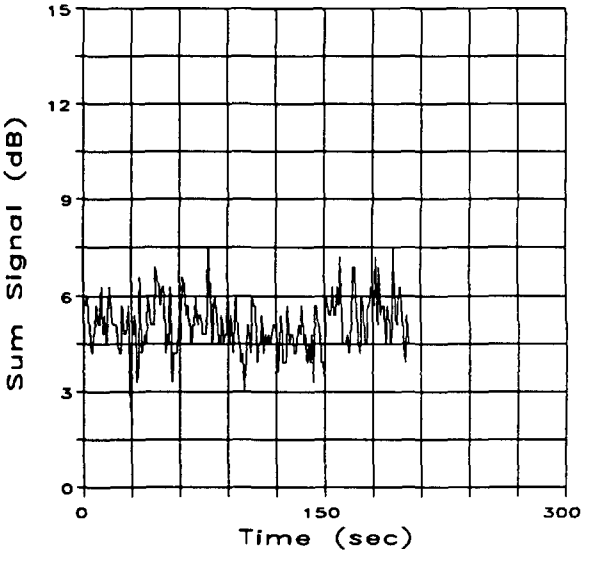

TR16, 12Sep91, 1430 hours

Figure B-5. Noise measurement at 0.4 km and 2 km, Trials 15 and 16.

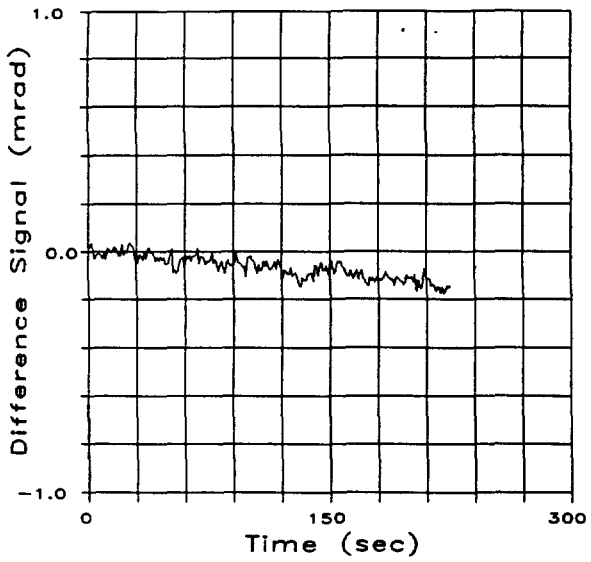

TR18, 13Sep91, 0828 hours

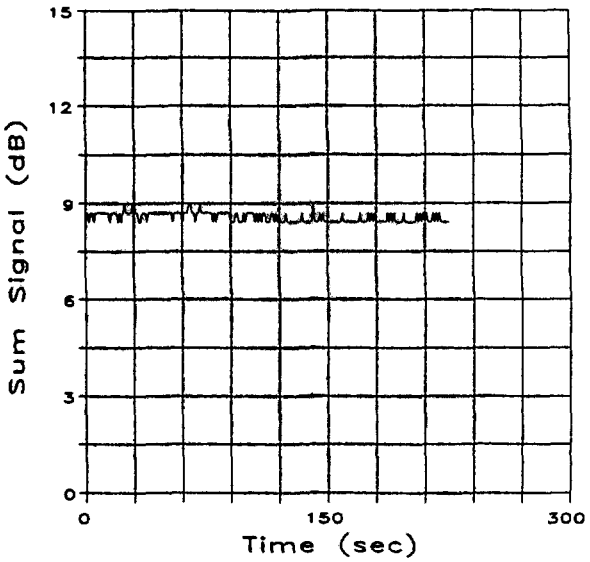

TR18, 13Sep91, 0828 hours

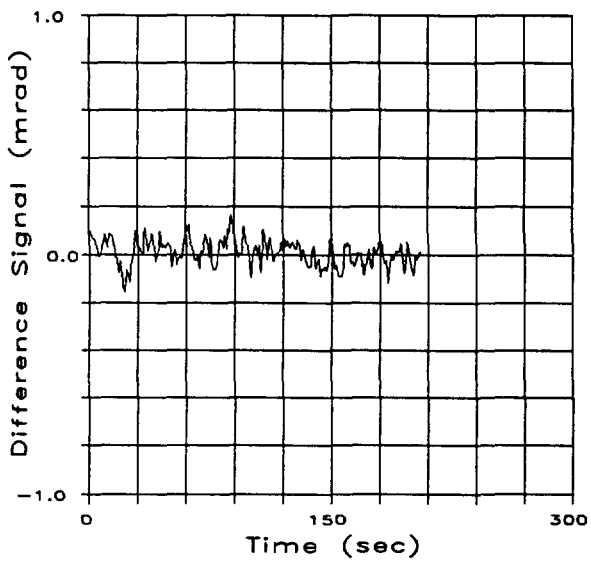

TR19, 13Sep91, 0840 hours

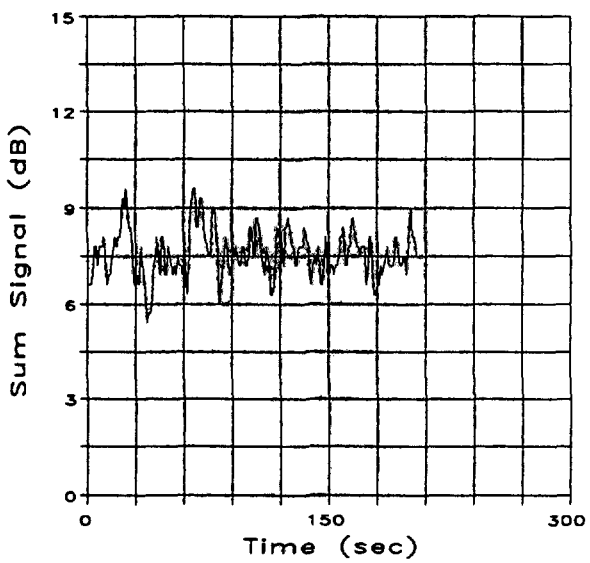

TR19, 13Sep91, 0840 hours

Figure B-6. Noise measurement at 0.4 km and 2 km, Trials 18 and 19.

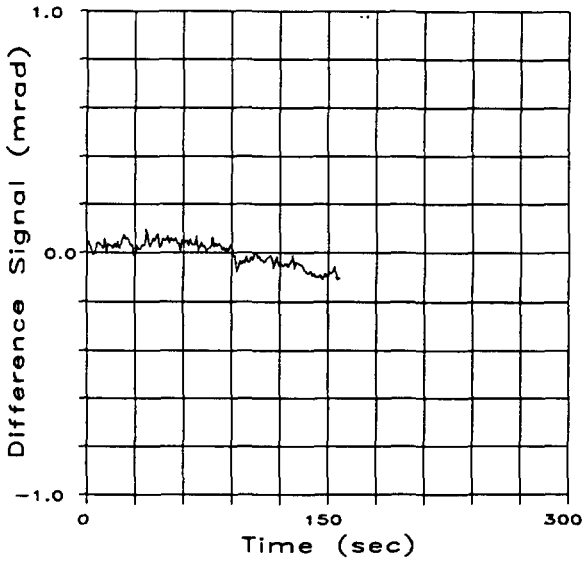

TR22, 13Sep91, 1054 hours

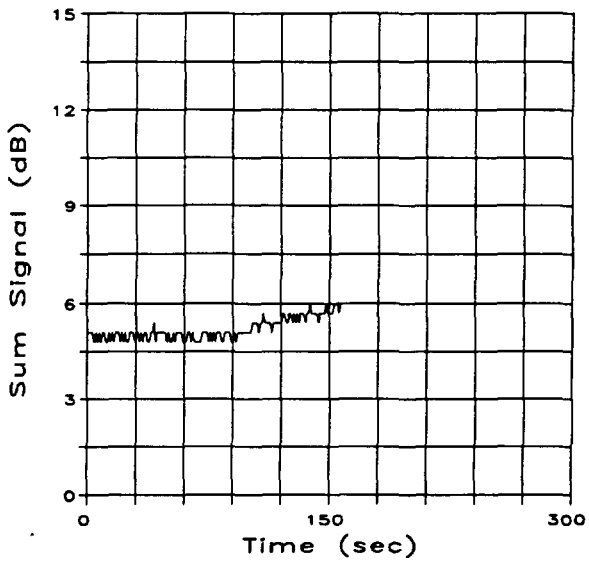

TR22, 13Sep91, 1054 hours

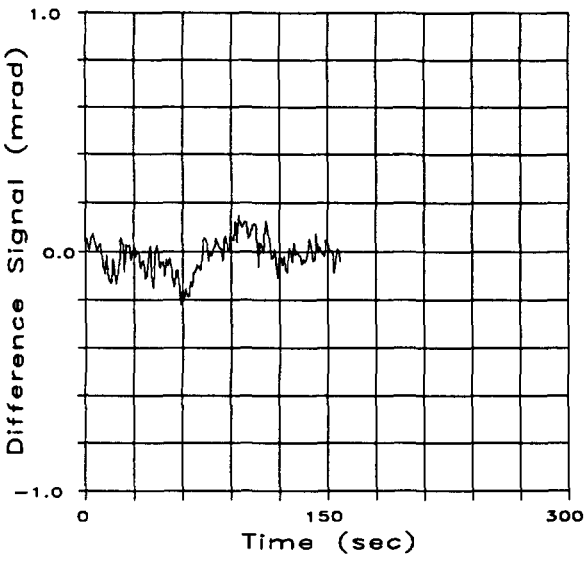

TR23, 13Sep91, 1110 hours

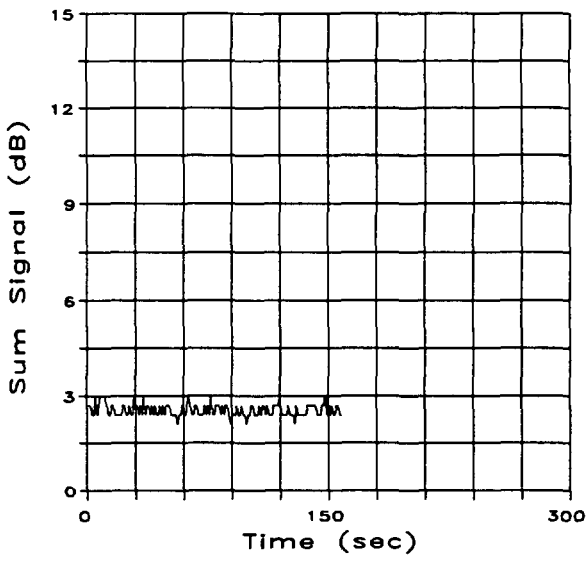

TR23, 13Sep91, 1110 hours

Figure B-7. Noise measurement at 0.4 km and 1 km, Trials 22 and 23.

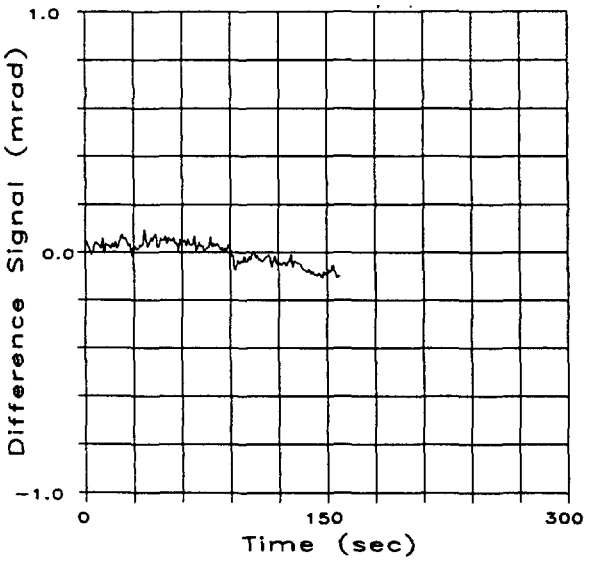

TR22, 13Sep91, 1054 hours

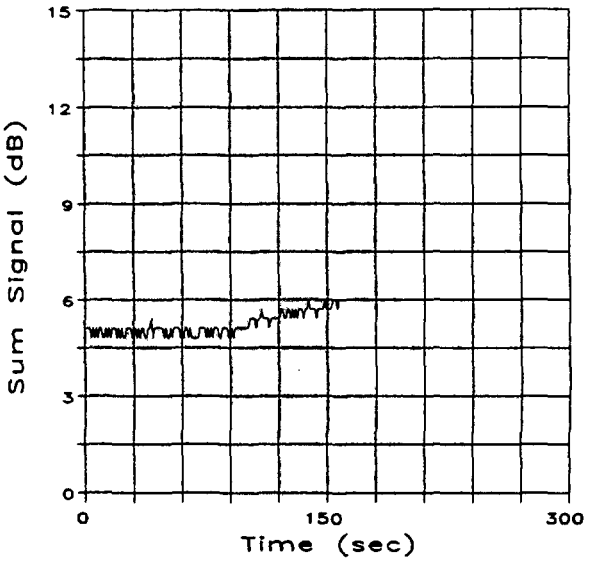

TR22, 13Sep91, 1054 hours

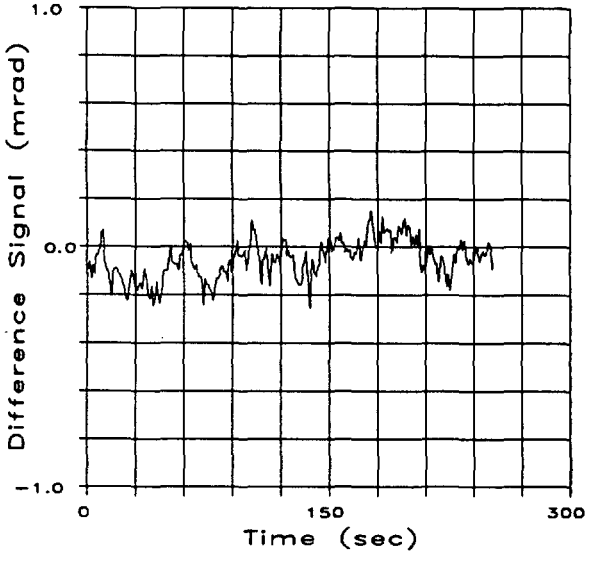

TR26, 13Sep91, 1505 hours

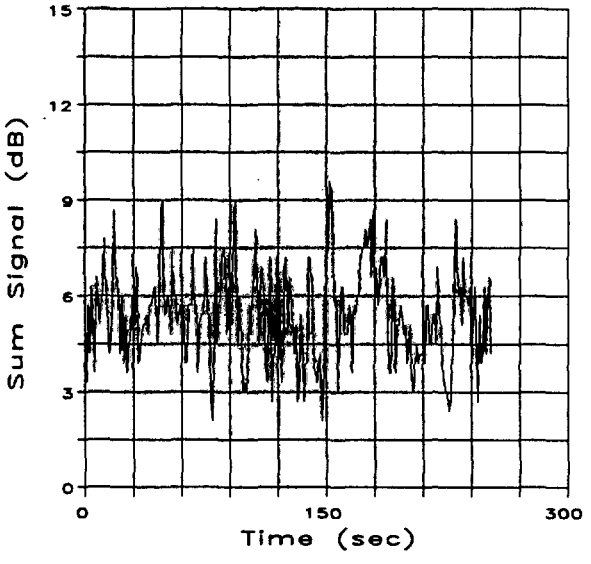

TR26, 13Sep91, 1505 hours

Figure B-8. Noise measurement at 0.4 km and 5 km, Trials 22 and 26.

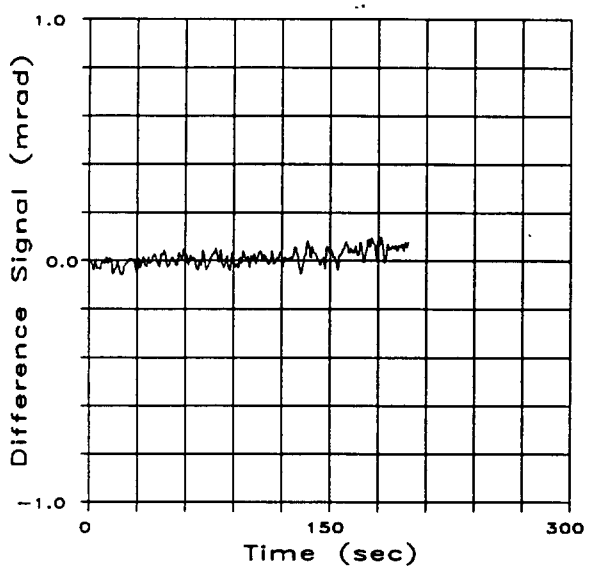

TR27, 16Sep91, 1129 hours

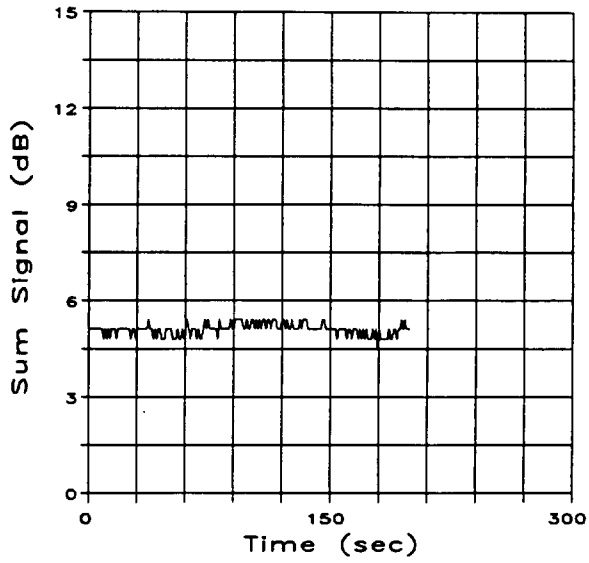

TR27, 16Sep91, 1129 hours

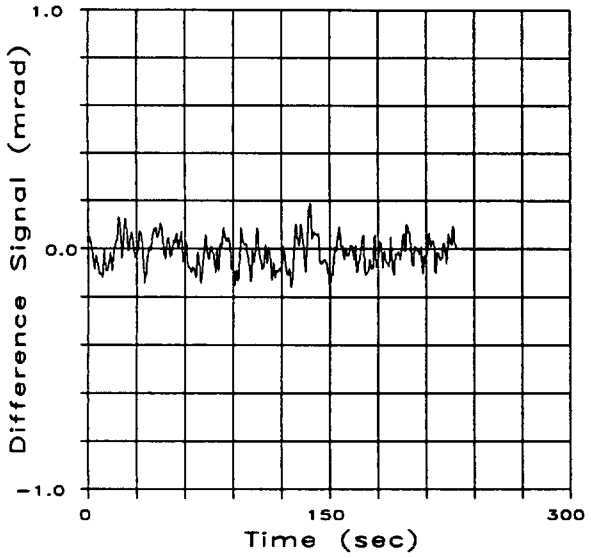

TR28, 16Sep91, 1142 hours

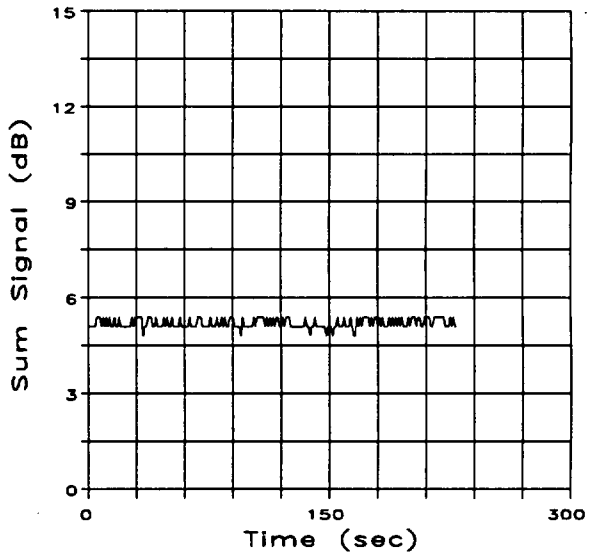

TR28, 16Sep91, 1142 hours

Figure B-9. Noise measurement at 0.4 km and 1 km, Trials 27 and 28.

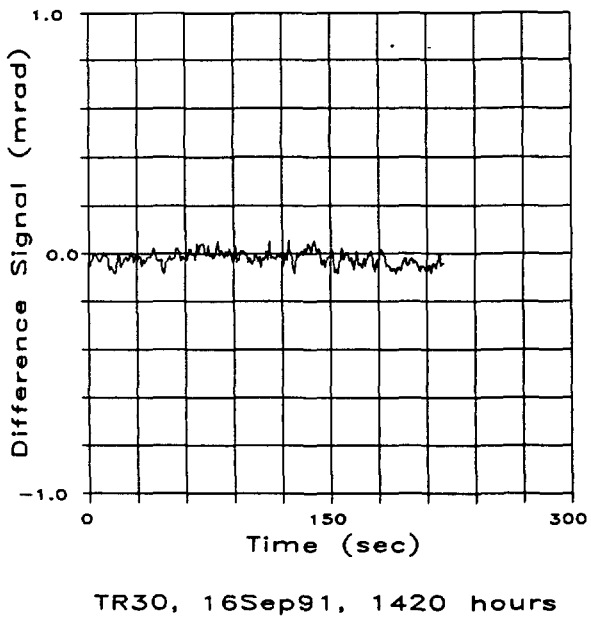

TR30, 16Sep91, 1420 hours

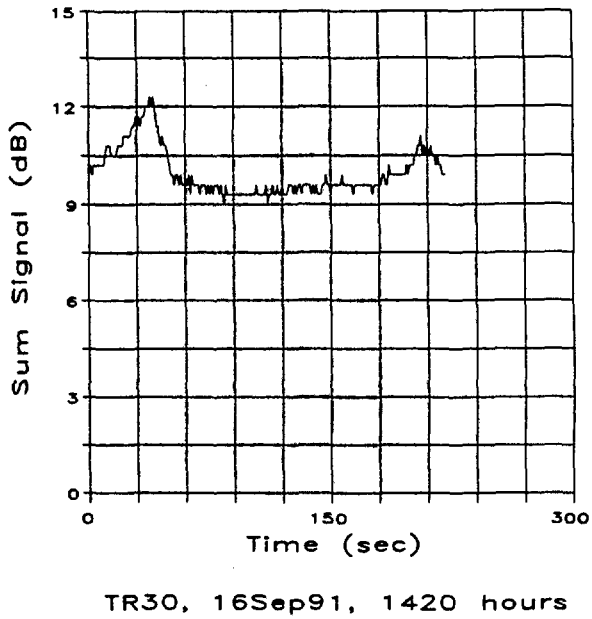

TR30, 16Sep91, 1420 hours

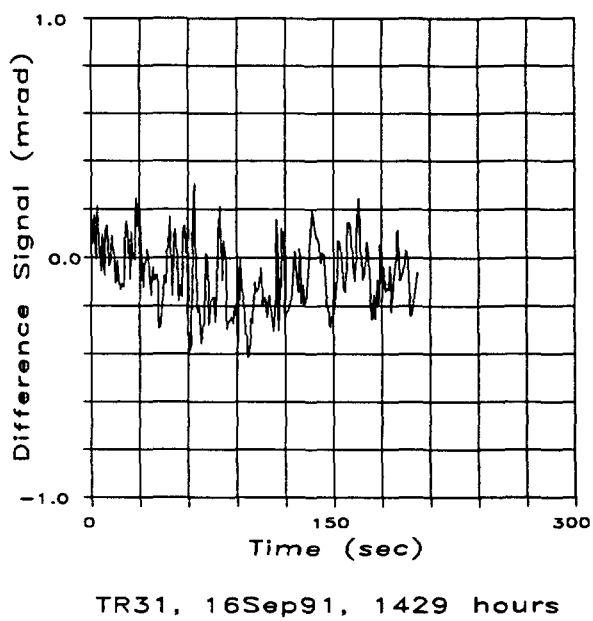

TR31, 16Sep91, 1429 hours

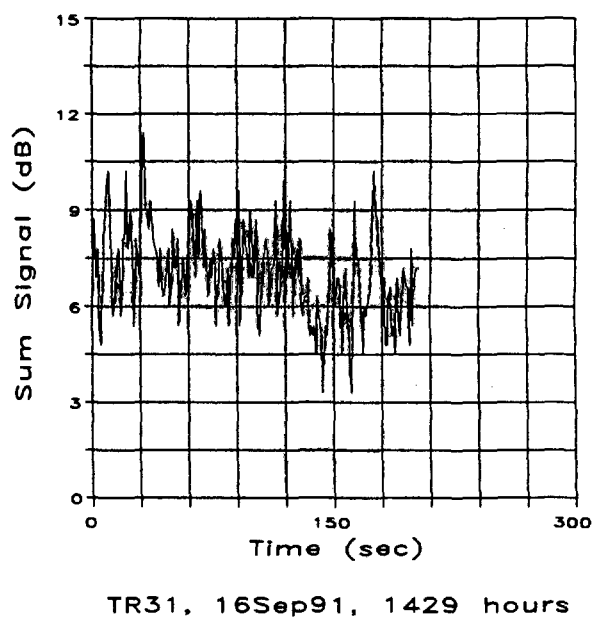

TR31, 16Sep91, 1429 hours

Figure B-10. Noise measurement at 0.4 km and 3 km, Trials 30 and 31.

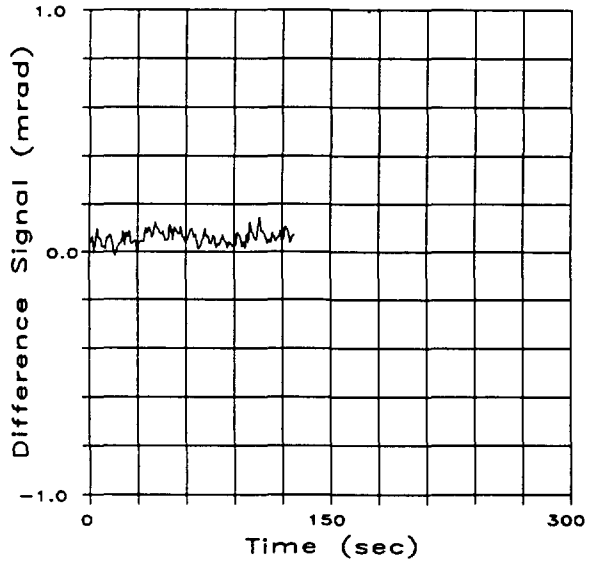

TR34, 17Sep91, 0843 hours

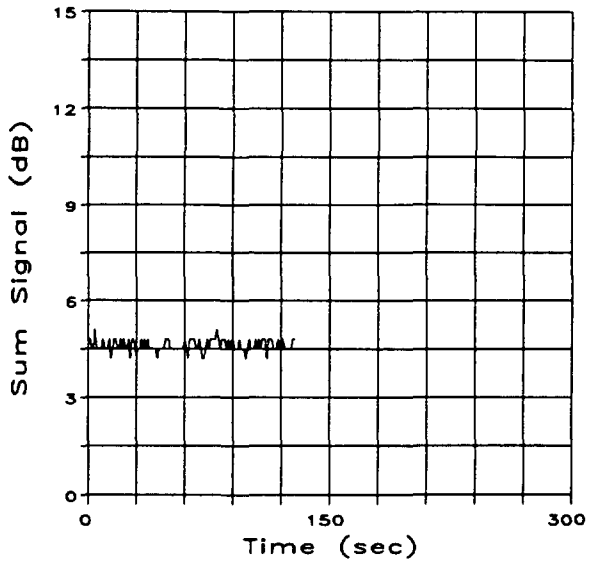

TR34, 17Sep91, 0843 hours

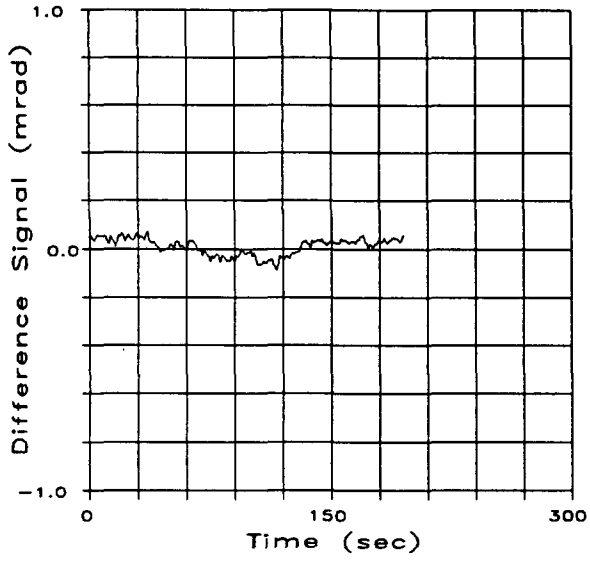

TR33, 17Sep91, 0710 hours

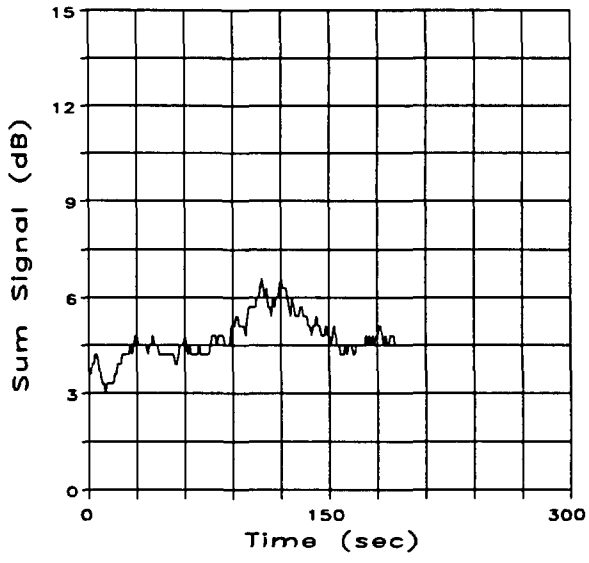

TR33, 17Sep91, 0710 hours

Figure B-11. Noise measurement at 0.4 km and 3 km, Trials 34 and 33.

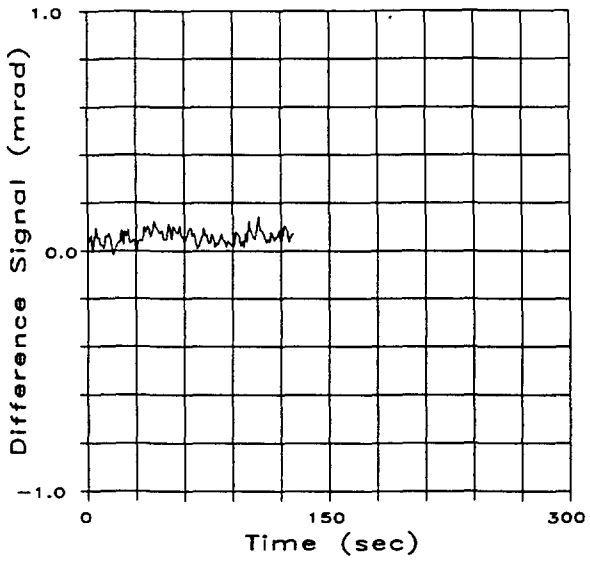

TR34, 17Sep91, 0843 hours

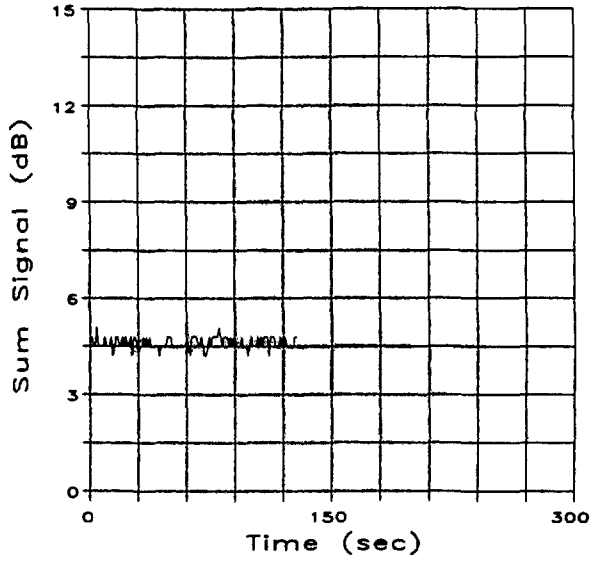

TR34, 17Sep91, 0843 hours

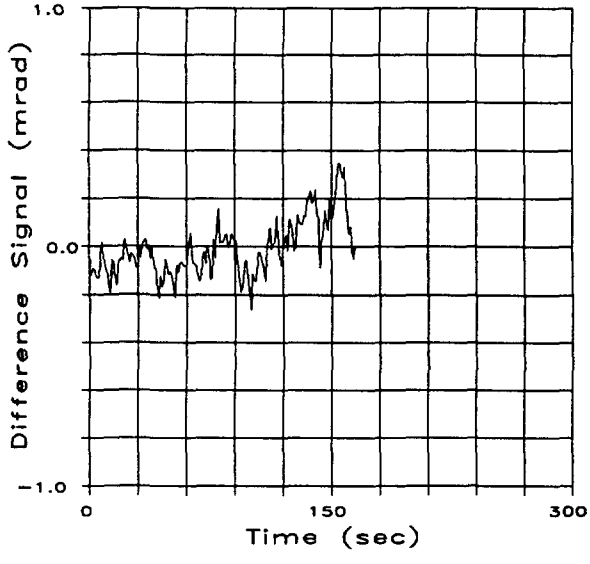

TR35, 17Sep91, 0854 hours

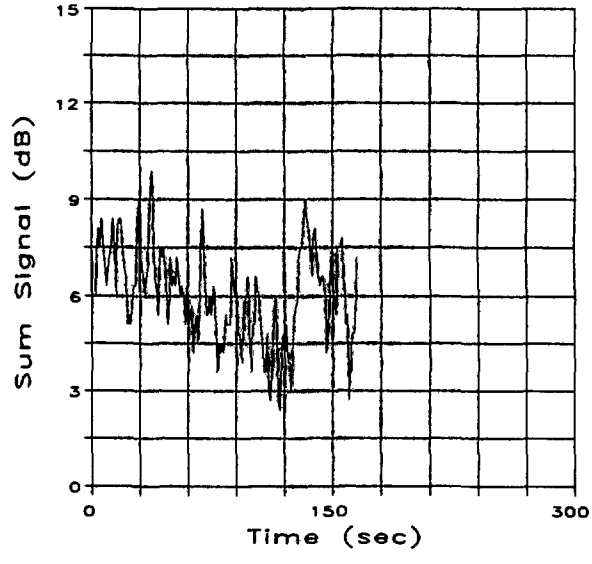

TR35, 17Sep91, 0854 hours

Figure B-12. Noise measurement at 0.4 km and 3 km, Trials 34 and 35.

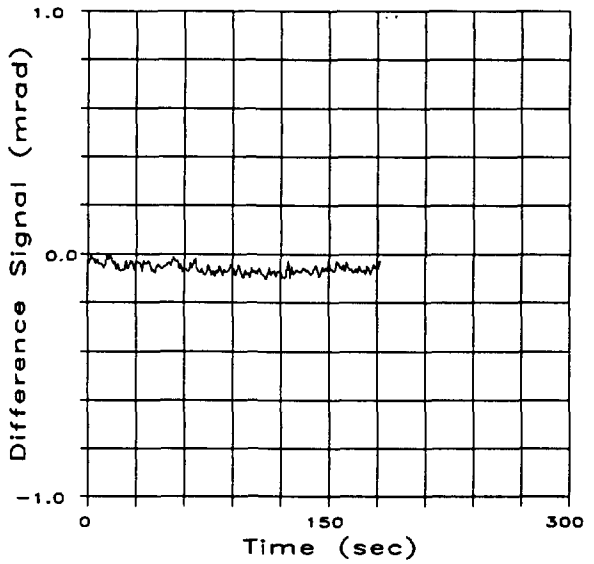

TR37, 17Sep91, 1059 hours

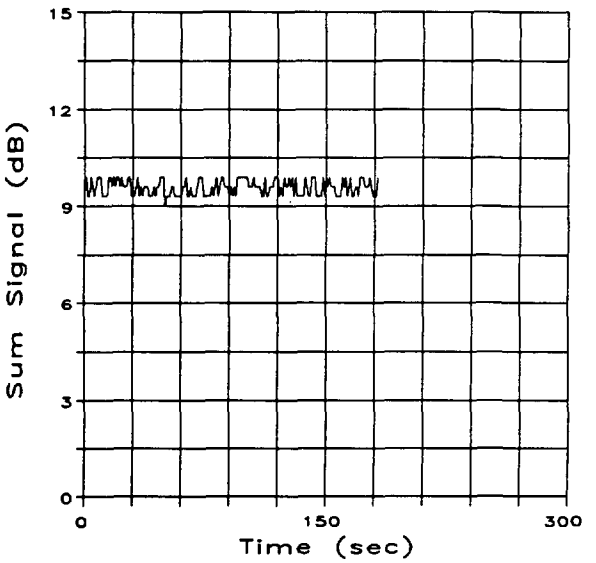

TR37, 17Sep91, 1059 hours

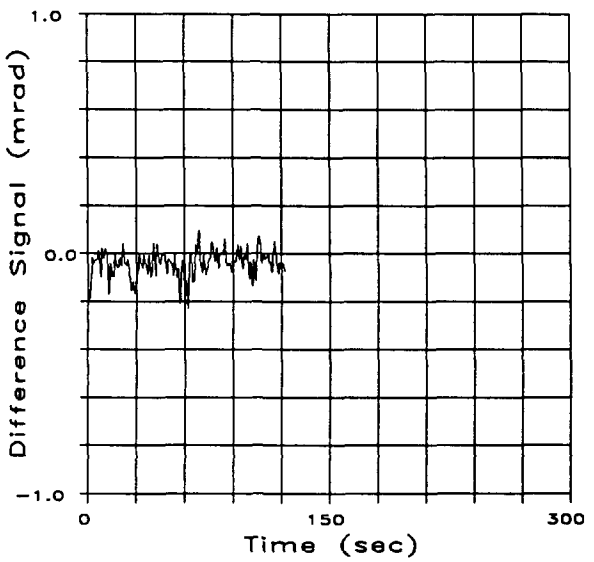

TR38, 17Sep91, 1130 hours

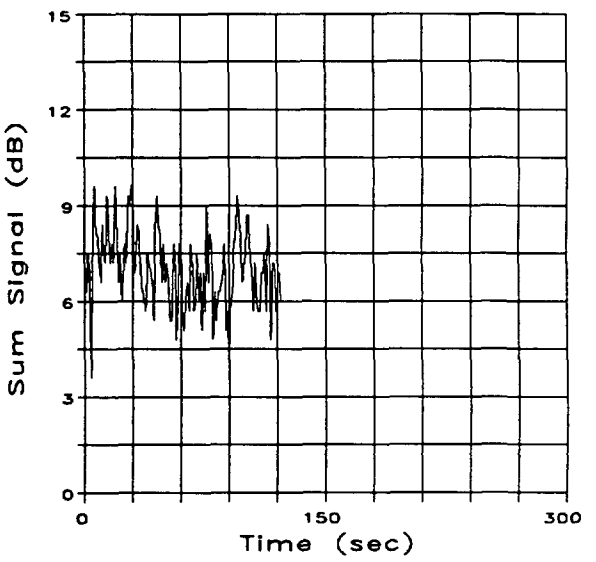

TR38, 17Sep91, 1130 hours

Figure B-13. Noise measurement at 0.4 km and 4 km, Trials 37 and 38.

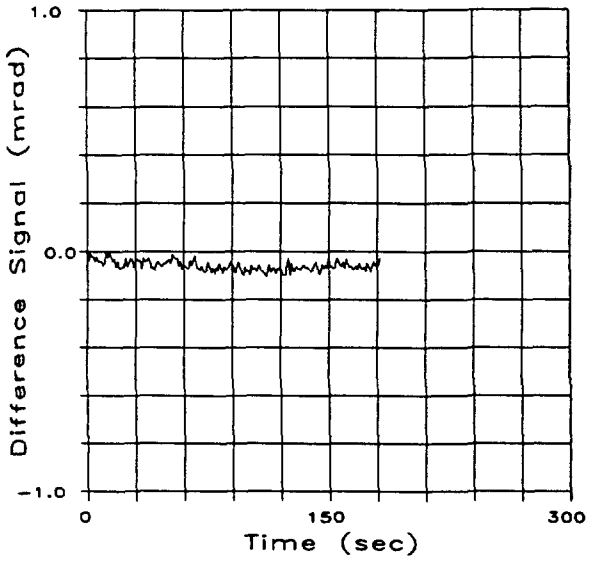

TR37, 17Sep91, 1059 hours

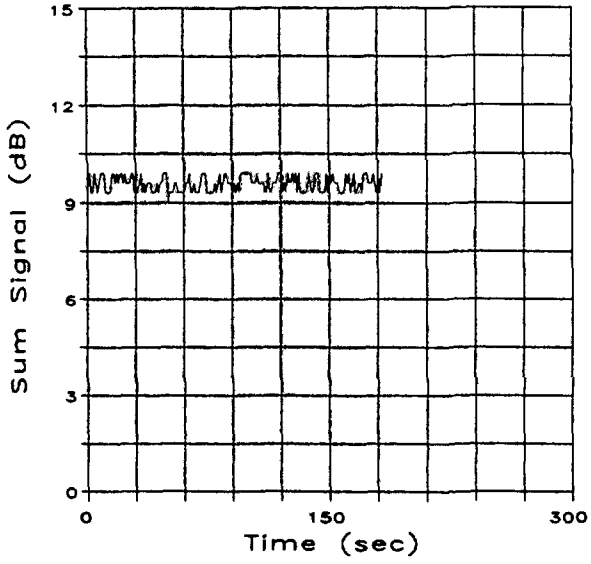

TR37, 17Sep91, 1059 hours

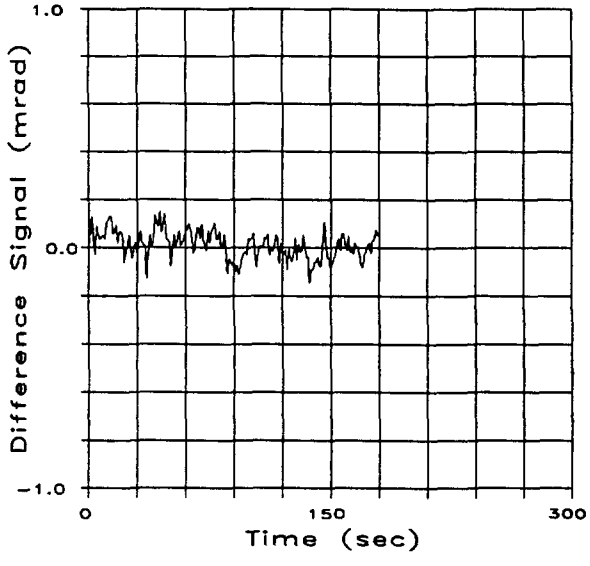

TR40, 17Sep91, 1301 hours

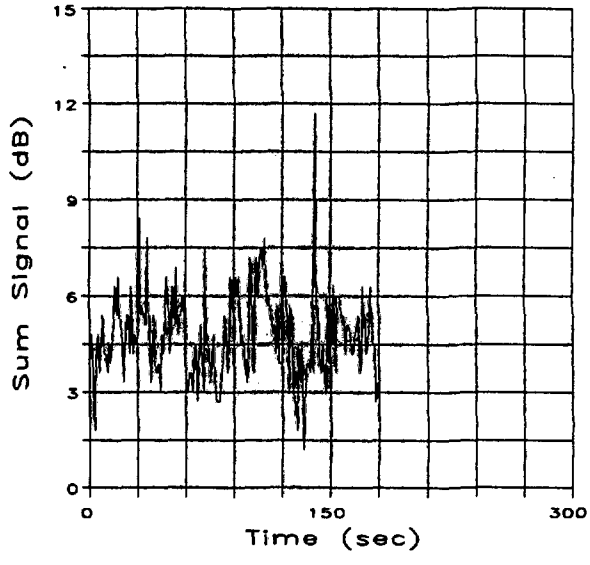

TR40, 17Sep91, 1301 hours

Figure B-14. Noise measurement at 0.4 km and 5 km, Trials 37 and 40.

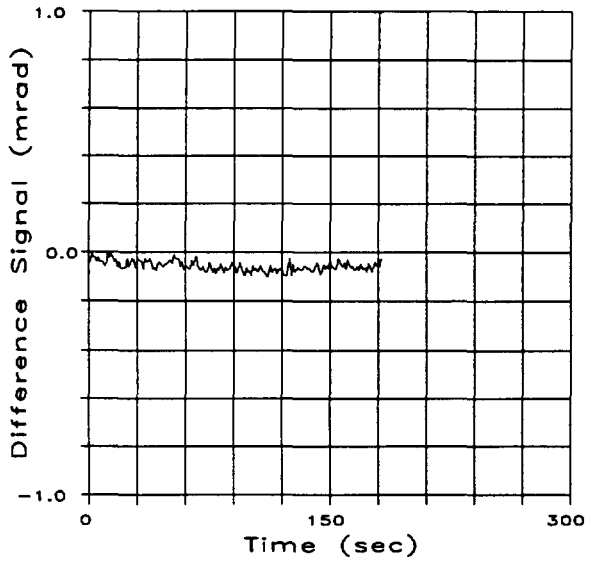

TR37, 17Sep91, 1059 hours

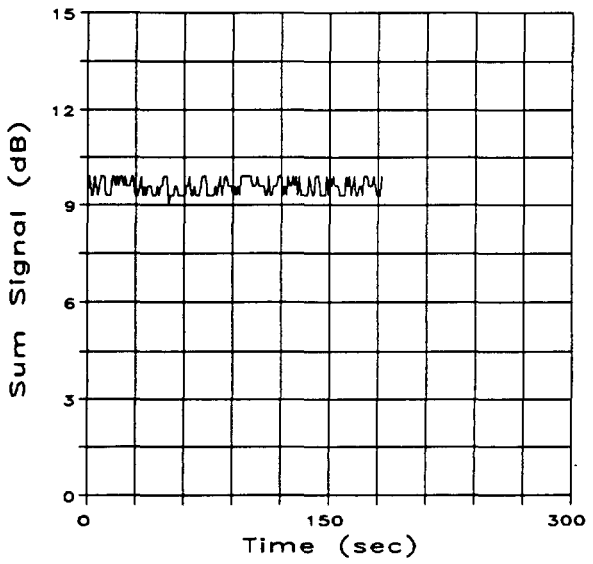

TR37, 17Sep91, 1059 hours

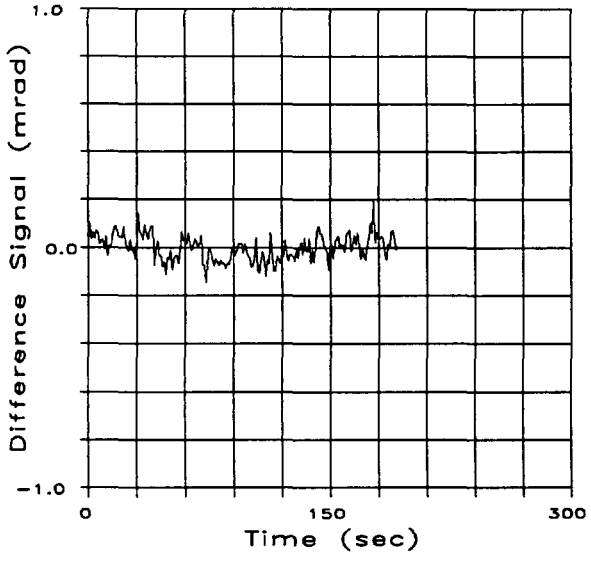

TR41, 17Sep91, 1401 hours

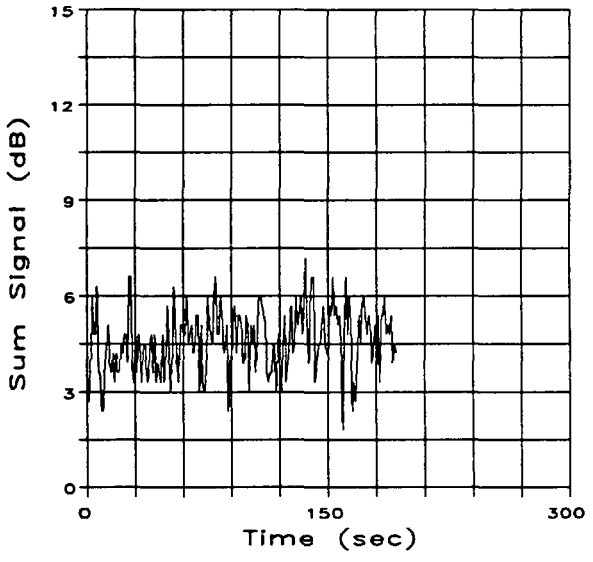

TR41, 17Sep91, 1401 hours

Figure B-15. Noise measurement at 0.4 km and 5 km, Trials 37 and 41.

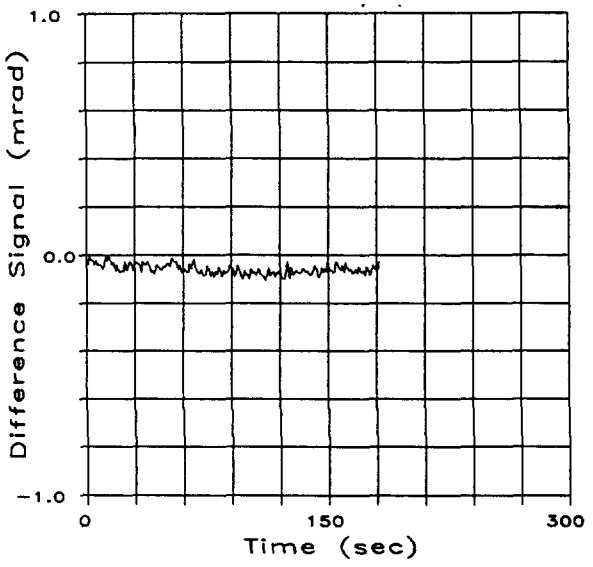

TR37, 17Sep91, 1059 hours

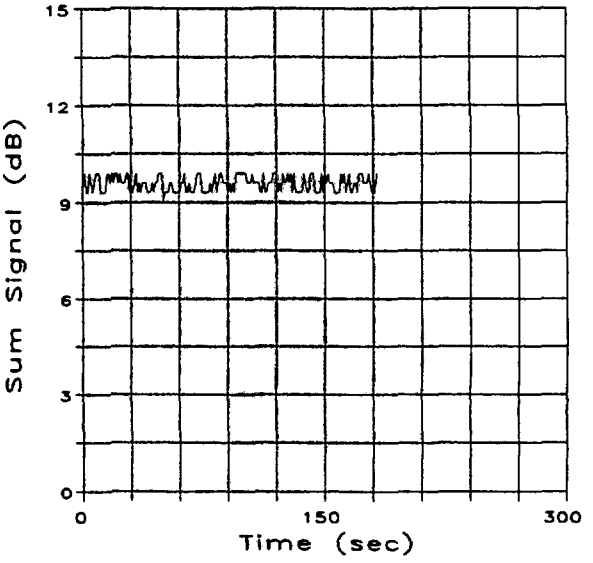

TR37, 17Sep91, 1059 hours

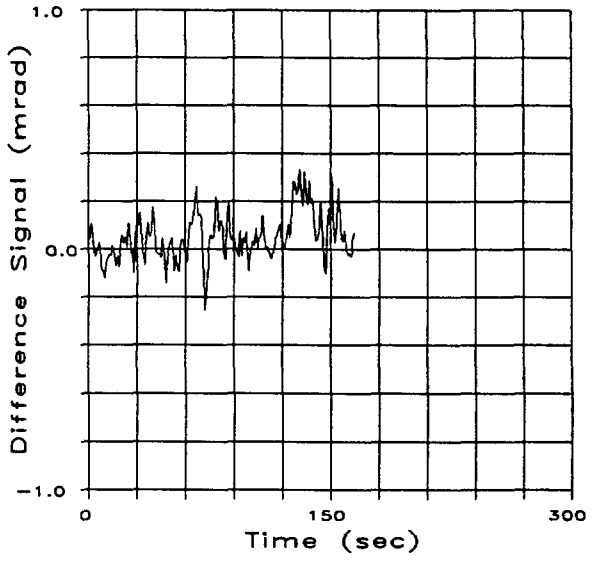

TR43, 17Sep91, 1511 hours

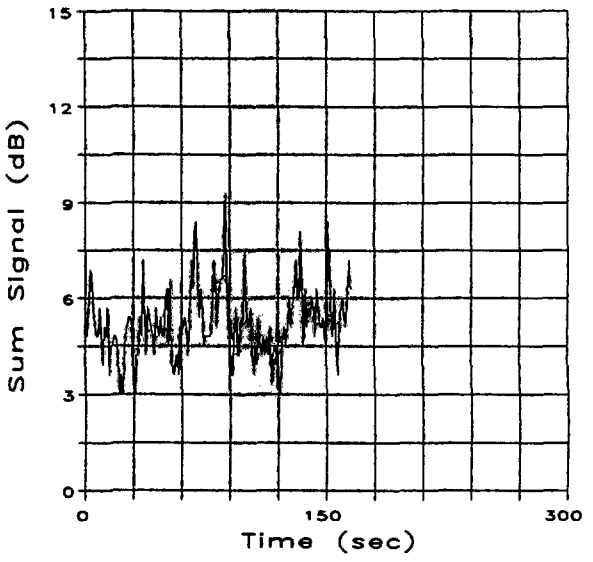

TR43, 17Sep91, 1511 hours

Figure B-16. Noise measurement at 0.4 km and 3 km, Trials 37 and 43.

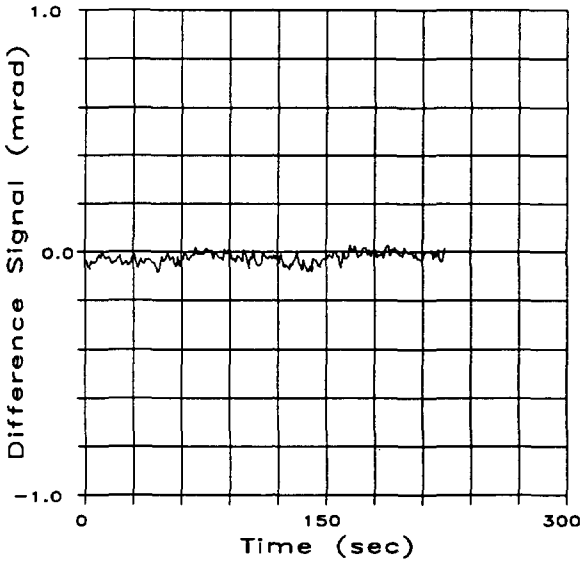

TR45, 18Sep91, 0853 hours

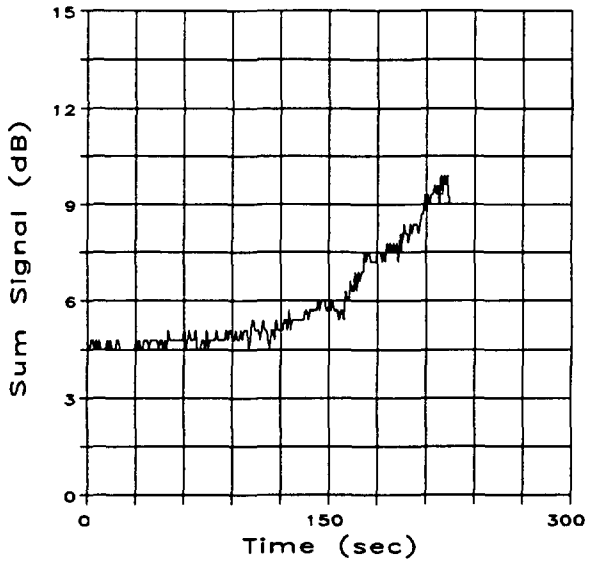

TR45, 18Sep91, 0853 hours

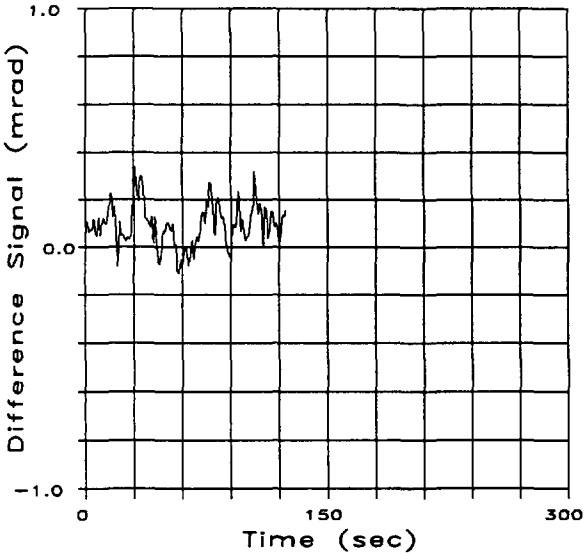

TR46, 18Sep91, 0903 hours

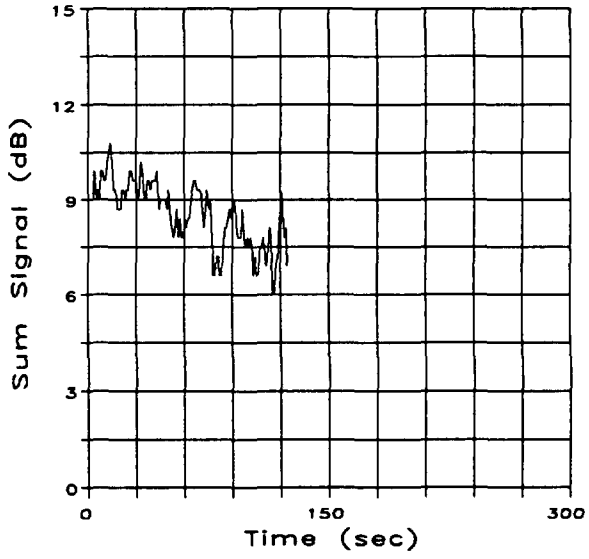

TR46, 18Sep91, 0903 hours

Figure B-17. Noise measurement at 0.4 km and 3 km, Trials 45 and 46.

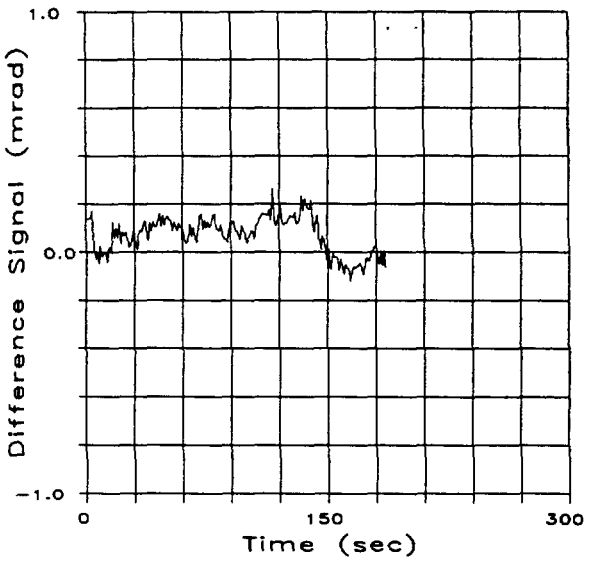

TR48, 18Sep91, 1000 hours

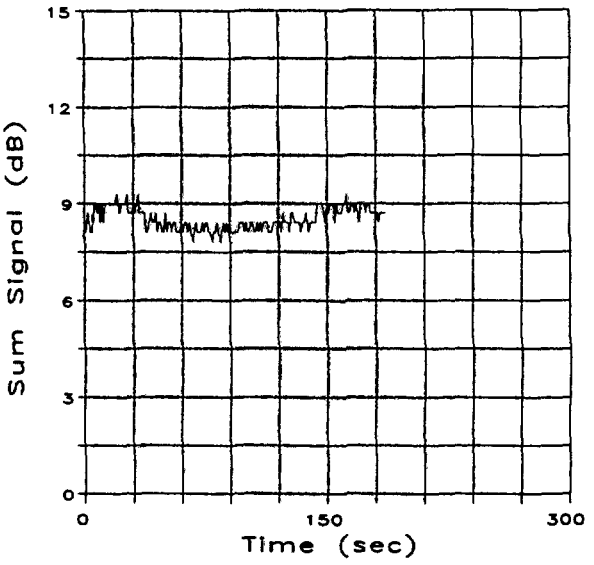

TR48, 18Sep91, 1000 hours

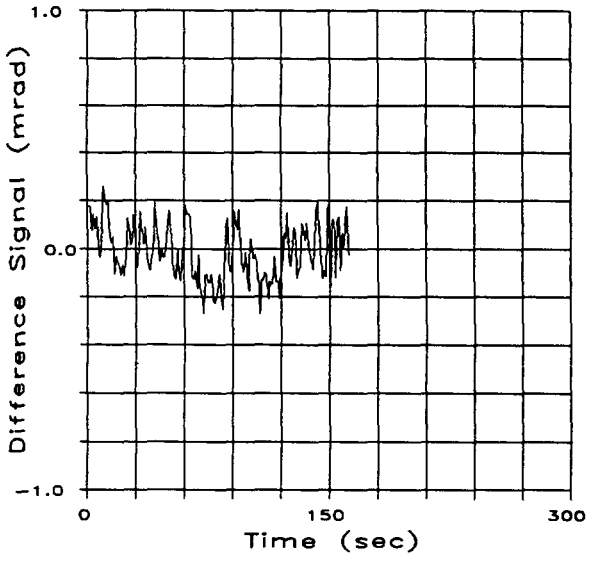

TR49, 18Sep91, 1011 hours

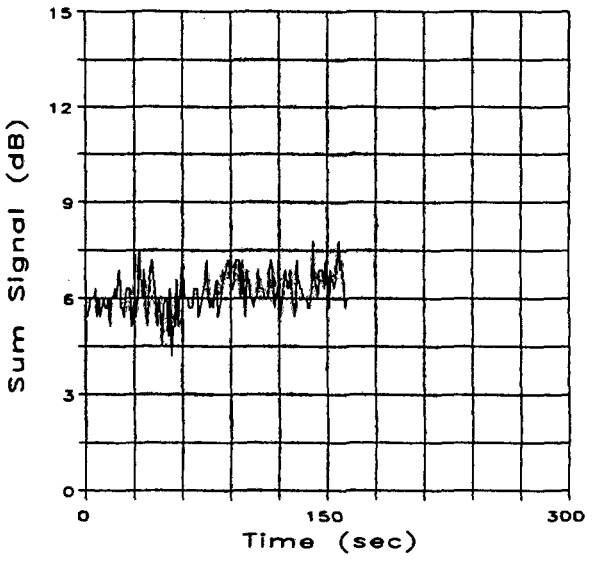

TR49, 18Sep91, 1011 hours

Figure B-18. Noise measurement at 0.4 km and 3 km, Trials 48 and 49.

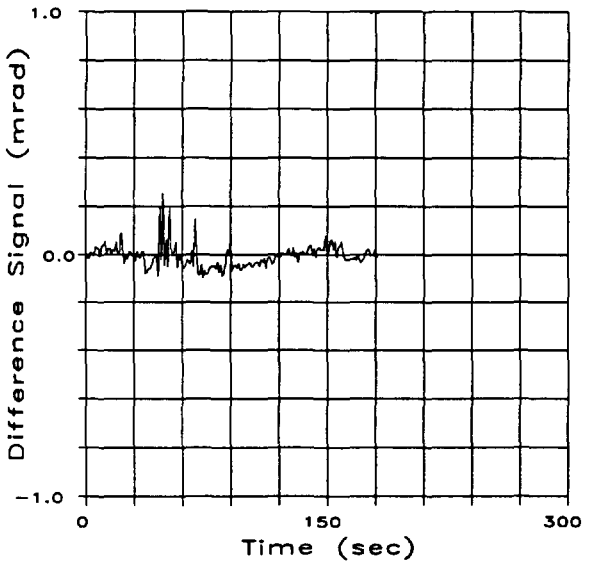

TR51, 18Sep91, 1418 hours

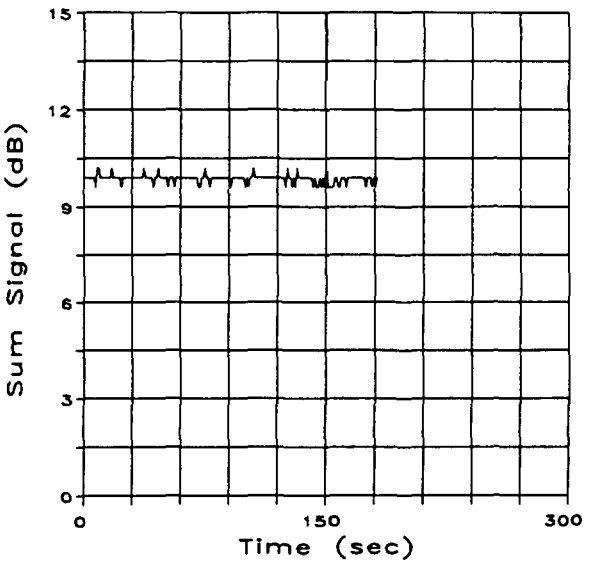

TR51, 18Sep91, 1418 hours

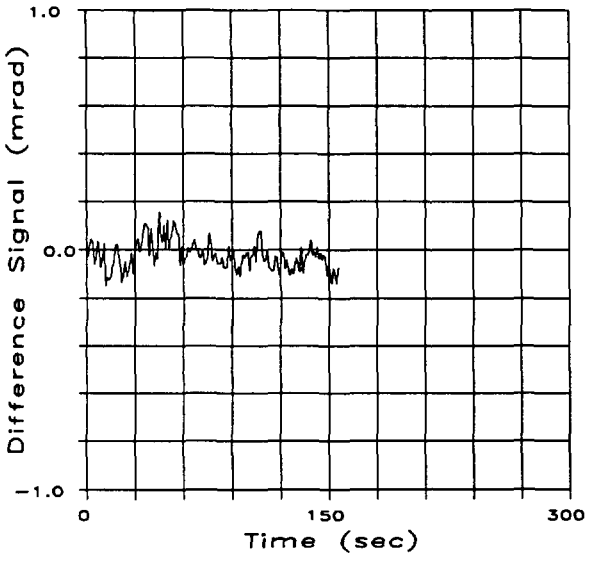

TR52, 18Sep91, 1430 hours

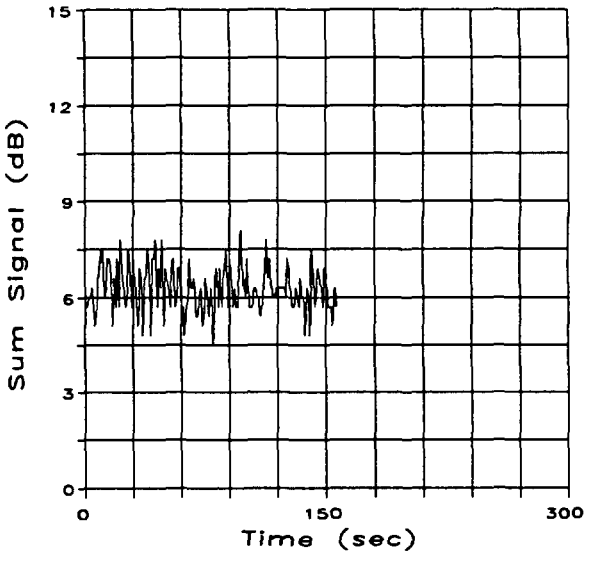

TR52, 18Sep91, 1430 hours

Figure B-19. Noise measurement at 0.4 km and 2 km, Trials 51 and 52.

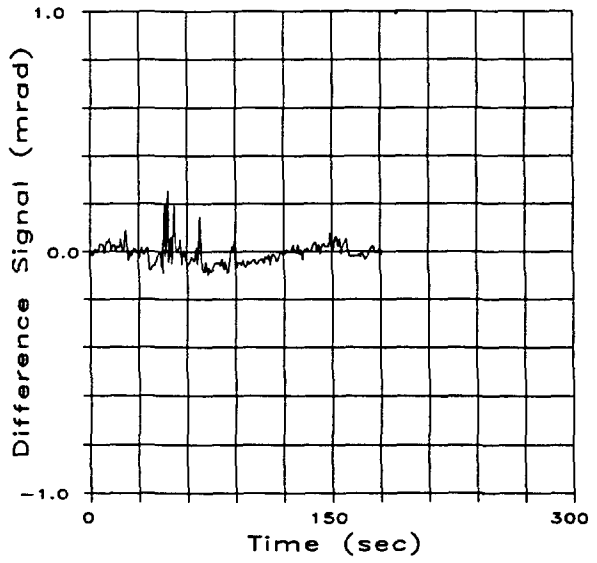

TR51, 18Sep91, 1418 hours

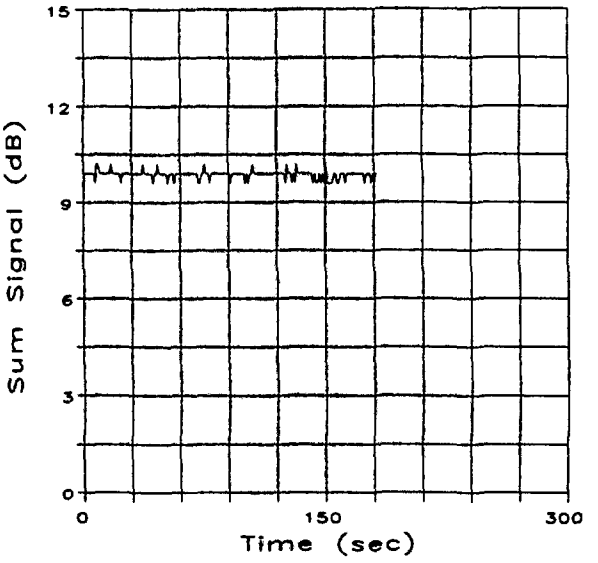

TR51, 18Sep91, 1418 hours

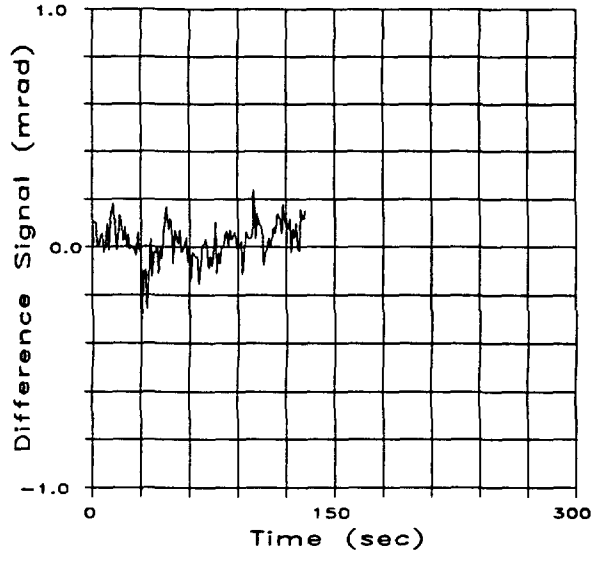

TR55, 18Sep91, 1536 hours

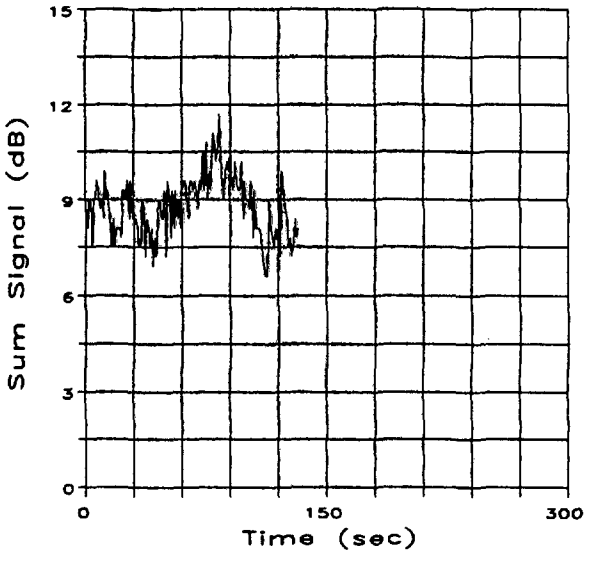

TR55, 18Sep91, 1536 hours

Figure B-20. Noise measurement at 0.4 km and 2 km, Trials 51 and 55.

APPENDIX C:

METEOROLOGICAL DATA

INTENTIONALLY LEFT BLANK.

Table C-1. Meteorological Data Recorded at 2-km Mark of Test Area 3

Date	Time (hr)	Visibility (mi)	Temp. (°F)	Rel. Hum. (%)	Water Vapor Density (g/m^3)
11 Sep	0745	2.4	68.2	89	0.1549
	0800	4.0	69.6	89	0.1620
	0815	4.2	71.5	88	0.1703
	0830	4.2	73.0	86	0.1746
	0845	5.1	73.7	83	0.1723
	0900	6.3	74.7	81	0.1735
	0915	8.3	75.3	78	0.1703
	1330	11.7	91.7	54	0.1941
	1345	12.0	90.7	55	0.1920
	1400	12.6	91.7	53	0.1905
	1415	13.1	91.8	52	0.1875
	1430	13.5	92.6	50	0.1845
	1445	13.6	92.1	50	0.1818
	1500	13.3	92.2	50	0.1824
12 Sep	0800	2.9	75.4	88	0.1927
	0815	4.3	77.1	86	0.1987
	0830	4.8	78.3	82	0.1966
	0845	5.7	79.9	79	0.1990
	0900	7.2	81.4	76	0.2005
	1200	15.0	90.4	61	0.2110
	1215	13.0	91.3	59	0.2096
	1230	13.8	90.9	59	0.2071
	1245	13.4	91.3	59	0.2096
	1300	12.9	93.4	55	0.2078
	1400	14.4	93.0	54	0.2016
	1415	14.8	94.7	50	0.1961
	1430	14.1	94.7	50	0.1961
	1445	15.4	95.1	48	0.1905
	1500	12.7	96.5	46	0.1901

Table C-1. Meteorological Data Recorded at 2-km Mark of Test Area 3 (continued)

Date	Time (hr)	Visibility (mi)	Temp. (°F)	Rel. Hum. (%)	Water Vapor Density (g/m^3)
13 Sep	0800	2.7	75.1	88	0.1909
	0815	4.2	77.6	87	0.2041
	0830	4.6	79.9	83	0.2091
	0845	5.4	81.2	79	0.2072
	0900	7.0	83.8	75	0.2129
	0915	8.2	85.1	71	0.2097
	0930	7.6	85.6	70	0.2099
	1030	12.9	88.9	62	0.2052
	1045	13.2	89.9	60	0.2045
	1100	9.3	90.8	58	0.2030
	1115	10.4	91.8	57	0.2055
	1130	11.9	92.3	55	0.2012
	1145	14.3	92.2	54	0.1970
	1500	9.9	95.6	41	0.1651
	1515	12.9	95.7	41	0.1655
16 Sep	1115	7.6	93.2	52	0.1953
	1130	7.2	93.4	52	0.1964
	1145	7.8	93.5	51	0.1932
	1200	7.7	92.7	51	0.1888
	1415	9.5	96.2	41	0.1679
	1430	9.9	96.4	40	0.1648
	1445	10.0	96.4	40	0.1648

Table C-1. Meteorological Data Recorded at 2-km Mark of Test Area 3 (continued)

Date	Time (hr)	Visibility (mi)	Temp. (°F)	Rel. Hum. (%)	Water Vapor Density (g/m^3)
17 Sep	0700	0.1	69.5	89	0.1615
	0715	2.1	70.2	89	0.1652
	0730	1.0	71.0	89	0.1695
	0830	2.7	78.7	83	0.2015
	0845	3.0	80.0	79	0.1997
	0900	5.1	81.1	75	0.1961
	0915	4.8	71.8	44	0.0860
	1045	8.8	87.6	48	0.1528
	1100	8.6	88.3	46	0.1495
	1115	10.3	89.1	45	0.1498
	1130	10.1	89.3	44	0.1473
	1145	9.6	90.5	42	0.1457
	1300	10.8	93.5	36	0.1364
	1400	11.0	94.7	33	0.1294
	1415	11.3	93.8	33	0.1261
	1500	11.0	94.1	31	0.1195
	1515	10.8	93.8	30	0.1146
	1530	11.6	94.1	27	0.1041
18 Sep	0845	5.8	76.6	75	0.1706
	9000	6.7	78.2	70	0.1673
	0915	7.1	79.7	67	0.1678
	0930	7.6	80.9	64	0.1663
	0945	7.8	82.5	61	0.1665
	1000	8.1	84.2	58	0.1667
	1015	8.5	85.4	54	0.1609
	1030	9.2	87.0	51	0.1595
	1415	13.6	94.7	32	0.1255
	1430	14.6	95.4	31	0.1241
	1445	11.9	95.6	28	0.1127
	1500	15.6	95.3	28	0.1118
	1515	15.7	94.9	28	0.1105
	1530	15.8	94.8	28	0.1102
	1545	15.8	94.9	28	0.1105

Table C-2. Meteorological Data Recorded at 5-km Mark of Test Area 3

Date	Time (hr)	Visibility (mi)	Temp. (°F)	Rel. Hum. (%)	Water Vapor Density (g/m^3)
11 Sep	0745	N/A	68.6	85	0.1498
	0800	N/A	69.6	85	0.1547
	0815	N/A	71.2	85	0.1629
	0830	N/A	72.2	84	0.1662
	0845	N/A	73.0	84	0.1705
	0900	N/A	74.0	83	0.1739
	0915	N/A	74.6	82	0.1751
	1330	N/A	90.7	55	0.1920
	1345	N/A	92.2	53	0.1933
	1400	N/A	92.2	53	0.1933
	1415	N/A	91.2	53	0.1877
	1430	N/A	92.0	51	0.1849
	1445	N/A	91.7	51	0.1833
	1500	N/A	91.4	51	0.1817
12 Sep	0800	N/A	74.1	84	0.1766
	0815	N/A	76.2	83	0.1864
	0830	N/A	77.6	82	0.1924
	0845	N/A	79.4	81	0.2010
	0900	N/A	79.9	79	0.1991
	1200	N/A	91.2	59	0.2090
	1215	N/A	91.7	58	0.2085
	1230	N/A	91.6	58	0.2079
	1245	N/A	92.1	57	0.2073
	1300	N/A	93.7	55	0.2096
	1400	N/A	92.8	54	0.2004
	1415	N/A	93.5	52	0.1970
	1430	N/A	94.2	51	0.1972
	1445	N/A	95.0	49	0.1939
	1500	N/A	95.2	48	0.1910
13 Sep	0800	N/A	74.6	84	0.1794
	0815	N/A	76.1	83	0.1858
	0830	N/A	78.1	82	0.1954
	0845	N/A	79.6	82	0.2047
	0900	N/A	81.4	79	0.2085
	0915	N/A	83.1	77	0.2140
	0930	N/A	84.9	74	0.2172

Table C-2. Meteorological Data Recorded at 5-km Mark of Test Area 3 (continued)

Date	Time (hr)	Visibility (mi)	Temp. (°F)	Rel. Hum. (%)	Water Vapor Density (g/m^3)
13 Sep (continued)	1030	N/A	88.4	62	0.2021
	1045	N/A	89.5	60	0.2021
	1100	N/A	90.2	59	0.2029
	1115	N/A	91.1	57	0.2013
	1130	N/A	92.0	55	0.1994
	1145	N/A	92.3	54	0.1975
	1500	N/A	96.1	41	0.1675
	1515	N/A	97.3	39	0.1649
16 Sep	1115	N/A	91.9	55	0.1988
	1130	N/A	92.5	54	0.1987
	1145	N/A	92.2	54	0.1970
	1200	N/A	92.3	54	0.1975
	1415	N/A	95.6	44	0.1771
	1430	N/A	96.9	41	0.1714
	1445	N/A	96.8	40	0.1667
17 Sep	---------- N/A ----------				
18 Sep	---------- N/A ----------				

INTENTIONALLY LEFT BLANK.

No. of Copies	Organization
2	Administrator Defense Technical Info Center ATTN: DTIC-DDA Cameron Station Alexandria, VA 22304-6145
1	Commander U.S. Army Materiel Command ATTN: AMCAM 5001 Eisenhower Ave. Alexandria, VA 22333-0001
1	Director U.S. Army Research Laboratory ATTN: AMSRL-OP-CI-AD, Tech Publishing 2800 Powder Mill Rd. Adelphi, MD 20783-1145
1	Director U.S. Army Research Laboratory ATTN: AMSRL-OP-CI-AD, Records Management 2800 Powder Mill Rd. Adelphi, MD 20783-1145
2	Commander U.S. Army Armament Research, Development, and Engineering Center ATTN: SMCAR-TDC Picatinny Arsenal, NJ 07806-5000
1	Director Benet Weapons Laboratory U.S. Army Armament Research, Development, and Engineering Center ATTN: SMCAR-CCB-TL Watervliet, NY 12189-4050
1	Director U.S. Army Advanced Systems Research and Analysis Office (ATCOM) ATTN: AMSAT-R-NR, M/S 219-1 Ames Research Center Moffett Field, CA 94035-1000

No. of Copies	Organization
1	Commander U.S. Army Missile Command ATTN: AMSMI-RD-CS-R (DOC) Redstone Arsenal, AL 35898-5010
1	Commander U.S. Army Tank-Automotive Command ATTN: AMSTA-JSK (Armor Eng. Br.) Warren, MI 48397-5000
1	Director U.S. Army TRADOC Analysis Command ATTN: ATRC-WSR White Sands Missile Range, NM 88002-5502
(Class. only) 1	Commandant U.S. Army Infantry School ATTN: ATSH-CD (Security Mgr.) Fort Benning, GA 31905-5660
(Unclass. only) 1	Commandant U.S. Army Infantry School ATTN: ATSH-WCB-O Fort Benning, GA 31905-5000
1	WL/MNOI Eglin AFB, FL 32542-5000
	Aberdeen Proving Ground
2	Dir, USAMSAA ATTN: AMXSY-D AMXSY-MP, H. Cohen
1	Cdr, USATECOM ATTN: AMSTE-TC
1	Dir, USAERDEC ATTN: SCBRD-RT
1	Cdr, USACBDCOM ATTN: AMSCB-CII
1	Dir, USARL ATTN: AMSRL-SL-I
5	Dir, USARL ATTN: AMSRL-OP-AP-L

No. of Copies	Organization
2	Commander U.S. Army Missile Command ATTN: AMSMI-RD-AS-MM, Mike Christian Redstone Arsenal, AL 35898-5253
1	Commander U.S. Army Armament Research, Development, and Engineering Center ATTN: SMCAR-FSP-AI, Murray Rosenbluth Bldg 353N Picatinny, NJ 07806-5000
1	Commander U.S. Army Armament Research, Development, and Engineering Center ATTN: SMCAR-FSP-BD, Larry Yung Bldg 353N Picatinny, NJ 07806-5000
1	Commander U.S. Army Communications and Electronics Command ATTN: Scott Mollica Fort Monmouth, NJ 07703
2	Commander Naval Surface Warfare Center ATTN: Code F41, Jim Morrissett Douglas Marker Dalhgren, VA 22448-5000
1	Commander U.S. Army Test and Evaluation Command ATTN: STEDP-MT-DA-0, Dennis Bodrero Dugway Proving Ground, UT 84022-5000
1	Institute for Defense Analysis Science and Technology Division ATTN: Dr. James M. Ralston 1801 N. Beauregard Street Alexandria, VA 22311-1772
1	Georgia Tech Research Institute Radar Systems Applications Laboratory ATTN: Jay Saffold Atlanta, GA 30332-0800

No. of Copies	Organization
2	AAI Corporation ATTN: David Cleveland, 100/444 Paul Shipley, 100/403 P.O. Box 126 Hunt Valley, MD 21030-0126
1	MIT Lincoln Laboratory ATTN: Pamela Reynolds 244 Wood St. Room A082 Lexington, MA 02173
1	MIT Lincoln Laboratory ATTN: Jack Fleischman, B363 244 Wood St. Lexington, MA 02173
1	University of Nebraska Electrical Engineering Dept. ATTN: Ram Narayanan Mail Stop 0511 Lincoln, NE 68588
2	Rockwell International MMW Radar Technology Dept. Tactical Systems Division ATTN: Keith Hull, MS-DC04 Roland H. Wright, MS-DD46 3370 Miraloma Ave P.O.Box 3170 Anaheim, CA 92803-3170
	Aberdeen Proving Ground
1	Dir, USAMSAA ATTN: AMXSY-GA, Floyd Wofford
11	Dir, USARL ATTN: AMSRL-SS-SD, Donald Bauerle Robert Bender Suzanne Stratton (5 cp) Bruce Wallace Joseph Nemarich (ADELPHI) AMSRL-WT-WB, Victor Leitzke Richard McGee

USER EVALUATION SHEET/CHANGE OF ADDRESS

This Laboratory undertakes a continuing effort to improve the quality of the reports it publishes. Your comments/answers to the items/questions below will aid us in our efforts.

1. ARL Report Number ARL-MR-140 Date of Report June 1994

2. Date Report Received _____

3. Does this report satisfy a need? (Comment on purpose, related project, or other area of interest for which the report will be used.) _____

4. Specifically, how is the report being used? (Information source, design data, procedure, source of ideas, etc.) _____

5. Has the information in this report led to any quantitative savings as far as man-hours or dollars saved, operating costs avoided, or efficiencies achieved, etc? If so, please elaborate. _____

6. General Comments. What do you think should be changed to improve future reports? (Indicate changes to organization, technical content, format, etc.) _____

CURRENT ADDRESS

_____
Organization

_____
Name

_____
Street or P.O. Box No.

_____
City, State, Zip Code

7. If indicating a Change of Address or Address Correction, please provide the Current or Correct address above and the Old or Incorrect address below.

OLD ADDRESS

_____
Organization

_____
Name

_____
Street or P.O. Box No.

_____
City, State, Zip Code

(Remove this sheet, fold as indicated, tape closed, and mail.)

(DO NOT STAPLE)

DEPARTMENT OF THE ARMY

OFFICIAL BUSINESS

BUSINESS REPLY MAIL
FIRST CLASS PERMIT No 0001, APG, MD

Postage will be paid by addressee.

Director
U.S. Army Research Laboratory
ATTN: AMSRL-OP-CI-B (Tech Lib)
Aberdeen Proving Ground, MD 21005-5066

NO POSTAGE
NECESSARY
IF MAILED
IN THE
UNITED STATE